J. Phys. G: Nucl. Part. Phys. **34** (2007) R165–R242 doi:10.1088/0954-3899/34/4/R01

TOPICAL REVIEW

Heaviest nuclei from ^{48}Ca-induced reactions

Yuri Oganessian

Flerov Laboratory of Nuclear Reactions, Joint Institute for Nuclear Research, 141980 Dubna, Moscow Region, Russia

E-mail: oganessian@jinr.ru

Received 30 October 2006
Published 16 March 2007
Online at stacks.iop.org/JPhysG/34/R165

Abstract

After a brief introduction of the role of shell effects in determining the limiting nuclear masses, the experimental investigation of the decay properties of the heaviest nuclei is presented. For the production of superheavy nuclides fusion, reactions of heavy actinide nuclei with ^{48}Ca-projectiles have been used. The properties of the new nuclei, the isotopes of elements 112–118, as well as of their decay products, together with the known data for the light isotopes with $Z \leqslant 113$, give evidence of the significant increase of the stability with the neutron number of the heavy nucleus. The obtained results are discussed in the context of the theoretical predictions about the 'island of stability' of the hypothetical superheavy elements.

(Some figures in this article are in colour only in the electronic version)

1. Introduction

Only 278 nuclides out of about 3000 hitherto known are found in nature. The change of the proton-to-neutron ratio in stable nuclei generates, as it is well known, their radioactive decay. The neutron excess in nuclei leads to decrease of the neutron separation energy; the limit comes at $B_n = 0$ (the neutron drip line). Similarly, the zero proton separation energy, $B_p = 0$ (the proton drip line), determines the limit of existence of proton-rich nuclei. Another limitation is the extreme nuclear mass, which is defined by the probability of spontaneous fission. In fact, when the fission barrier vanishes ($B_f = 0$), the nucleus thoroughly loses its stability even with respect to small variations of the nuclear shape, which in turn brings forth fast division into two fragments ($T_{SF} \sim 10^{-19}$ s). In the macroscopic approach (the liquid-drop model is a typical example), which for a long time has been used to describe the nuclear masses in the ground and highly deformed states, spontaneous fission dominates already in nuclei with $Z^2/A \geqslant 39$ [1, 2]. This decay mode defines the extreme masses of the heaviest nuclei, as well as the limits of existence of the chemical elements ($T_{1/2} > 10^{-14}$ s). In this model, the limit of existence of nuclei is located practically immediately after $Z \approx 100$ [1].

 © 2007 IOP Publishing Ltd Printed in the UK

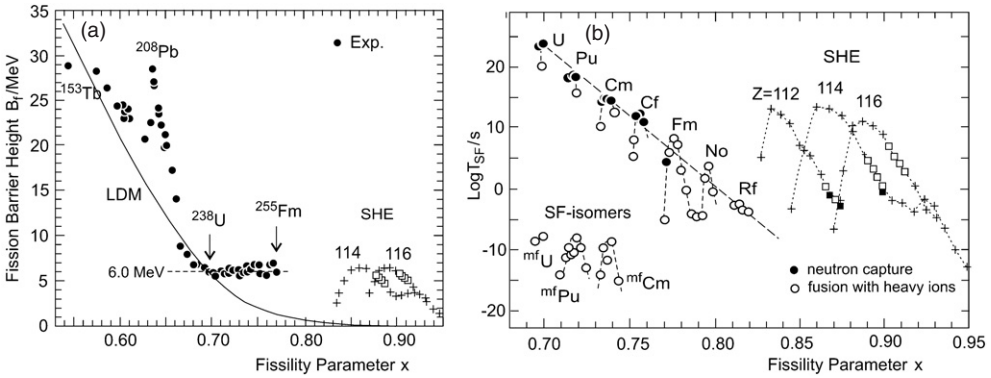

Figure 1. (a) Fission barrier heights as a function of the fissility parameter $x = (Z^2/A)/(Z^2/A)_{\rm crit}$ [5] at $(Z^2/A)_{\rm crit} = 50.883$. The black points are experimental data, the solid line is calculations in the liquid-drop model [3, 6], crosses are calculated fission barrier heights in the macro-microscopic model for the isotopes of elements 114 and 116 [7], the open squares are nuclei, produced in the ^{242,244}Pu, ^{245,248}Cm + ^{48}Ca reactions. (b) Half-lives with respect to spontaneous fission as a function of the fissility parameter x. The black points and the open circles denote experimental values $T_{\rm SF}$(exp) for spontaneous fission of even–even nuclei from the ground and isomeric states. The dashed line is an extrapolation into the trans-actinide region before the synthesis of heavy nuclei in heavy-ion-induced reactions (macroscopic concept). Crosses are calculated values $T_{\rm SF}$(th) in the macro-microscopic model for even–even isotopes of elements 114 and 116 [7], open squares are nuclei, produced in the reactions ^{242,244}Pu, ^{245,248}Cm + ^{48}Ca, black squares are isotopes for which the SF-half-lives have been measured.

At the same time, it has been observed that in the binding energy of nuclei in their ground state, even for spherical nuclei, there are large fluctuations depending on the proton or neutron number (nuclear shells).

This was illustrated long time ago by comparison of the liquid-drop model calculations with experimental masses and fission barriers for the known relatively heavy nuclei with $160 \leqslant A \leqslant 260$ (see, for example, [3, 4]). The experimental masses were found to differ from the calculated ones both for the spherical nuclei close to ^{208}Pb and for the rather deformed actinide nuclei with $Z \geqslant 90$. Another question is to what extent the nuclear structure at the ground state will manifest itself at large deformations in the fission process.

Already the first calculations of the nuclear potential energy surface in the macroscopic approximation revealed the difficulties standing in the way of describing many of the experimentally observed characteristics of nuclear fission. A strong disagreement is found in the fission barrier heights (figure 1(a)) and in the probabilities of spontaneous fission (figure 1(b)) which, as it is well known, is determined not only by the height, but also by the shape of the fission barrier. The smooth reduction of the liquid-drop fission barrier height with the increase of the fissility parameter $x \sim Z^2/A$ cannot explain the variations of the fission barriers of heavy nuclei, namely the two times higher barrier in ^{208}Pb ($B_f \approx 28$ MeV) and the practically unchanged fission barrier heights in the isotopes of the actinides from U to Fm ($B_f \approx 6$ MeV). As a result, the partial spontaneous-fission half-lives $T_{\rm SF}$(th) strongly differ from $T_{\rm SF}$(exp), see figure 1(b). In macroscopic approaches it is impossible to find an explanation of the nuclear shape isomerism [8], which manifests itself in heavy nuclei as 33 SF-isomers [9], as well as of the strong change in $T_{\rm SF}$ for the actinide isotopes at small variations of their nucleon composition [10] and many other effects, which have been seen in different experiments.

1.1. Theoretical concept

Based on the saturation property and low compressibility of nuclear matter an analogy has been suggested with a charge liquid droplet. Since then, the main field of application of the liquid-drop model (LDM) has been the description of the average properties of the nuclear masses and deformation energies. The attempts to extend the analogy between the nucleus and a liquid droplet to get some information about the dynamic properties of nuclear matter (by assuming an irrotational and incompressible collective flow in the nucleus) have not been successful.

The reason is that the macroscopic description completely neglects the effect of non-uniformities in the distribution of nucleons in phase space that depend on Z and N and are, therefore, unique for each nucleus. It had become obvious that the macroscopic approaches needed corrections to the 'smooth' dependence of the nuclear potential energy by means of the shell model [11, 12], which predicted the gaps in the single particle level distribution corresponding to the magic numbers . . . 50, 82, 126. From the point of view of nuclear stability with respect to spontaneous fission, there is the question concerning the changes of the shell effect with the increase of deformation.

The main achievements of the macro-microscopic theory are connected with the development of the method of calculating such corrections for the ground and highly deformed states [13, 14] based on the Nilsson or Wood–Saxon single particle potential to the smooth, macroscopic part of the energy. The concept of nuclear shells is here defined as a large-scale non-uniformity in the energy distribution of the individual particle states near the Fermi energy [15] directly connected to the nuclear binding energy. In such an approach, the model corrects the energy according to the nuclear structure (effect of nuclear shells, pairing), based on the calculation of the nuclear levels [16, 17].

In many publications (e.g., see the reviews [15, 18–20] and references therein), a number of the existing disagreements between the macroscopic (liquid drop) model and experiment were explained by taking into account the shell effect when calculating the nuclear energy. One important consequence of these calculations was the disclosure of a significant gap in the spectrum of low-lying levels in the region of the hypothetical superheavy nuclei, namely of a new (following $N = 126$) closed spherical neutron shell $N = 184$ [21–23]. It was also shown that the considerable variations of the binding energy of spherical nuclei were due to the nuclear shells and that shell effects might also be present in deformed 'magic nuclei' (deformed shells) [13–15, 24]. And finally, at further and quite significant increase of the deformation arising in fission, *the shell effects continued to play an important role* in defining the potential energy and the nuclear inertial masses [15, 25].

In the region of heavy nuclei with $A \geqslant 200$ that concern us, the agreement with experimental ground-state masses and deformations was obtained by taking into account the closed spherical shells $Z = 82$ and $N = 126$ ($\Delta E_{\text{Shell}} = -14.3$ MeV) and the deformed shells $Z \approx 100$ and $N = 152$ ($\Delta E_{\text{Shell}} = -5.2$ MeV) [26]. These shells are responsible for the variations in the fission barrier heights (figure 1(a)) and shapes (like the two-humped fission barriers of actinides) and, hence, for the nuclear stability against spontaneous fission. They qualitatively reflect the variations of $T_{\text{SF}}(\text{exp})$ versus Z and N in the region of the actinides, including SF-isomers (figure 1(b)), bimodal spontaneous fission of neutron-rich Fm–No isotopes and many other regularities in the properties of spontaneously fissioning nuclei.

When moving into the region of heavier nuclei, as shown in figure 2, the variation of the amplitude $\Delta E_{\text{Shell}}(Z, N)$ evidences the appearance of new closed shells $Z = 108$, $N = 162$ ($\Delta E_{\text{Shell}} = -7.2$ MeV) and $Z = 114$, $N = 184$ ($\Delta E_{\text{Shell}} = -7.2$ MeV) [24, 26]. Nuclei, situated in close proximity to the $N = 162$, as well as to the $N = 152$ shell, in the ground state have

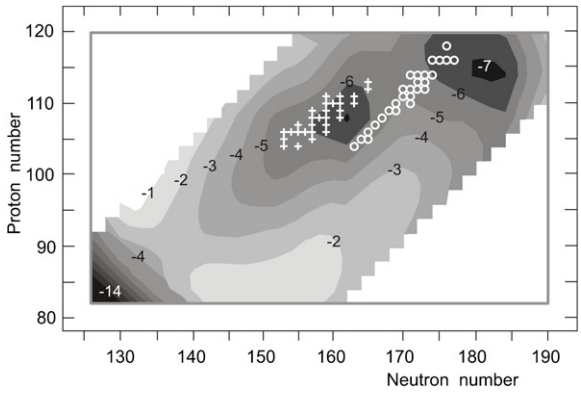

Figure 2. The map of the shell corrections ΔE_{shell} to the nuclear macroscopic potential energy [24, 26]. The numbers at the contour curves correspond to the amplitude of the shell correction (in MeV). Crosses denote nuclei with $Z \geqslant 104$, obtained in cold fusion reactions, open circles in Act. + ^{48}Ca reactions.

a large enough deformation ($\beta_2 \approx 0.24$). In the region of heavier masses, nuclei with $N = 184$ similarly to the 'magic nucleus' ^{208}Pb ($N = 126$, $Z = 82$) are spherical. The properties of the nuclei change significantly depending on the effect of the new shells. The strongest difference is observed for heavy nuclei with $Z \geqslant 100$, where $B_f(\text{LD}) \approx 0$. The sum of the smooth part of the deformation energy $E_d(\text{LD})$ and the shell correction $\Delta E_d(\text{Shell})$ brings forth the appearance of a fission barrier with height roughly equal to the magnitude of the shell correction. For the heaviest nuclei with $Z = 112$–114 and $N = 180$–184 (see figure 1(a)), the fission barrier height may amount to $B_f > 6$ MeV (higher than for ^{238}U). Therefore, the partial spontaneous-fission half-lives, as shown in the calculations of [7], increase up to almost 10^6 years. Then, T_{SF} exceeds the estimates of the macroscopic models by a factor of 10^{30}! Less striking, but also quite strong, is the effect expected for deformed nuclei with $Z = 106$–108 and $N \approx 162$; the effect of the deformed shells suppresses the probability of spontaneous fission by a factor of $>10^{20}$.

Here an interesting situation arises. Because of the high stability with respect to spontaneous fission, the heaviest nuclei will undergo α- or β-decay (T_α, $T_\beta \ll T_{\text{SF}}$). The energy and probability of these decays will depend on the ground-state nuclear masses; they can be calculated within theoretical models, based on different concepts about the fundamental properties of nuclei. From this point of view, the experimental results, obtained in the mentioned region of strong effects of the new nuclear shells, are very informative for testing the theory.

As follows from the calculations, the shell effect considerably increases the stability of heavy nuclei relative to α-decay. For the magic nuclei $N \approx 184$ with $Z = 112$ and 114, according to [7], T_α amounts to 10^6 s and 10^3 s, respectively. The deformed nucleus ($Z = 106$, $N = 162$) will have $T_\alpha \sim 10^2$ s.

In this way, without going into details and not neglecting some uncertainties in the theoretical predictions (quantitatively, the results of different calculations vary), we have an alternative to the macroscopic approaches which concern the determination of the extreme nuclear masses. Contrary to the smooth variation of nuclear binding energy leading to considerable loss of stability, when going into the region $Z > 100$, strong energy variations occur due to the nuclear structure. The theoretical predictions for the new shells, which in fact

are not too far from the well-established region of the actinides (it is a question of nuclei with mass ∼290–300), push far away the limits of nuclear masses and extend the region of existing elements at least as far as $Z \sim 120$ and even more.

Earlier as an illustration we mentioned the calculations of the macro-microscopic models (MMM). Other, purely microscopic self-consistent approaches to the description of nuclear binding energies, such as the Hartree–Fock–Bogoliubov (HFB) model with effective density-dependent interactions (with zero range forces of Skyrme type [27–31] or finite range forces of Gogny type [32–34]) and the relativistic-mean-field (RMF) theory (based on an effective Lagrangian containing both nucleonic and mesonic degrees of freedom [35, 36]), also predict significant increase of the binding energy of heavy nuclei at $N \approx 162$ and $N = 184$. It seems the conclusion that in the region of superheavy elements one may expect a strong influence of the above-mentioned nuclear shells follows from all microscopic models. In models such as HFB, the description of the experimental masses in a wide region of heavy nuclei is obtained by choosing suitable forces. Among them, as shown in [37], the best agreement in the known region of the heavy nuclei is achieved in the HFB-Sly4 calculations [27] and in the model with Gogny DIS forces [38]. For superheavy nuclei depending on the choice of parameters, the calculated energies, shapes and fission barriers somewhat differ from each other. However, in most cases, the nuclear binding energy is bigger and the fission barriers are noticeably higher than in the predictions of the MM-model [39]. Like the MMM-calculations, in microscopic models the maximum shell effect at the $N = 184$ spherical shell closure is expected, but for nuclei with a higher number of protons: $Z = 120$, 122, 124 or even 126 [40–42]. We shall present a quantitative comparison of the calculations within different models and in different versions in the last paragraph of this review together with the comparison of the experimental results.

The above-mentioned uncertainties in the quantitative estimations of the nuclear shell effects do not change the general conclusion of theory that in the large interval of masses from 250 to 320, an '*island of stability*' may arise, considerably changing the limits of existence of atomic nuclei.

The theoretical studies of the properties of the heaviest nuclei, which have been carried out during the past 40 years and have undergone intensive development during the very recent years, are nowadays an enormous domain of modern nuclear theory. It is not our aim to discuss in detail the concept and conclusions of the different models and the outcoming quantitative descriptions of mass, deformation, energy levels, etc of all known nuclei. The more so, we are not going to discuss their advantages or shortcomings. Such an analysis has been done in some reviews written recently [37, 43, 44]. Of main interest to us are the basic consequences of these models which concern the properties of the heaviest nuclei; in fact, from the point of view of their experimental verification, this is the main purpose of the present review.

1.2. Experimental approaches

In order to be able to estimate the real feasibility of such experiments, it is necessary to understand at what distance from the known regions are the hypothetical nuclides to be looked for and what are the scales of any changes in their structure (the shell effects) that are to be found experimentally.

First of all we should note that the new 'magic nuclei' possess considerable neutron excess. For the products of heavy-ion reactions the neutron excess will be notably smaller. This will, in turn, lead to a decrease of the shell effect and to loss of stability. In figure 3, as contour plots, we have shown the calculated half-lives and decay modes of nuclei with different proton and neutron numbers [45, 46]. It can be seen that a significant increase of

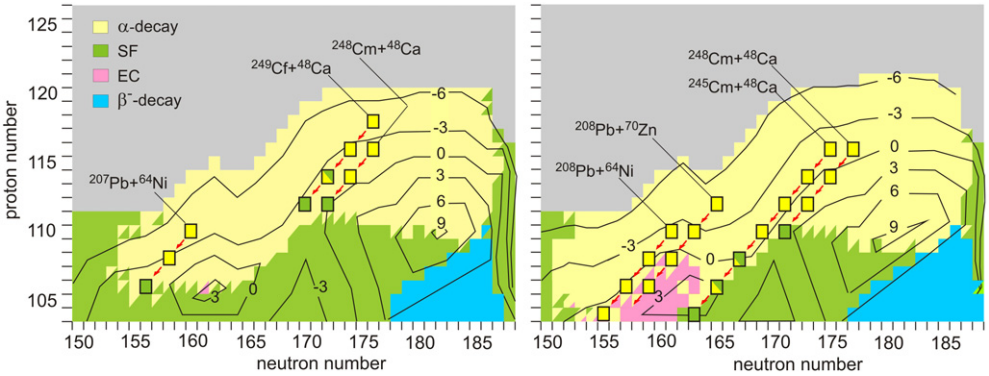

Figure 3. Contour map of the calculated half-lives as Log $T_{1/2}$ (in seconds) and decay modes of nuclei with different proton and neutron numbers (after [47]). The left graph refers to even–even nuclei, the right one to even–odd nuclei. The regions corresponding to different decay modes are shown in different colours. The consecutive decay of nuclei, produced in cold fusion and Act. + ^{48}Ca reactions is also shown (see the text for details).

stability may be expected in the regions around the magic nuclei. The remarkable success in the past few years achieved in the synthesis of heavy nuclei in cold fusion reactions is related basically to isotopes in the vicinity of the $N = 162$ shell, mainly at $N < 162$ [47]. The decay properties (α-decay energies and half-lives, as well as spontaneous-fission half-lives) of practically all synthesized nuclei up to the heaviest one (^{277}112) are well explained by model calculations reflecting the effect of the deformed shells $Z = 108$ and $N = 162$.

But in order to probe the effect of the next, spherical shells, which influence a much wider charge and mass region of heavier nuclei, it is necessary to synthesize nuclei with $Z \geqslant 112$ and $N \geqslant 172$. This is hard to achieve in cold fusion reactions. One of the key questions pertains to the production of new 'magic' nuclei in heavy-ion-induced reactions. The withdrawal from the well-studied cold fusion reactions, which have been used for a long time to synthesize the heaviest elements, and the choice of new reactions, in particular, hot fusion reactions with massive nuclei, need a separate investigation. The low yield (in all earlier attempts only upper limits of cross sections were obtained [48–54]) and the rather limited information on the reaction mechanism in the new, yet unknown region of heaviest nuclei made it necessary to carry out a series of additional experiments. The setting up of experiments aimed at the fusion of nuclei with different mass ratios in the entrance channel is presented in this review. Comparative analysis of the experimental data obtained in cold and hot fusion reactions is discussed in the section 'Reactions of synthesis'. We shall come back to this issue in the section 'Discussions', after the cross sections of the production of evaporation residues in fusion reactions of ^{48}Ca with actinide nuclei have been shown.

From the calculated partial half-lives T_α, $T_{\mathrm{EC},\,\beta}$ and T_{SF}, as shown in figure 3, we may get an impression of the scenarios and the decay properties of the heaviest nuclei depending on Z and N. It is seen that in the new regions, due to the considerable increase of nuclear stability relative to spontaneous fission, the nuclei will undergo α-decay. The consecutive α-decays will follow until the shell effect weakens and spontaneous fission becomes the main decay mode. In the region of $N < 162$ this is observed for even–even isotopes [47]. In the case of odd nuclei, due to the large hindrances to spontaneous-fission α-decay may occur down to long-living nuclei without competition from spontaneous fission. In fact, this is also observed in the experiments. For the heavier neutron-rich nuclei, the decay sequences of both even and

odd isotopes will end by spontaneous fission. The total decay time will be then determined to a great extent by the neutron number of the parent nucleus. When approaching the $N = 184$ shell, we may expect a strong increase in the decay time.

The experimental setup for separation of the evaporation residues from a huge amount of by-products, the characteristics and operation mode of the cyclotron–separator–detector array, the analysis of the background sources and random coincidence probabilities in the sequential decays of the evaporation residues are presented in the section 'Setting of experiments'.

The characteristics in the observed decay sequences are presented in the section 'Experimental results'. In this section, the issues connected with the identification of nuclei in the new region are also considered. The transition to the neutron-rich side leads, as seen from figure 3, to nuclei with new, previously unknown, properties. The recently widely used method of identification of neutron-deficient nuclei by means of the known final product in the decay chain of parent nuclei is not applicable here. In this section, we present the experimental results and perform the analysis (including those from chemical experiments) of the data so as to determine the atomic and mass numbers of the synthesized nuclei.

The comparative analysis of the decay properties of the new nuclides with the energy and half-lives of α-decay and spontaneous fission, obtained in a wide region of nuclei, as well as their consistency with the theoretical predictions, are given in the section 'Discussions'.

Finally, starting from the performed experiments and the acquired data we briefly discuss the perspectives of further investigations in the field of synthesis and studies of the nuclear structure, spontaneous fission and chemical properties of the heaviest nuclei. In the same brief manner we discuss the search for superheavy elements in nature, an issue to which many investigations have been lately dedicated (see the review article [55] and references therein).

2. Reactions of synthesis of superheavy nuclei

It is known that elements heavier than plutonium were synthesized mostly in (n, γ) reactions by successive capture of neutrons in long expositions at high-flux nuclear reactors. The high capture cross sections for thermal and resonance neutrons, followed by consecutive β^--decays, made it possible to synthesize new elements with atomic numbers up to 100 [56]. The mass limit was set by the isotope ^{257}Fm. The chain of sequential neutron capture was blocked by the short-lived isotope ^{258}Fm ($T_{SF} \approx 0.3$ ms) [57]. The following attempts to overcome this constraint by means of the much higher pulsed neutron flux in nuclear explosions were also limited by the observation of ^{257}Fm. Perhaps, this is a matter of history, but the first attempts to penetrate the region of superheavy elements were undertaken with neutron capture reactions [58].

The transition from neutron- to heavy-ion-induced reactions considerably complicated the problem of the synthesis of new elements, first of all from the technical point of view. The small cross sections, the short half-lives of the synthesized nuclides, the significant decrease of the luminosity of the experiments and the considerable increase of the background from by-products called for a radical change of the approaches to the synthesis of new elements. Along with this, the physical issue of the interaction of massive nuclei, leading to the formation of heavy and particularly superheavy nuclei, is far from being clear even today. Because of this, without claiming to analyse all modern views on this problem, we shall try to motivate the choice of reactions, which have been used for the synthesis of superheavy elements. We shall consider the fusion process and point briefly to some other reactions that were investigated and even used several times to synthesize heavy nuclei, but proved to be useless where the superheavy elements were concerned.

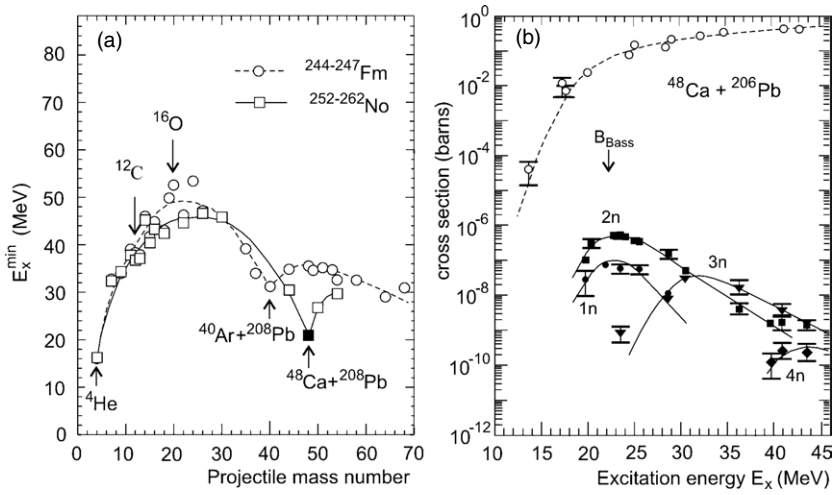

Figure 4. (a) Excitation energy at the Coulomb barrier of the compound nuclei Fm and No as a function of the projectile mass. (b) Experimental fission cross sections (open circles) in the ^{208}Pb + ^{48}Ca reaction [66–68] and cross sections of the xn-evaporation channels in the ^{206}Pb + ^{48}Ca reaction (black symbols) [62], obtained at different compound nucleus excitation energies. The dashed and solid lines are results of calculations [69] (see also calculations in [70]).

In the standard fusion theory, tested in many experiments with light projectiles (from ^{4}He to ^{26}Mg), the evaporation-residue cross section, $\sigma_{\rm EVR}(E_x) = \Sigma\sigma_{xn}(E_x)$, is determined by the cross section for the formation of the compound nucleus with excitation energy E_x and by the probability of its survival, $P_{xn}(E_x)$, during de-excitation by emission of x-nucleons (for the heavy nuclei—mainly neutrons) and γ-rays:

$$\sigma_{xn}(E_x) = \sigma_{\rm CN}(E_x) \cdot P_{xn}(E_x).$$

It is then assumed that for all collisions with $\ell \leqslant \ell_{\rm crit}$, fusion (amalgamation of the interacting nuclei) takes place automatically in a very short time after overcoming the Coulomb barrier. Indeed, if the nuclear attractive force were stronger than the Coulomb repulsion, this simple fusion pattern would be quite defensible. The reason is that at contact, the size of the contact area (sometimes called 'the neck' or 'contact window') increases faster than the other degrees of freedom. The potential energy of the formed nuclear system with summed mass is higher than the compact shape near the ground state.

The difference in mass of the initial nuclei A_P, A_T and the final nucleus $A_{\rm CN} = A_P + A_T$ defines the excitation energy of the compound nucleus E_x. The minimum value of E_x at the reaction Coulomb barrier B_C is

$$E_x^{\rm min} = B_C - Q,$$

with $Q = M_{\rm CN} - (M_P + M_T)$.

It is easy to show that $E_x^{\rm min}$ depends on the masses of the interacting nuclei: when the mass ratio A_P/A_T decreases, the excitation energy E_x increases (in turn, the Coulomb barrier rises), but further decreases with increasing Q (figure 4(a)). The first experiments revealed the advantages of cold fusion reactions compared to the asymmetric hot fusion ones for the production of heavy nuclei with $Z \geqslant 100$ [59, 60]. The advance to the nuclei with closed proton or neutron shells leads to an additional reduction of the excitation energy $E_x^{\rm min}$. It has been shown that when the two magic nuclei ^{208}Pb and ^{48}Ca fuse (figure 4(b)), the maximum cross

sections for evaporation residues are reached in the channels with small number of evaporated neutrons ($x = 1$–3) [61–64].

Since 1974 the cold fusion reactions ^{208}Pb, ^{209}Bi + massive projectile ($A_P \geqslant 50$) have been used in the synthesis of the heaviest elements. In reactions of this type, with practically the same target mass (^{208}Pb or ^{209}Bi), the increase of the atomic and mass numbers of the evaporation products is entirely connected with the increase of the mass (charge) of the projectile. When the projectile becomes more and more heavy, the excitation energy of the compound nuclei decreases (down to $E_x \approx 15$–10 MeV) and the transition to the ground state takes place by the emission of only one neutron and γ-rays [65]. As a result, the survivability of the compound nucleus $P_{xn}(E_x)$ significantly increases, this being the main advantage of the cold fusion reactions.

Another peculiarity of this type of reactions is that fusion of the stable nuclei ^{208}Pb or ^{209}Bi with stable isotopes from ^{54}Cr to ^{70}Zn as projectiles leads to the formation of compound nuclei with small neutron excess: $\Delta N_{\rm CN} = N_{CN} - Z_{\rm CN} = 50$–54. The evaporation residues are some 10–15 mass units shifted from the β-stability line. This, in turn, leads to a considerable decrease in their half-lives.

Both factors lying at the basis of the cold-fusion reaction method, namely the production of intense beams of ions with $A_P \geqslant 50$ and the necessity to use fast techniques for separation and detection of the new nuclei, considerably changed the setting up of experiments aimed at the synthesis of new elements. A successful way to solve the problem was found in 1975 at GSI (Darmstadt) with the heavy-ion accelerator UNILAC and the separator SHIP, which was capable of separating in-flight, for about 10 μs, the atoms of the new elements among the huge background caused by reaction by-products. Finally, in cold fusion reactions the six heaviest elements with $Z = 107$–112 were synthesized for the first time. A detailed description of the experiments and the analysis of the obtained data can be found in the original publications and reviews [65, 71, 72], which have been written during the last 20 years of studying the heaviest elements. At present, at RIKEN (Tokyo) experiments on the synthesis of element 113 in the ^{209}Bi + ^{70}Zn reaction are being performed and first results have been obtained on the decay properties of the isotope ^{278}113 [73].

Going back to the question of the fusion of massive nuclei, let us look at the cross sections of the evaporation products, measured in cold fusion reactions. As can be seen from figure 5, the cross section $\sigma_{1n}(Z_{\rm CN})$—of the main channel of the synthesis reaction—exponentially decreases with the increase of $Z_{\rm CN}$. When $Z_{\rm CN}$ changes from 102 to 113 the cross section decreases almost by a factor of 10^7. The further advance into the region of $Z > 113$ seems to be problematic, because the experiments on the production of element 113 are carried out today at the limit of experimental sensitivity. The observed strong decrease in the cross section with the increase of $Z_{\rm CN}$ in cold fusion is evidence that strong obstacles arise on the way of formation of the cold compound nucleus itself.

Obviously, the mechanism of fusion of massive nuclei, such as ^{208}Pb and ^{70}Zn, significantly differs from the above-considered simple scenario of formation of compound nuclei using light projectiles just by a substantial (more than twice) increase of the Coulomb repulsion between the interacting nuclei. The exchange of nucleons at the contact point and the following formation of a composite system of summed mass are far from guaranteeing its evolution to a more compact shape near the ground state. This transition is the result of a complex collective motion of the system in conditions of strong Coulomb repulsion. As an illustration, the calculated potential energy surface of the ^{278}112 nucleus is presented in figure 6(a) at fixed deformations of the fragments; the trajectory from the touching point of the two nuclei ^{208}Pb and ^{70}Zn to the compact shape of the compound nucleus is indicated. It can be seen that the motion in the direction of decreasing deformation is connected with the increase of

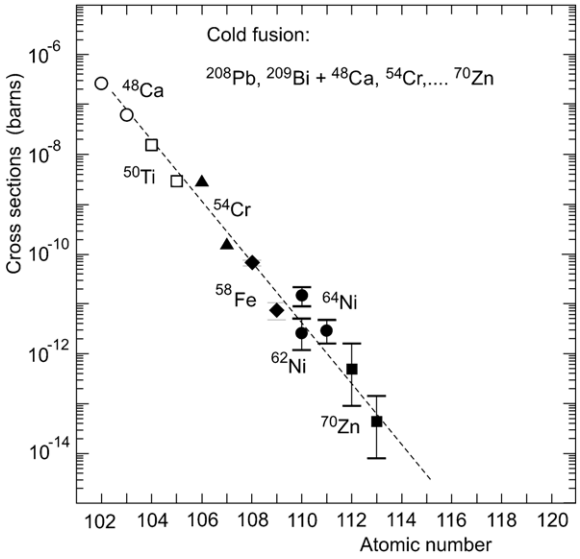

Figure 5. Maximal cross sections of the 1*n*-evaporation channel in the cold fusion reactions of ^{208}Pb and ^{209}Bi target nuclei with different projectiles (indicated in the figure) as a function of the compound nucleus atomic number [65, 73]. The dashed line is drawn to guide the eye.

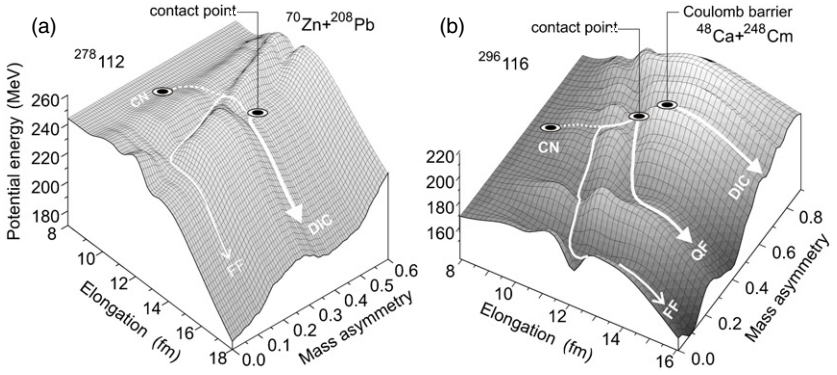

Figure 6. An illustration of the possible trajectories of collective motion of the nucleus on the potential energy surface [74] as a function of the deformation corresponding to the nuclear shape evolving from the touching point to the compact configuration of the compound nucleus. For convenient visualization, the calculated nuclear potential energy is shown at fixed deformations of the fragments. (a) ^{278}112—in the cold fusion reaction ^{208}Pb + ^{70}Zn, (b) ^{296}116—in the reaction ^{248}Cm + ^{48}Ca.

the potential energy of the system. The heavy nuclear system with large deformation hardly can overcome this potential barrier solely by shape fluctuation ($P_{\rm dyn} \ll 1$). The amplitude of the fluctuation, in turn, depends on the dynamical properties of the nuclear system and its temperature. The rise of the temperature is disastrous, because cold fusion stops being 'cold' and loses its basic advantage—the high survivability of the compound nucleus.

Now, the process of formation of the evaporation residues takes place via three stages: capture, motion along the collective trajectory, survival [74–76]; the resulting cross section is

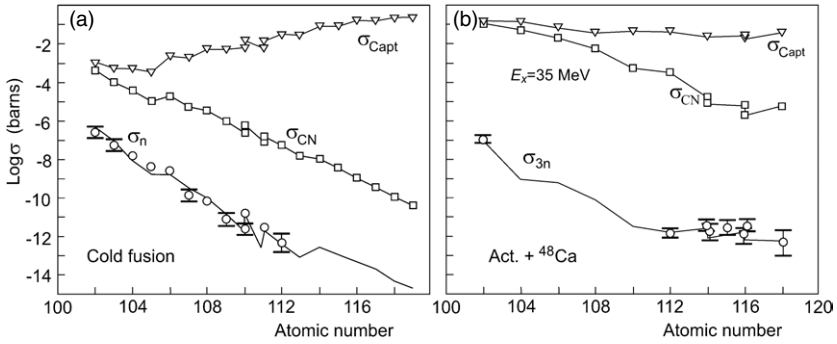

Figure 7. (a) Calculated cross sections for sticking (formation of a mono-nucleus) are denoted by triangles, compound nucleus by squares and evaporation residues at energies corresponding to the maximum cross sections of the $1n$-evaporation channel (experimental points) by circles [65]. The solid lines are drawn through the calculated values. The data are taken from [75]. (b) The same presentation as (a), but for the Act. + ^{48}Ca reactions at fixed excitation energy of the compound nucleus $E_x = 35$ MeV, based on calculations from [74] and on the experimental cross sections presented in the figures 17, 19–21 and 23.

defined by the product:

$$\sigma_{\mathrm{EVR}} = \sigma_{\mathrm{capt}} \cdot P_{\mathrm{dyn}} \cdot P_{\mathrm{sur}}.$$

Transport models, describing the stage of collective motion in different assumptions about the dynamical properties of the nuclear system, indicate a strong decrease of P_{dyn} with the increase of the proton number. The results of calculations for σ_{CN}, obtained in [75] for the reactions ^{208}Pb, ^{209}Bi + ^{48}Ca, ^{50}Ti, . . . ,^{70}Zn at E_x, corresponding to the maximum cross section σ_n, are shown in figure 7(a).

The last stage—the survivability of the compound nucleus in the mentioned reactions—is defined by the probability for its de-excitation by emission of a neutron and γ-rays in competition with fission. The probability $P_{\mathrm{sur}} \approx [\Gamma_n/(\Gamma_n + \Gamma_f)] \cdot P_\gamma$ was also calculated in [74–77] for a given neutron binding energy B_n and fission barrier height B_f, taking into account shell and pairing effects on the level densities of the excited nucleus. Although the theoretical models describe rather qualitatively and less quantitatively the process of cold fusion, they give a physical picture of the collective motion of heavy nuclear systems and the dynamical hindrances arising on the path of formation of extremely heavy nuclei. From this point of view, we can estimate and finally find the way to synthesize heavier (superheavy) nuclei, situated near the closed spherical shells $N = 184$ and $Z = 114$ (or 120, 122).

Unfortunately, the forecasts for cold fusion reactions are not optimistic because of two reasons: the increase of the projectile mass ($A_P > 70$) will lead to further considerable decrease of the cross section (see figure 7(a)), and the evaporation products have small neutron excess. Indeed, the cross section of the reaction ^{208}Pb(^{76}Ge, n)^{283}114 for the synthesis of element 114 will amount, by extrapolations, to $\sigma_n \leqslant 0.05$ pb; the isotope ^{283}114 will have 169 neutrons, while the rise in nuclear stability, according to theoretical predictions (see above), is expected at $N > 170$–172. Obviously, for the synthesis of nuclei with $Z \geqslant 114$, it is necessary to look for other approaches.

In order to decrease the factors hindering fusion, it is desirable to make use of more asymmetric reactions and to obtain an increase in the neutron number of the evaporation residues by using both target and projectile nuclei with maximum neutron excess. However, the choice of reactions meeting these conditions is rather poor. As target material, it is

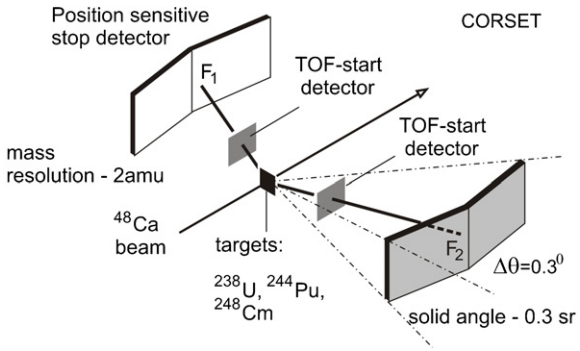

Figure 8. Layout of the CORSET setup for measuring masses and energies of fission fragments [80].

reasonable to use neutron-rich isotopes of the actinides (Act.), such as ^{244}Pu, ^{248}Cm and ^{249}Cf, produced in high-flux reactors and thus having largest neutron excess. Among the projectiles, undoubted advantage has the doubly magic nucleus of the rare isotope ^{48}Ca (only 0.14% in the natural isotopic abundance of Ca) [48, 78, 79]. The compound nucleus ^{292}114, produced, for example, in the fusion of ^{244}Pu and ^{48}Ca, acquires eight additional neutrons compared to the mentioned case of the ^{208}Pb + ^{76}Ge reaction. These eight neutrons, as will be shown below, play a key role in the production and study of the decay properties of superheavy nuclei.

Compared to the cold fusion reaction ^{208}Pb + ^{76}Ge ($Z_P \cdot Z_T = 2624$), the Coulomb repulsion in the reaction ^{244}Pu + ^{48}Ca ($Z_P \cdot Z_T = 1880$) decreases by almost 40%, which in turn should lead to the decrease of the factors hindering the formation of the compound nucleus. On the other hand, due to the magic structure of ^{48}Ca, the excitation energy $E_x^{\min}$ of the compound nucleus ^{292}114 amounts to approximately 30 MeV, a value by 10–15 MeV lower than in typical hot fusion reactions induced by lighter projectiles.

However, unlike the cold fusion reactions, the asymmetric reactions Act. + ^{48}Ca have not been investigated so far. A few experiments devoted to the synthesis of nuclei in reactions such as ^{238}U, ^{242}Pu, ^{243}Am and even ^{248}Cm + ^{48}Ca, undertaken in 1967–1985 in different laboratories and using on-line physical and off-line chemical techniques, as was already mentioned above, have given only upper limits for the production cross sections of new elements. Therefore, 15 years later, when addressing this issue again, it was necessary to understand more about the mechanism of these reactions and of the opportunities they would provide for the synthesis of new elements. For this purpose, we carried out a series of experimental investigations, the main point of which was the following.

The compound nucleus, if formed in a fusion reaction, will prevailingly undergo fission from its initial (excited) state. The fission fragments of a compound nucleus have the characteristic mass and energy distributions, which distinguish them from fragments, formed in other exit channels: quasi-elastic scattering, deep-inelastic collisions, etc. The task is to separate the channel pertaining to the compound nucleus fission.

The time-of-flight spectrometer CORSET [80], used in these experiments, is presented schematically in figure 8. It is capable of registering the angles, masses and energies of correlated fragments in a large solid angle ∼0.3 sr.

The total kinetic energies (TKE) of two correlated fragments, produced in the ^{208}Pb + ^{48}Ca reaction corresponding to full momentum transfer from the ^{48}Ca ions to the composite system ^{256}102 at $E_x = 18$ MeV, are shown in figure 9(a) as a function of the fragment mass (A_F). The

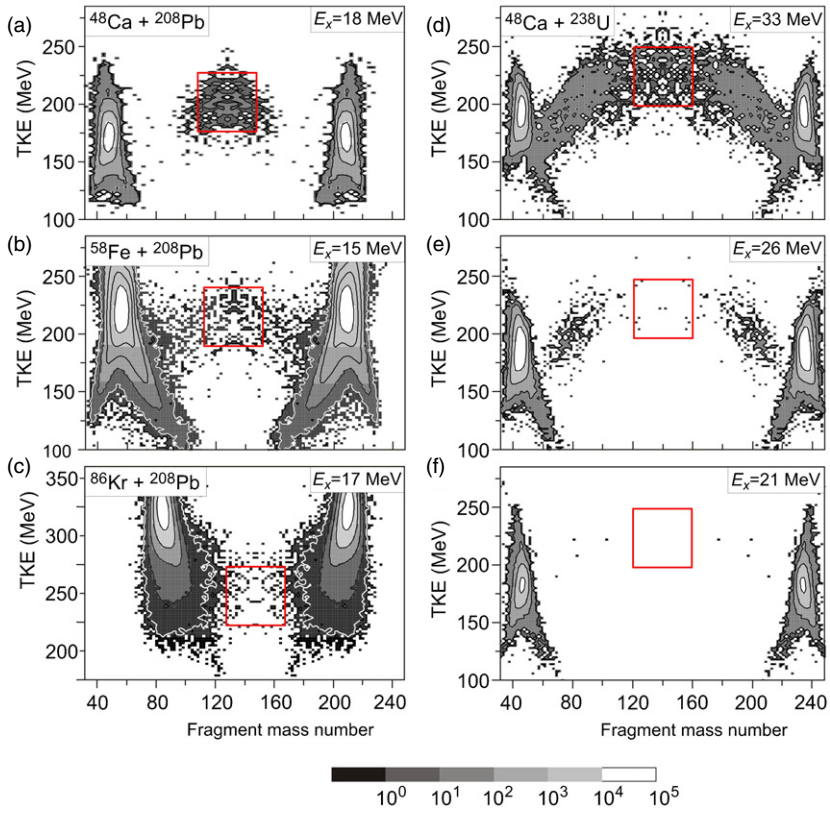

Figure 9. Two-dimensional spectra of TKE(A_F) of correlated fragments from cold fusion reactions (indicated in the graphs (a) [81], (b) [82] and (c) [83]). The excitation energies of the nuclei ^{256}102, ^{266}108 and ^{294}118 are shown in the graphs. The red line encircles the region of fragment mass $A_{CN}/2 \pm 20$ amu with summed kinetic energy $\langle$TKE$\rangle \pm 50$ MeV. The spectra, measured in the ^{238}U + ^{48}Ca reaction at different excitation energies of the ^{286}112 nucleus, are given in the graphs (d), (e) and (f) [84].

observed fragments with mass around $A_P = 48$ (projectile-like) and $A_T = 208$ (target-like) are products of multi-nucleon transfer in quasi-elastic (QE) and deep-inelastic (DIC) collisions. The region of mass and energy $A_F = A_{CN}/2 \pm 20$ and TKE $= 200 \pm 50$ MeV, according to known data, covers about 60% of the fission fragments of ^{256}No [81]. From the measurements at various energies, the fusion–fission cross section $\sigma_{FF}(E_x)$ was determined, which, in first approximation, for the reaction ^{208}Pb + ^{48}Ca can be taken as $\sigma_{CN}(E_x)$. Simultaneously, in the $^{206–208}$Pb + ^{48}Ca reaction, in the experiments [62, 63] the cross sections of evaporation residues $\sigma_{xn}(E_x)$ were measured in the energy interval $E_x \approx 15$–42 MeV for the xn-evaporation channels, when $x = 1$–4. Thus, from the experiments with the ^{206,208}Pb + ^{48}Ca reaction, the complete pattern of fusion and survival of the compound No nuclei at different excitation energies could be drawn (figure 4(b)). Similar measurements were also performed for element 104 (Rf) in the ^{208}Pb + ^{50}Ti reaction [85].

In the experiments that followed, either the projectile mass was increased keeping ^{208}Pb as a target (cold fusion) or the target mass was increased and the projectile used was ^{48}Ca (hot fusion). The two-dimensional plot TKE versus A_F, measured in the ^{208}Pb + ^{58}Fe reaction, is

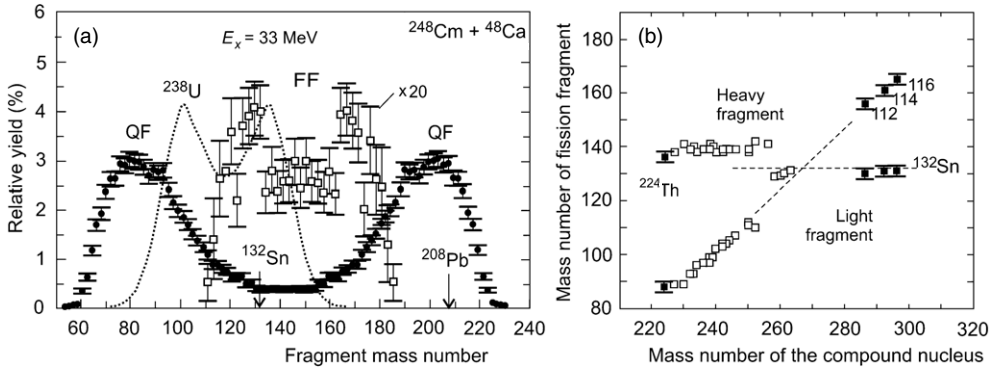

Figure 10. (a) Mass distributions of quasi-fission fragments (black points) and fission in the symmetric mass region (open squares) in the ^{248}Cm + ^{48}Ca reaction at $E_x = 33$ MeV. The dashed line is the fission-fragment mass distribution of ^{238}U at $E_x = 30$ MeV [87]. (b) The most probable mass of the primary fission fragments as a function of the mass of the fissioning nucleus. The open squares denote low-energy fission of actinides, the black squares denote fission of the excited nuclei with $Z = 112$, 114, 116 in the reactions ^{238}U, ^{244}Pu, ^{248}Cm + ^{48}Ca. Data for ^{224}Th in the reaction ^{208}Pb + ^{16}O at $E_x \approx 26$ MeV, obtained with the CORSET setup, are also shown in the figure [89].

shown in figure 9(b). It is seen that when the projectile mass is increased from ^{48}Ca to ^{58}Fe, the picture changes drastically. The yields of the projectile-like and target-like products have increased significantly, whereas the yield of fragments corresponding to the region expected for the fission of the compound nucleus ^{266}Hs has decreased by more than two orders of magnitude [86]. Indeed, as it has been shown by different model calculations (as was mentioned before), here dynamical hindrances to the formation of the compound nucleus start to play an important role. Finally, in the reaction ^{208}Pb + ^{86}Kr (figure 9(c)), in the mass region $A_{CN}/2$ only few events were registered; the upper limit for the formation of the compound nucleus with $Z = 118$ was estimated to be $\sigma_{CN} \leqslant 200$ nb. Having thus obtained a consistent picture of the cold fusion reactions, the experiments at the CORSET setup were continued using the reactions Act. + ^{48}Ca [82].

The data for the ^{238}U + ^{48}Ca reaction at $E_x = 33$ MeV are presented in figure 9(d). In this reaction again a large yield of projectile-like and target-like nuclei was observed, along with events in the region where fission fragments from the compound ^{286}112 nucleus were expected. However, in contrast to the experiment with the ^{208}Pb-target, the observed fragments are typical for strongly asymmetric fission (two egg-like distributions, symmetric relative to $A_{CN}/2$) and are situated outside the place where the compound nucleus fission fragments would come. Obviously, this process (we call it 'quasi-fission') is not connected with the formation of the compound nucleus ^{286}112, but its tails create a background in the symmetric mass region $A_F \approx A_{CN}/2$. The separation of these two types of fission is possible only by means of systematic measurements at various excitation energies, since the yields of the two types of fission vary at the different excitation energies (see figures 9(d)–(f)). It should be noted that the peak of the heavy fragments of quasi-fission (QF) is located close to $A_F \approx 208$ (^{208}Pb). Similar measurements were also done for many other reactions, with targets lighter or heavier than ^{238}U [87, 88].

The fission-fragment mass distributions, obtained in one of these reactions, namely ^{248}Cm + ^{48}Ca at $E_x = 33$ MeV, are presented in figure 10(a). The difference between the two types of fission is well seen: the main channel is QF, with mass ratio of the fragments

$A_{F1}/A_{F2} \approx 2.35$, and the other one, of much less intensity (FF), with $A_{F1}/A_{F2} \approx 1.24$. In the same figure, the known fission-fragment mass distribution of ^{238}U at $E_x \approx 30$ MeV is shown; its shape is quite similar to that of the FF mass spectrum from the reaction ^{248}Cm + ^{48}Ca. The overlap of the mass of the heavy fragment from ^{238}U and the mass of the light fragment from ^{296}116 may be a sign that the fission in both cases is governed by the effect of the closed shells $Z = 50$, $N = 82$. The difference lies in that in the fission of ^{238}U the shell effect is connected with the formation of the heavy fragment, while in the case of the heavy nucleus ($A = 296$) it manifests itself in the light fragment. As can be seen from figure 10(b), the mass distributions of the fragments from the FF-channel and the data, obtained for the actinides, show that the fission mode of all nuclei with $Z = 90$ to $Z = 116$ is very much the same. The mass and energy spectra of the fission fragments are characterized by a small change in the mass of one of the fragments (the $Z = 50$, $N = 82$ shell effect) and a large variation of the mass of the complementary fragment (depending on the mass of the fissioning nucleus). Due to the same reasons, in the intermediate mass region $A = 258$–272, the mass-symmetric fission mode may prevail when the $Z = 50$, $N = 82$ shell effect works simultaneously on both fragments [90].

The results, obtained in the ^{238}U, ^{244}Pu and ^{248}Cm + ^{48}Ca experiments, can be shown in the form of collective motion of the heavy nuclear system with $A = 296$ over the potential energy surface. As illustrated in figure 6(b) for the reaction ^{248}Cm + ^{48}Ca, at the contact point of the ^{248}Cm and ^{48}Ca nuclei, the potential energy of the nascent ^{296}116 nucleus is *higher* than the energy of the compound nucleus. That is why in the reactions Act. + ^{48}Ca, contrary to cold fusion (see for comparison figure 6(a)), the hindrances to the formation of compact shapes must be considerably suppressed. This will in turn lead to an increase in the probability $P_{\rm dyn}$. At the same time, at the early stage of the reaction, the system can, with high probability, enter the deeper valley of quasi-fission. Because of this loss, only a small part of the nuclei will reach compact forms close to the top of the compound nucleus fission barrier. The ratio of the yields of QF and FF displays the competition between these two processes. As is seen from figure 6(b), the cross section $\sigma_{\rm CN}$ can be less than $\sigma_{\rm FF}$, since the nucleus may enter the compound nucleus fission valley and demonstrate at the scission point the characteristics of fission without transition over the fission barrier [91] (i.e., by-passing the stage of forming a compound nucleus, see figure 6(b)). Essentially, this is a second obstacle on the way to compound nucleus formation. The calculated cross sections $\sigma_{\rm CN}(Z)$ shown in figure 7(b) account for such a limitation in the last stage of the collective nuclear motion. We shall return to the discussion of this problem after the experimental data on the cross sections for the evaporation residues have been shown.

The last stage—the survival of the compound nucleus—is the decisive one in the given method of synthesis of the heaviest nuclei. As was mentioned earlier, the estimations of $E_x^{\rm min}$ and the following experiments, aimed to measure the excitation functions for evaporation products, have shown that the compound nuclei with $Z_{\rm CN} = 112$–118, when formed in Act. + ^{48}Ca reactions, may attain excitation energy from 30 to 55 MeV. This energy will be released by a cascade emission of 2–5 neutrons (the evaporation of charged particles is significantly less probable) and γ-rays. At each step, neutron evaporation and fission compete strongly. The survival probability can be simply expressed as

$$P_{\rm sur} \sim \prod_{i=1}^{x} (\Gamma_n/\Gamma_f)i \sim \prod_{i=1}^{x} \exp[(B_f - B_n)/T]_i,$$

where B_f and B_n are the fission barrier height and the binding energy of the neutron, respectively, T is the temperature of the compound nucleus and x is the number of emitted neutrons.

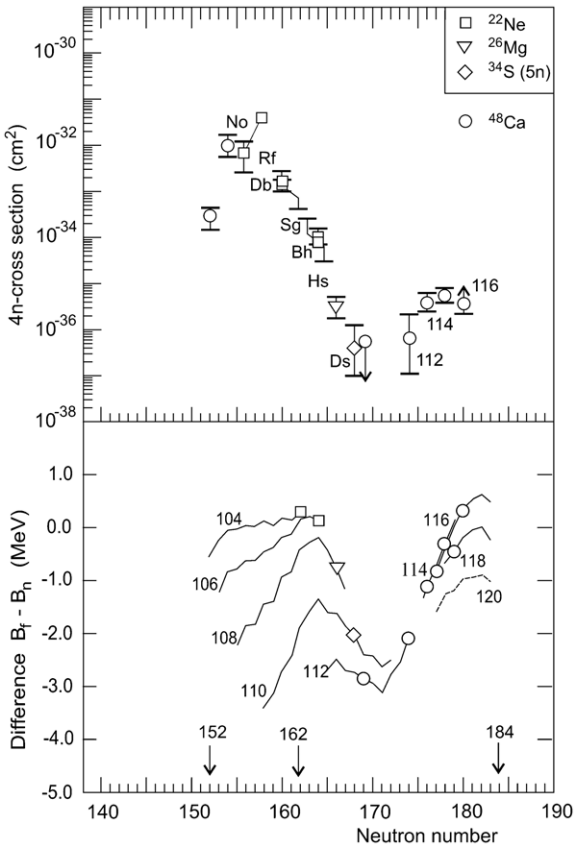

Figure 11. Upper panel: experimental cross sections at the maximum of $4n$-evaporation channels in hot fusion reactions leading to the formation of isotopes of elements 102–110 at different neutron numbers of the compound nucleus. Squares, triangle and diamond denote the reactions Act. + ^{22}Ne, ^{26}Mg and ^{34}S [94–100], open circles denote Act. + ^{48}Ca reactions. Lower panel: calculated values of $(B_n - B_f)$ for isotopes of elements 102–120 with different neutron numbers [39, 144]. The symbols denote isotopes corresponding to the compound nuclei in the above-mentioned reactions.

Unfortunately, in the region of the superheavy nuclei the calculated P_{sur} depends strongly on the choice of B_n and B_f, predicted by different models in a rather wide range (especially the fission barrier heights) [25, 39, 92, 93].

In such a situation, the analysis of the experimental data, obtained during the synthesis of the heaviest nuclei in hot fusion reactions, seems to be more informative.

The cross sections of nuclei with $Z = 102$–110, produced in the $4n$-evaporation channel of the fusion reactions Act. + ^{22}Ne, ^{26}Mg and ^{36}S($5n$), are presented in figure 11(a) [94–100] (the neutron number of the corresponding compound nuclei is shown on the horizontal axis). Since there is no significant hindrance for fusion in such mass-asymmetric reactions ($Z_P \cdot Z_T = 920$–1500), the strong decrease in the cross section σ_{4n} is connected mainly with the survivability of the nuclei. The relatively high production cross section of isotopes with $Z \leqslant 105$ is a consequence of the high fission barrier, which is almost completely determined by the shell effect of the two closed neutron shells $N = 152$ and $N = 162$. At neutron numbers $N_{\text{CN}} > 162$, as can be seen from figure 11(b), the fission probability significantly increases with the decrease of B_f. This reduces the cross section of Ds ($Z_{\text{CN}} = 110$) relative to Db

($Z_{CN} = 105$) by almost four orders of magnitude. However, if the predictions of the theoretical models (see above) about the existence of the next closed shell $N = 184$ are justified, the fission barrier height will again increase when advancing to the region where $N_{CN} \geqslant 174$ and $Z_{CN} \geqslant 112$. In turn, the nuclear survivability will increase too and as a result one can expect even a rise in the cross section σ_{EVR} for heavy nuclei with large neutron excess.

For a more detailed consideration of the feasibility of the Act. + ^{48}Ca fusion reactions for the synthesis of the heaviest nuclei, it is necessary to have experimental measurements of σ_{xn} (or at least their limits). We shall return to this question with the measured cross sections σ_{xn}(exp) in the general discussion of the experimental results.

In other reactions, the opportunities to synthesize superheavy elements are strongly reduced. Deep-inelastic transfer of massive clusters, even in reactions with extremely heavy nuclei such as ^{238}U + ^{136}Xe, ^{238}U + ^{238}U or ^{248}Cm + ^{238}U, as has been shown in some experiments [101–103], leads to very small cross sections. In mass-asymmetric reactions the necessity to use targets heavier than ^{248}Cm is limited by the chance to produce isotopes with $Z \leqslant 103$ in reactions with ^{254}Es-targets [104].

Hence, reactions such as Act. + ^{48}Ca turn out to be, from our point of view, the most promising ones for the synthesis of the heaviest nuclei with large neutron excess. In spite of the fact that quasi-fission strongly competes with the formation of a compound nucleus, the expected cross section σ_{CN} is essentially higher than in cold fusion reactions. The main losses take place in the stage of survival of the excited nuclei, and this strongly depends on their fissility. At the same time, the theoretically predicted rise in the fission barrier, when approaching the closed shell $N = 184$, must manifest itself in the growth of the evaporation-residue cross sections depending on the number of neutrons (less on the proton number) in the compound nucleus.

Nevertheless, the expected (and observed) cross sections of the new nuclides with $Z \geqslant 112$, produced via the evaporation channels of the Act. + ^{48}Ca reactions, are of the order of picobarns ($\equiv 10^{-36}$ cm^2) and in some cases even lower, which in turn imposes strong requirements for high luminosity and high sensitivity in launching new experiments aimed at the production of the heaviest nuclei.

3. Setting the experiments

The expected half-lives of the heavy nuclei from Act. + ^{48}Ca reactions, as it can be seen in figure 3, can vary in a wide range: from a few μs (for the even–even isotopes of the heavy elements) up to tens of hours (for the products of sequential decay of the odd nuclei). Because of this, the separation and registration of the looked-for nuclei must possess wide-range operating speed. The expected cross sections for the evaporation residues produced at energies above the Coulomb barrier are calculated to be of the order of picobarns (or a fraction of pb), which is a factor 10^{11}–10^{12} smaller than the total reaction cross section. The recoiling nuclei from fusion reactions, formed with full momentum transfer from the projectile to the compound nucleus, leave the target layer in the direction of the beam. Therefore, the separation system must be capable of 'relieving' the detector from the beam particles and from other by-products.

There are technical difficulties too. For the acceptable ion-optical characteristics of the recoil separator, the ^{48}Ca beam with intensity of about 1.0–1.5 pμA (beam power $\sim$0.3 kW) should give a spot at the target position of $\sim$0.3–0.5 cm^2. At this, the target must withstand a huge beam dose ($\sim 10^{19}$ particles and even more) during a long-term irradiation. These conditions demand the fulfilment of certain requirements with respect to the technology and construction of the target from unique highly enriched isotopes of Pu, Am, Cm and Cf (which

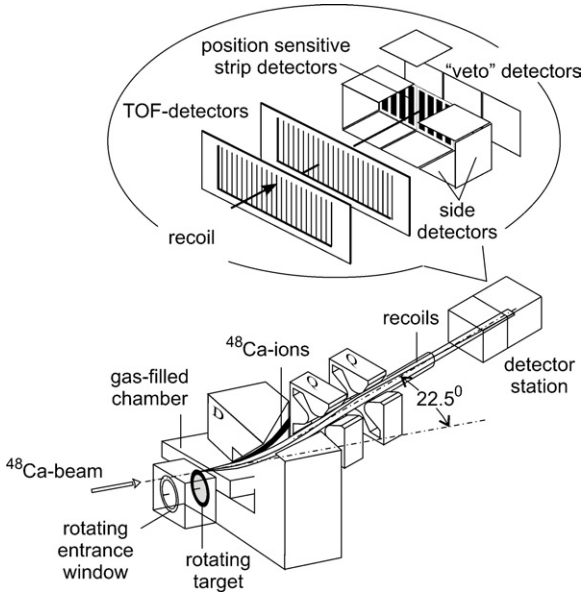

Figure 12. Layout of DGFRS (the Dubna gas-filled recoil separator). D is the dipole magnet and Q is the quadrupole doublet.

are a great deficit), and to the systems of continuous control of the working radioactive target layer during the whole experiment.

We considered different versions of setting up experiments with Act. + ^{48}Ca reactions by taking into account the great and successful experience of working with recoil separators (such as the velocity selector—SHIP [105] or the energy selector—VASSILISSA [106]), and nevertheless, chose another system—the gas-filled separator, which to our opinion better corresponds to the high demands of the experiments.

3.1. The Dubna gas-filled recoil separator (DGFRS)

The gas-filled recoil separator (DGFRS) is schematically presented in figure 12. The principle of operation of such experimental setups is well known [107–116].

Due to the interaction of the projectiles with the target nuclei the reaction products, which are emitted in the direction of the beam, come into the region of an external magnetic field that separates them by their magnetic rigidity. If the magnetic dipole field region is filled with a dilute-gas medium, the moving ions change their initial ionic charge due to collisions with the atoms of the gas. Coming into the gas, an initially homogeneous ion beam splits up into several components, corresponding to the different charge states. After a statistically large number of collisions with the atoms of the medium, the charge distribution approaches equilibrium and the ions follow some mean trajectory determined by the mean charge value ($\overline{q}$). The shape of the equilibrium charge distribution is described by a Gaussian centred at the average charge $\overline{q}$, as expressed approximately by the Bohr formula [117]: $\overline{q} \approx (v/v_0) \cdot Z^{1/3}$, where Z is the ion atomic number and $v_0 = 2.19 \times 10^6$ m s^{-1} is the Bohr velocity. Since $B\rho = mv/q$, the magnetic rigidity of an ion is defined by the simple relation: $B\rho = 0.02267 \times A/Z^{1/3}$ (Tm).

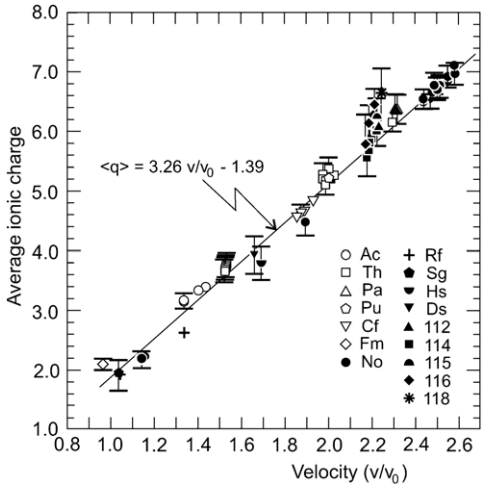

Figure 13. Average ionic charge of heavy nuclei moving in hydrogen medium with different velocities (in Bohr's units of velocity $v_0 = 2.19 \times 10^8$ cm s^{-1}), measured at DGFRS. The line is the calculation of $\overline{q}(v/v_0)$ with the ANAMARI computer code [113].

Thus, in first approximation, the curvature radius of the ion in a magnetic field is determined mainly by the mass, to a lesser degree by the atomic number, and becomes charge and velocity independent. Ions of different mass will be deflected from the central ray trajectory, moving through different curvature radii that are, to first order, proportional to the $A^{2/3}$ value. The evaporation residues (EVRs) of fusion reactions have the largest possible mass, with corresponding trajectories of highest radius of curvature. Accordingly, the other reaction products—target-like or projectile-like ions—will be separated from the EVRs following the trajectories with lower curvature radii. To illustrate, the DGFRS has a dispersion of 7.5 mm per 1% of $B\rho$, while the ratios of rigidities of the EVRs, scattered target-like and primary beam ions, for systems such as ^{48}Ca + ^{244}Pu and ^{22}Ne + ^{244}Pu, are 1.0/0.89/0.29 and 1.0/0.95/0.18, respectively [113]. The width of the trajectory with a given v/q ratio and thus the mass resolution of the gas-filled separator depend on the optical dispersion of the system and on the width of the spatial distribution of the EVRs, which is due to interactions with the target material and the separator gas.

The accurate setting of the spectrometer magnetic rigidity requires precise knowledge of the relevant v/q ratio. The dependence of the average charge states on the velocities of actinide and trans-actinide nuclei in dilute hydrogen was determined at the DGFRS by measurement of the magnetic rigidities of EVRs synthesized and identified in various reactions (figure 13) [118]. An interpolation or extrapolation of these data allows determination of the v/q ratios and, consequently, of the magnetic rigidity settings of the DGFRS for the superheavy nuclei that are synthesized in fusion–evaporation reactions induced by ^{48}Ca-projectiles (they are also shown in figure 13). A specific characteristic of the DGFRS is the hydrogen gas used in the separator, which enables better suppression of projectile- and target-like recoils at the focal plane than the helium gas [119]. The suppression factors exceed 10^{15} and 10^4 for beam and target-like particles, respectively [112], depending on the projectile–target combinations. Just after the exit of the dipole, there is a quadrupole doublet, with a 20 cm aperture, which focuses the recoil nuclei onto the separator focal plane located 4 m downstream. The superheavy nuclei, leaving the target with energy of 30–40 MeV, fly over this distance for $\sim$1 μs.

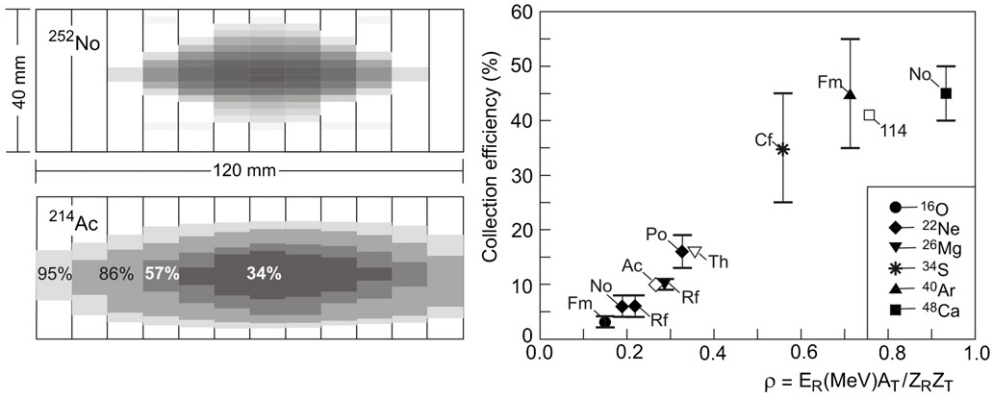

Figure 14. Left panel: the distribution in the focal plane of DGFRS of the ^{252}No recoils, exiting the target with an energy ≈41.2 MeV and of ^{214}Ac with an energy ≈10.5 MeV, produced in the ^{206}Pb(^{48}Ca, 2n) and ^{197}Au(^{22}Ne, 5n) reactions, respectively. The images are projected onto an area of 120 × 40 mm^2 of the front strip detector. Right side: collection efficiency (the transmission of evaporation residues) of the DGFRS, obtained in reactions with a different ion/target mass ratio (the projectiles are shown by different symbols). Black symbols denote experimental results, open symbols denote calculations with the ANAMARI computer code [113], ρ is a scaling parameter.

The image size at the focal plane, which defines the sensitive area of the detector, is the result of the interplay of the ion-optical effects and charge-exchanging and multiple scattering interactions in the target and separator media that determine the velocity, angle and charge dispersions of the ions. The velocity dispersion is negligible in first approximation. Multiple scattering and charge-exchange effects, as well as focusing, are increased with pressure. It has been shown that the vertical width of the EVR spatial distribution depends only on the optical effects and multiple scattering in the gas (that is pressure dependent), while the horizontal distribution is proportional to the squares of the effective charge-exchange cross section and gas pressure [110]. Consequently, the widths of the distributions are optimized by appropriate choice of the gas pressure. For the ^{48}Ca-induced fusion reactions, which we have investigated, the pressure in the separator was about 1 Torr.

The transmission of the evaporation residues and their distribution on the focal plane were determined experimentally in asymmetric fusion reactions with different projectile/target mass ratios. The results are shown in figure 14. With the obtained data and the dependence of the average charge states on the velocities of recoils shown in figure 13, using Monte Carlo techniques the ANAMARI computer code was developed and used for the calculation of the EVRs trajectories in the separator [113]. ANAMARI accounts for reaction kinematics, energy losses and multiple scattering in target and separator media, equilibrium charge states of the EVRs and the magnetic optical system of the separator. The code successfully reproduces the distributions of the EVRs on the focal plane detector array and their collection efficiencies for the numerous reactions studied. By performing fast calculations of the position spectra and collection efficiencies, it allows the optimal separator system settings to be determined.

An example of the tuning of DGFRS for the separation of No isotopes, formed in the ^{206}Pb(^{48}Ca, xn)$^{254-x}$ No reaction, can be given.

The maximum yield of the 2n-evaporation channel of the reaction ^{206}Pb + ^{48}Ca, used for calibration of the detectors, was measured at the projectile energy of 217 MeV in the middle of the target layer [62]. The evaporation residues ^{252}No were produced with an average kinetic

energy of 40.8 MeV; because of energy losses in the target layer and the hydrogen gas (at a pressure of 1 Torr), the average EVR energy is reduced to 38 MeV in the centre of the dipole magnet. The measured equilibrium ion charge in hydrogen of 38 MeV EVRs is 6.6^{+}, which corresponds to a magnetic rigidity ($B\rho$) of 2.14 Tm for the central trajectory in the DGFRS. With a dispersion of 7.5 mm/%$B\rho$, an acceptance interval ($\Delta B\rho$) of $\pm$0.17 Tm ($\pm$8%) is defined by the horizontal 120 mm size of the focal-plane detector. Therefore, the magnetic rigidity interval $B\rho = 2.14 \pm 0.17$ Tm is optimal for the transmission of ^{252}No EVRs; other reaction products with rigidities outside this interval should miss the focal-plane detectors. The variation of projectile energy within 30 MeV ($E_{\mathrm{lab}} \approx$ 213–243 MeV) resulted in variation of the initial EVR kinetic energy within an interval of 40.0–45.5 MeV ($\approx$37–42 MeV in the centre of the dipole magnet) and corresponding change of the average ^{252}No ion charge $q \approx 6.5$–7.0. However, due to the linear dependence of the average charge of the ion on its velocity v, the rigidity of EVRs with mass m, $B\rho = mv/q$, remains practically the same ($\Delta B\rho = 0.03$). Thus, collection efficiencies of the separator for nuclides, produced in the reaction in a wide projectile energy range, as well as for its neighbouring isotopes, are very similar. This makes it possible to perform measurements of EVRs production cross sections as a function of the excitation energy of the compound nucleus (excitation functions) with a constant efficiency without changing the separator settings.

Obviously, in experiments on the synthesis of superheavy elements in fusion reactions of ^{48}Ca with ^{233}U–^{249}Cf (the projectile/target mass ratio being 0.206–0.192), the distribution of the evaporation residues on the focal plane of DGFRS is close to the one observed for the ^{252}No nuclei (shown on the left-hand side of figure 14). For this reason, the chosen size of the focal-plane detector (120 $\times$ 40 mm^2) allows registration of separated superheavy nuclei with efficiency close to 100%.

The calculated transmission efficiency of the separator for $Z = 112$–118 nuclei is about 35–40% [113], whereas full-energy ^{48}Ca-projectiles, projectile-like ions, and target-like nuclei are suppressed by factors $\sim 10^{17}$, 6×10^{14} and 10^4–10^6, respectively.

3.2. The ^{48}Ca beam

The $^{48}Ca^{+5}$ ions, produced by the ECR (14 GHz) ion source, were accelerated by the U400 cyclotron to an energy of up to 5.65 A MeV. The measurement and the continuous control of the beam energy were done in two ways: by Si(Au)-detectors measuring the energy spectrum of the ^{48}Ca-projectiles scattered at an angle of $\theta_{\mathrm{Lab}} = 30^{\circ}$ and by TOF-detectors directly measuring the energy of the primary beam. In turn, the calibration of both the Si(Au)- and TOF-detectors was performed by measuring the beam energy by the high-resolution magnetic spectrometer MSP-144 [120]. The energy dispersion of the ^{48}Ca beam in the middle of the target, determined by the energy resolution of the beam coming from the cyclotron, the weak variation of energy over the long irradiation, the energy loss in the entrance window (0.72 mg cm^{-2} Ti) and in the target backing (0.72 mg cm^{-2} Ti), as well as by the thickness of the target layer ($\sim$0.35 mg cm^{-2}), amounted to about 4.5 MeV.

The typical beam intensity at the target was 0.5–0.7 pμA (in the years 2000–2001), consequently (2004–2005) it increased to 1.2 pμA. The consumption of the ^{48}Ca isotope, enriched to 68%, amounted to about 0.5 mg h^{-1}.

3.3. The targets

The thickness of the target was chosen by a compromise between the luminosity and the transmission of the evaporation residues through the separator. The yield of ^{252}No in the

Table 1. Experimental conditions and number of registered decay events from evaporation residues in Act. + ^{48}Ca reactions.

Reaction	Target thickness (mg cm^{-2})	Isotope enrichment (%)	E_{LAB} (MeV)	E_x (MeV)	Beam dose ($\times 10^{19}$)	Number of events				Reference
						2n	3n	4n	5n	
^{233}U + ^{48}Ca	0.44	99.97	240	32.7–37.1	0.7	–	–	–	–	[121]
^{238}U + ^{48}Ca	0.35	99.3	230	29.3–33.5	0.58	–	1	–	–	[121]
	0.35		234	32.9–37.2	0.71	–	6	–	–	[121]
	0.35		240	37.7–41.9	0.52	–	–	1	–	[121]
^{237}Np + ^{48}Ca	0.35	99.3	244	36.9–41.2	1.10	–	2	–	–	See the text
^{242}Pu + ^{48}Ca	0.40	99.98	235	30.4–34.7	0.50	1	5	–	–	[121]
	0.40		238	33.1–37.4	0.49	–	5	–	–	[121]
	0.40		244	38.0–42.4	0.47	–	5	7	–	[121]
	0.40		250	43.0–47.2	0.32	–	–	2	–	[121]
Chemistry	1.4	99.98	235		0.16	–	2	–	–	See the text
^{244}Pu + ^{48}Ca	0.38	98.6	231	29.8–32.9	0.46	–	–	–	–	[122, 123]
			236	32.9–37.4	1.50	–	2	–	–	[122, 123]
			243	38.9–43.0	0.40	–	2	7	–	[123]
			250	44.9–49.0	0.31	–	1	4	–	[123]
			257	50.4–54.7	0.29	–	–	1	1	[123]
^{243}Am + ^{48}Ca	0.36	99.9	248	38.0–42.3	0.43	–	3	–	–	[124, 125]
			253	42.4–46.5	0.43	–	–	1	–	[124, 125]
Chemistry	1.2	99.9	247	35.0–43.8	0.34	–	15	–	–	[126, 127]
Chemistry	1.2	99.9	247	35.0–43.8	0.35	–	5	–	–	[128]
^{245}Cm + ^{48}Ca	0.35	98.7	243	30.9–35.0	1.20	2	3	–	–	[123]
			249	35.9–39.9	0.54	1	5	–	–	[127]
			255	40.7–44.8	0.83	–	4	–	–	[127]
^{248}Cm + ^{48}Ca	0.35	97.4	240	31.2–34.9	2.30	–	3	–	–	[129]
			247	36.8–41.1	0.70	–	2	6	–	[121]
^{249}Cf + ^{48}Ca	0.23	97.3	245	26.6–31.7	2.50	–	1	–	–	[130]
	0.34	>98	251	32.1–36.6	1.60	–	2	–	–	[131]

^{206}Pb + ^{48}Ca reaction revealed that the effective layer thickness of the metallic ^{206}Pb-target is limited to ∼0.5 mg cm^{-2}. Because of this, in the experiments on the synthesis of superheavy nuclei, targets of actinide oxides were used with thickness of ≈0.35 mg cm^{-2} (by working material) deposited on a 1.5 μm Ti foil and covered by a protective carbon layer ∼35 μg cm^{-2} thick. Enriched isotopes of U, Np, Pu, Am, Cm and Cf were used as target material (see table 1). Each of the six targets had an area of 5.3 cm^2 in the shape of an arc segment with an angular extension of 60° and an average radius of 60 mm. The segments were mounted on a disc that was rotated at 2000 rpm perpendicular to the beam direction. The total area of the target was 32 cm^2, the total weight of the isotopes was about 10 mg. The ion beam falling on the target was scanned in the vertical direction with a frequency of 1 kHz in the range of a limiting diaphragm of a 9 mm diameter. The tests with intense beams of ^{22}Ne and ^{34}S showed that targets with this construction could accept a maximal ^{48}Ca-beam intensity of up to

5–6 pμA and could be repeatedly used in long-term irradiations with a dose of up to $\sim 5 \times 10^{19}$ beam particles and possibly even more.

3.4. The detector array

EVRs passing through the separator were implanted in a 4×12 cm^2 semiconductor detector with 12 vertical position-sensitive strips. The detection efficiency of the focal-plane front detector for α-particles, emitted from the decays of the implanted nuclei, is 52% of 4π. To detect escaping α's, the front detector was surrounded by eight 4×4 cm^2 side detectors (without position sensitivity), forming a box open to the front (beam) side (see figure 12). In this geometry, the position-averaged detection efficiency for full-energy α-particles of implanted nuclei increases to 87% of 4π.

Before implantation into the front detector, the separated EVRs pass through a time-of-flight (TOF) measuring system that consists of two (start and stop) multiwire proportional chambers placed within 6 cm from each other and filled with $\sim$1.5 Torr pentane. The TOF system with registration efficiency of 99.9% allows distinguishing recoil nuclei coming from the separator and passing through the TOF-detector from signals, arising from α-decay or from spontaneous fission of the implanted nuclei (without a TOF signal). In order to eliminate the background from the fast light charged particles (p, α) with signal amplitudes lower than the registration threshold of the TOF-detector, occurring in the interaction of the projectiles with the hydrogen gas, a 'veto' silicon detector was placed behind the front detector (figure 12).

The detection system was calibrated by registering the recoil nuclei and decays (α or SF) of known isotopes of No and Th and their descendants, produced in the reactions ^{206}Pb(^{48}Ca, 2n) and ^{nat}Yb(^{48}Ca, 3–5n), respectively. The typical full-width-at-half-maximum (FWHM) energy resolution for α-particles, implanted in the focal-plane detector, was 60–80 keV, depending on the strip and the position on the strip. The α-particles that escaped the focal-plane detector at different angles and were registered in a side detector had an energy resolution of the summed signals (side detector plus residual focal-plane detector) of 140–200 keV. If the energy deposited by an α-particle as it recoiled out of the focal-plane detector was lower than the detection threshold of 1.2 MeV (thus its position was lost) and was detected only by a side detector, its total energy was estimated as the sum of the energy measured by the side detector and half of the threshold energy (0.6 MeV), thus the uncertainty in determining the total energy was increased to $\pm$0.6 MeV. The assignment of such α-particles to the observed decay chains was made using the calculated probability of random correlations based on the decay rate in the side detectors associated with actual experimental conditions.

The FWHM position resolution from the signals of correlated decays of nuclei implanted in the detectors was 0.9–1.9 mm for EVR-α signals and 0.5–0.9 mm for EVR-SF signals. If an α-particle was detected by both the focal plane ($\Delta E_{\alpha 1}$) and a side detector ($\Delta E_{\alpha 2}$), i.e. $E_\alpha = \Delta E_{\alpha 1} + \Delta E_{\alpha 2}$, the position resolution depended on the amplitude $\Delta E_{\alpha 1}$, but was generally inferior to that obtained for the full-energy signal.

Fission fragments from the decay of ^{252}No implants, produced in the ^{206}Pb + ^{48}Ca reaction, were used for the mean total kinetic energy (TKE) calibration. The measured fragment energies ($E_{\rm tot} = E_{F1} + E_{F2}$) were not corrected for the pulse-height defect of the detectors, the energy loss in the detectors' entrance windows or dead layers or for the energy loss of the escaping fragment (E_{F2}) in the pentane gas, filling the detection system (at a pressure of about 1.7 Torr). The mean sum energy loss of fission fragments from the SF-decay of ^{252}No was about 20 MeV. The TKE of nuclei with $Z > 102$ was determined as the sum $E_{\rm tot}$ + 20 MeV. The systematic

uncertainty in estimating the TKE value was about 5–7 MeV when both fission fragments were detected.

3.5. DGFRS operating mode

From model calculations and the available experimental data, one can estimate the expected α-particle energies of the evaporation products and their descendant nuclei that could be produced in a specific reaction of synthesis. For α-particles emitted by the parent or daughter nuclei, it is possible to choose wide enough energy and time gates $\delta E_{\alpha 1}$, $\delta t_{\alpha 1}$ and $\delta E_{\alpha 2}$, $\delta t_{\alpha 2}$ (accounting for all the uncertainties in the estimation of the expected energies and half-lives of the synthesized nuclei) and employ a special low-background detection scheme [122, 123, 129, 132, 133]. During the irradiation of the target, the beam was switched off after a recoil signal was detected with parameters of implantation energy and TOF expected for evaporation residues, followed by an α-like signal with an energy in the interval $\delta E_{\alpha 1}$ in the same strip within a 1.4–1.9 mm wide position window and a time interval $\delta t_{\alpha 1}$ of up to 8 s. If the first α-particle was not detected (the probability being about 13%), then the switching-off the beam was done when a second α-particle in the corresponding $\delta E_{\alpha 2}$ and $\delta t_{\alpha 2}$ intervals was detected.

Such a running condition was a compromise between the inevitable loss of beam dose (10% of the beam time was lost) and the necessity of a beam pause for the registration of long-duration sequential decays of the daughter nuclides with $Z \leqslant Z_{\mathrm{CN}} - 2$ under very low background conditions.

This operating mode of DGFRS can be illustrated by detection of long decay chains of the odd–odd isotopes of element 115, produced in the ^{243}Am(^{48}Ca, $3n$)^{288}115 reaction [134].

The beam was switched off, if in the time interval $\delta t_{\alpha 1} = 8$ s both the recoil nucleus (response in the TOF-detector) and an α-like signal (without a TOF signal) with an energy 9.6 MeV $\leqslant E_\alpha \leqslant$ 11.0 MeV ($\delta E_{\alpha 1} = 1.4$ MeV) were detected in the same strip and in the position window $\Delta y \approx 2$ mm. The beam-off interval was initially set as $\delta t_{\alpha 2} = 2$ min. In this time interval, if an α-particle with $E_\alpha > 8.6$ MeV was registered in any position of the same strip, the beam-off interval was automatically extended to $\delta t_{\alpha 3} = 12$ min. In the 12 min period, if other α-particles with energies expected for heavy nuclei were observed, the beam-off pause was prolonged up to 2.7 h.

In this experiment, which continued 270 h, there were 577 short turn-offs of the beam, each lasting $\delta t_{\alpha 2} = 2$ min (the total beam-off time was about 19 h).

The spectrum of α-like signals (all events without a TOF signal) in all the strips in the energy range of $7 \leqslant E_\alpha \leqslant 11$ MeV is shown in figure 15(a). In the figure, we also show the α-particle spectrum detected in beam-off time intervals (see above). In the beam-off α-particle spectrum mainly the peaks originating from Po isotopes, the decay products of the long-lived isotopes of Ra–Th, produced in transfer reactions, were observed. The isotope ^{211}Po is the descendant nucleus of ^{219}Th, produced in calibration experiments with the $^{\mathrm{nat}}$Yb-target.

The majority of events with $E_\alpha = 8.0$–9.5 MeV is the result of α-decays of the short-lived descendants ^{212}Po ($T_{1/2} = 0.3$ μs, $E_\alpha = 8.78$ MeV) and ^{213}Po ($T_{1/2} = 4.2$ μs, $E_\alpha = 8.38$ MeV) detected in coincidence with β^--decays of the precursors ^{212}Bi and ^{213}Bi (see, e.g., [123, 132]). For α-particles with $E_\alpha > 8.9$ MeV, the total counting rate of the whole detector array during beam-off pauses was 0.7 h^{-1}. Note that in the high-energy part of the α-particle spectrum ($E_\alpha \geqslant 9.5$ MeV) only eight events were detected, seven of them (marked black), as we shall demonstrate below, belonging to the decay chains of the isotope ^{288}115.

Figure 15(a) shows that switching the beam off essentially eliminates the background at $E_\alpha > 9$ MeV, where sequential α-particle emission was observed in three decay chains (see figure 15(b)). The probability that any one of the four α-particles, observed during about

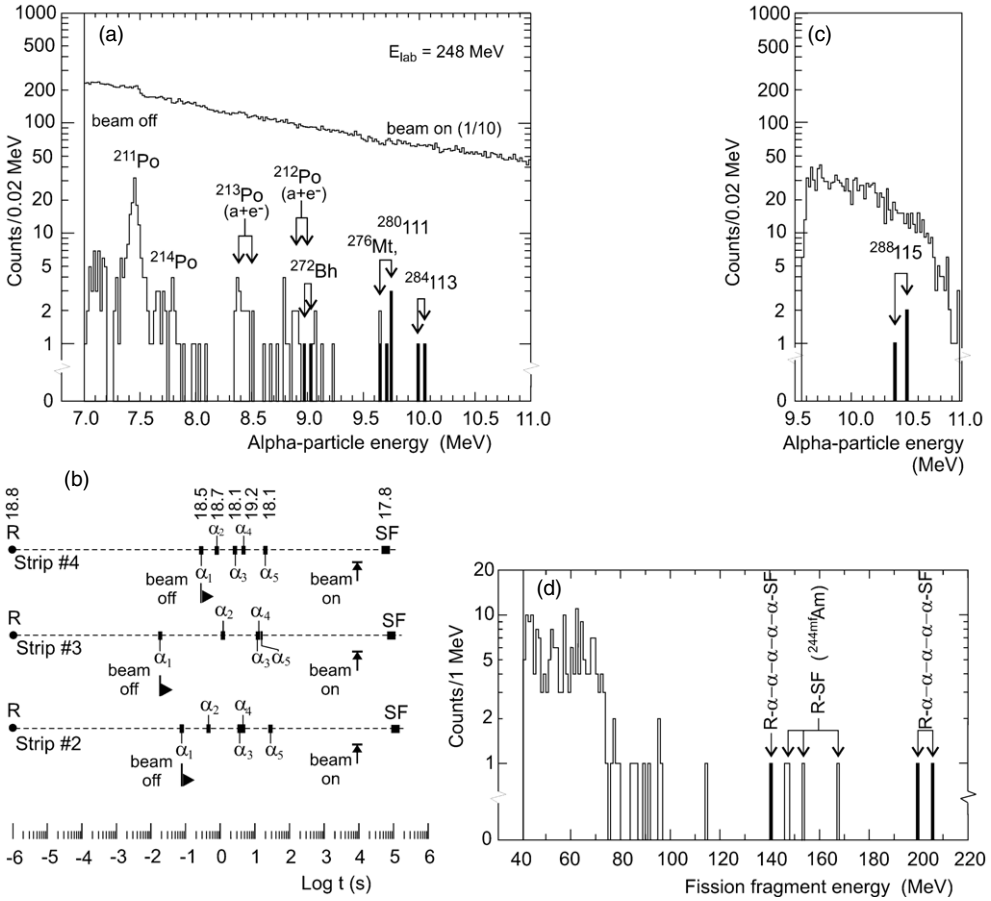

Figure 15. (a) Total beam-on α-like signal and beam-off α-particle energy spectra of events registered by the detectors of DGFRS in the reaction ^{243}Am + ^{48}Ca at the projectile energy: $E_{\mathrm{LAB}} =$ 248 MeV. The solid histogram shows the energies of events observed during beam-off periods in the correlated decay chains. (b) Detector signals observed during consecutive decays of the isotope of element 115, produced in the ^{243}Am(^{48}Ca, $3n$)^{288}115 reaction at $E_{\mathrm{LAB}} = 248$ MeV. For the event registered in strip no. 4 indicated are the position coordinates (in mm) of seven signals: the recoil nucleus (R), five α-particles and SF fission fragments. (c) Total energy spectrum of α-like events that stopped the beam during the ^{243}Am + ^{48}Ca experiment. The solid histogram shows the energies of α-particles that switched off the beam and were followed by two or more beam-off α-particles with $E_\alpha = 8.5$–11 MeV. (d) Total fission-fragment energy spectra; the solid histogram shows the energies of events, observed in the correlated decay chains.

30 s, is due to random detector background amounts to about 6×10^{-3}, even without taking into account the correlation in position and strip number for the subsequent events. Applying both of these factors will further reduce this probability by more than two orders of magnitude.

Comparing beam-off with beam-on events, one can determine the probability of random appearance of the first pair EVR-α_1 signals that switched off the beam. The total spectrum of α-like particles that caused the beam to be switched off is shown in figure 15(c). Here, the solid histogram shows the energies of events that caused the beam to be switched off.

These events were followed by two or more beam-off α-particles with $E_\alpha = 8.5$–11 MeV, without taking into account the position and strip number for the subsequent events. Thus, the probability that each one of the EVR-α_1 events followed by a subsequent α_2-...-α_5-SF decay chain randomly caused the beam to be switched off was about 10^{-5}.

The total spectrum of high-energy signals with $E \geqslant 40$ MeV (without an associated TOF signal) is presented in figure 15(d). For cases when fission signals were registered by both the front and the side detectors, the sum energy is given. The background signals (scattered ^{48}Ca ions, fragments of the induced fission of the target, etc) appear in the energy range $E \leqslant 120$ MeV; they are not observed in the beam-off spectrum. The signals of SF-fragments arising in the decays of heavy nuclei are expected at higher energies, with $E \geqslant 130$ MeV [123, 132, 133].

In the experiment with 248 MeV ^{48}Ca ions, we only observed seven spontaneous-fission events with $E_F \geqslant 130$ MeV. The three SF-events with measured energies of 147 MeV, 168 MeV and 154 MeV were detected 0.51 ms, 4.1 ms and 2.07 ms after the implantation of corresponding recoil nuclei in strips 12, 10 and 11, respectively. For the second and third events, both the front and side detectors registered fission fragments. Based on the apparent lifetime, it was reasonable to assign these events to the spontaneous fission of the 0.9 ms ^{244mf}Am isomer, a product of transfer reactions with the ^{243}Am target [135]. The DGFRS suppresses the yield of such products by a factor of 10^5 [123, 132]. For one event with $E_{tot} =$ 146 MeV, no appropriate EVR-SF correlation was found. However, before the ^{243}Am + ^{48}Ca experiment, during a 390 h off-line background measurement, we detected three SF-decays of long-lived nuclei, e.g. ^{252}Cf ($T_{1/2} = 2.65$ years), produced in incomplete fusion reactions in the previous experiments [130] where the same set of detectors was used. Thus, the registration of one more SF-event ($E_{tot} = 146$ MeV, strip 2) from the decay of long-lived nuclei corresponded to the background level of Cf isotopes and was to be expected.

Three more SF-events, which were observed in the strips and positions corresponding to the three R-α_1-...-α_5 decay chains, were registered with high total kinetic energies $E_{tot} =$ 205 MeV (150 + 55 MeV), 200 MeV (148 + 52 MeV) and $E_{F1} = 140$ MeV (only the front detector registered a fission fragment). Taking into account the above-mentioned energy losses by the spontaneous-fission fragments in the separator and detector, the total kinetic energy of these SF-events was estimated to be about 225 MeV. The probability that these SF-events appeared in the detector as random events and were not the members of the three preceding R-α_1-...-α_5 decay chains was less than 10^{-7}.

The position deviations of the detected seven signals of recoil nuclei and subsequent sequential decays (α and SF) for all three decay chains, observed in this experiment (for one decay chain in strip 4 the position coordinates are shown in figure 15(b)), indicate a strong *position correlation* between the observed decays. The analysis of the data obtained in this experiment and the properties of the isotopes of element 115, synthesized in the ^{243}Am + ^{48}Ca reaction, will be presented below.

Counting rates of the α-like and SF-like signals from the ^{243}Am + ^{48}Ca reaction, as well as the spectra, obtained in two operating DGFRS conditions—beam-on and beam-off, differ only slightly from the reactions with other targets shown in table 1. In spite of the certain increase in the yield of spontaneous-fission fragments when going from ^{243}Am to ^{248}Cm or ^{249}Cf targets (the main background is due to the long-lived SF-nuclei ^{252,254}Cf from transfer reactions), the probability of random coincidences of the fragments with preceding α-decays remains at the level of less than 10^{-6}.

In the operating modes, mentioned above, the setup allowed detection of rare events and decay characteristics of superheavy nuclei with decay time of up to 1 d and even longer. The most short-lived nuclei are detected in DGFRS in a special operating mode

of 'fast' data acquisition from the detectors, corresponding to $t \geqslant 5$ μs. In this way, the setup allows investigation of nuclei in a wide range of half-lives—from 10^{-5} s to more than 10^5 s.

From the characteristics of the DGFRS, which are given above, it follows that with a ^{48}Ca-beam intensity of 1.2 pμA, 0.35 mg cm^{-2} target thickness and a beam dose 5×10^{18} (realized for 200 h of operation) the observation of one decay event corresponds to the production cross section of about 0.7 pb.

Since 2000, the sensitivity of the experiments at DGFRS has exceeded by 10^2–10^4 times all earlier attempts to produce heaviest nuclei in ^{48}Ca-induced reactions and was the main factor in the progress achieved in the task of synthesis and studying the properties of superheavy elements.

4. Experimental results

For the synthesis of superheavy nuclei at DGFRS, the fusion reactions of ^{48}Ca with target nuclei, the isotopes of U, Np, Pu, Am, Cm and Cf (nine isotopes of six actinide elements), were used. They are presented in table 1. As will be shown in the following, in the investigations carried out at different ^{48}Ca energies, 29 new nuclides (34, including preliminary data for the decay chain of ^{282}113) were detected, all of them being evaporation products and their daughter nuclei in the region of $Z = 104$–118 and $A = 266$–294.

4.1. General characteristics

In the listed reactions, altogether 86 decay chains were registered. All decay chains are characterized, in their majority, by sequential α-decays (from one to six), which are terminated by spontaneous fission. In few cases, spontaneous fission occurred after detecting the recoil nucleus. In the observed chains, there were altogether 232 nuclear decays. The chains with similar characteristics, namely nuclear decay mode, energy and half-life, were attributed to the decay of the same nucleus no matter how it was produced—as an evaporation residue or as a daughter nucleus in the α-decay (or decays) of a heavier ancestor. In order to reduce the length of this overview, it is convenient to present the experimental data from different reactions by combining the identical events of each experiment as one chain and showing the number of events, the energy of the α-particles (E_α) and the average decay time $\bar{t}_\alpha$ of the chain nuclei together with the experimental uncertainties. For this reason, the chains of different type are denoted by symbols: $\boldsymbol{k}$, $\boldsymbol{l}$, $\boldsymbol{m}$, ..., $\boldsymbol{x}$, $\boldsymbol{y}$, $\boldsymbol{z}$ (15 types altogether). Finally, the analysis of these decay chains will allow us to identify the decay characteristics of each of the synthesized nuclei.

Let us first consider how reliably the data observed in the experiments with DGFRS may be attributed to the formation and decay of superheavy nuclei, namely to what extent the measured characteristics defined by the experimental setup satisfy the criteria of observation of evaporation residues from ^{48}Ca-induced reactions and their subsequent decays. In this respect, we should keep in mind that the kinematics of the investigated fusion reactions are practically the same when the mass of the target varies from ^{238}U to ^{249}Cf and the ^{48}Ca-beam energy changes by less than 30 MeV. We should also note that in all sequences only two decay modes are registered: α-decay and spontaneous fission. As a consequence, we have three kinds of signals from the detector array that characterize the decay of the reaction products: the recoil nuclei (R) and their decay by α-particle emission (α) or spontaneous fission (SF).

4.1.1. Recoil nuclei. Indeed, small variations of the target mass and the ^{48}Ca-beam energy, when occurring in complete fusion reactions, bring forth the formation of recoil nuclei in the middle of the target layer in a rather narrow energy range $E_{R(1/2)} \approx$ 38–42 MeV (0.131–0.146 A MeV). Taking into account the energy loss in the target layer, in hydrogen and in the TOF-detector, the kinetic energy of the recoiling nuclei entering the front detector is estimated to be $E_R^{\text{in}} \approx$ 15–20 MeV. The energy spectrum of the recoils from all the 86 registered sequences together with the spectrum of ^{252}No ($E_R^{\text{in}} \approx 21$ MeV) from the ^{206}Pb(^{48}Ca, $2n$)^{252}No reaction as a reference is shown in figure 16(a). The spectrum of the recoils, as can be seen from the figure, is consistent with the one expected for the evaporation products, obtained in the complete fusion reactions U − Cf + ^{48}Ca.

4.1.2. Sequential α-decays. In order to separate from the background those signals, which correspond to the correlated decay of heavy recoils implanted in the detector, it is necessary that they satisfy some specific conditions. The signals from the decay chains must have position correlation on the surface of the front detector, they should appear in a definite order with a TOF-mark for the recoiling nuclei, without a TOF-mark for decays (α-particles, SF fission fragments) and should be observed with a corresponding amplitude and time intervals.

Among the 86 decay chains, 164 nuclei undergo α-decay. In 17 cases, the α-particles were lost (emission in the backward direction to the open window). This is in agreement (within the obtained statistics) with the efficiency of the detector, which is 87%. For 26 α-particles, emitted in the backward hemisphere and registered by the side detectors, the deposited energy in the front detector was lower than the registration threshold. These events were not accompanied by position signals. For the remaining events, the position signals of the α-particles could be used as a parameter, pointing both to correlations between the sequentially emitted α-particles and to their relation to the preceding signal from the recoil nucleus and the subsequent signal from the spontaneous-fission fragment(s). The position deviation of the signals (in mm) relative to the average coordinates of the recoil nucleus, the α-particles and the SF fission fragments for each decay sequence summed over all the decay chains is shown in figure 16(b). As can be seen from the figure, the width of the distribution is FWHM ≈0.65 mm. In some cases, the deviations $\Delta y \geqslant 1$ mm are connected with the low energy deposited by the α-particle in the front detector, because the position resolution of the detector strongly deteriorates when approaching the registration threshold [130]. For 96% of the events, the deviations are within $\Delta y \leqslant 1$ mm, which underlines the strict correlation in all the observed decays. A position signal is necessary as a sign to switch the beam off, when a correlation has to be established between the recoil nucleus and the first α-particle in the prescribed energy range (for this purpose, wide-open gates are chosen: $\Delta y_{R\text{-}\alpha} \approx 2$ mm, ΔE_α up to 1.5 MeV). After switching the beam off, the coordinates of the next signals often simply demonstrate the correlation of the subsequent decays, due to the small probability for random coincidences (even without considering the positions), because of the low counting rate in the detector during the 'beam-off' operating time.

For each α-transition in the decay sequences, the energy E_α and the time of registration t_α of the emitted α-particle were measured. It was already mentioned that the energy resolution of the detector array depended on how the α-particle was measured. The best resolution (in most cases it amounted to ≈60–70 keV) corresponded to the full deposition of the α-particle energy in the front detector (according to calibration and estimation, the efficiency $\varepsilon_\alpha \approx 52\%$ of 4π). In 101 cases out of a total of 164, the α-particles of the decay chains were measured by the front detector. The identity of the nuclei, present in different sequences, and the decay energies Q_α were determined by the data taken from the front detector. Only in this case, the difference in the measured E_α could be considered as α-transitions to excited states.

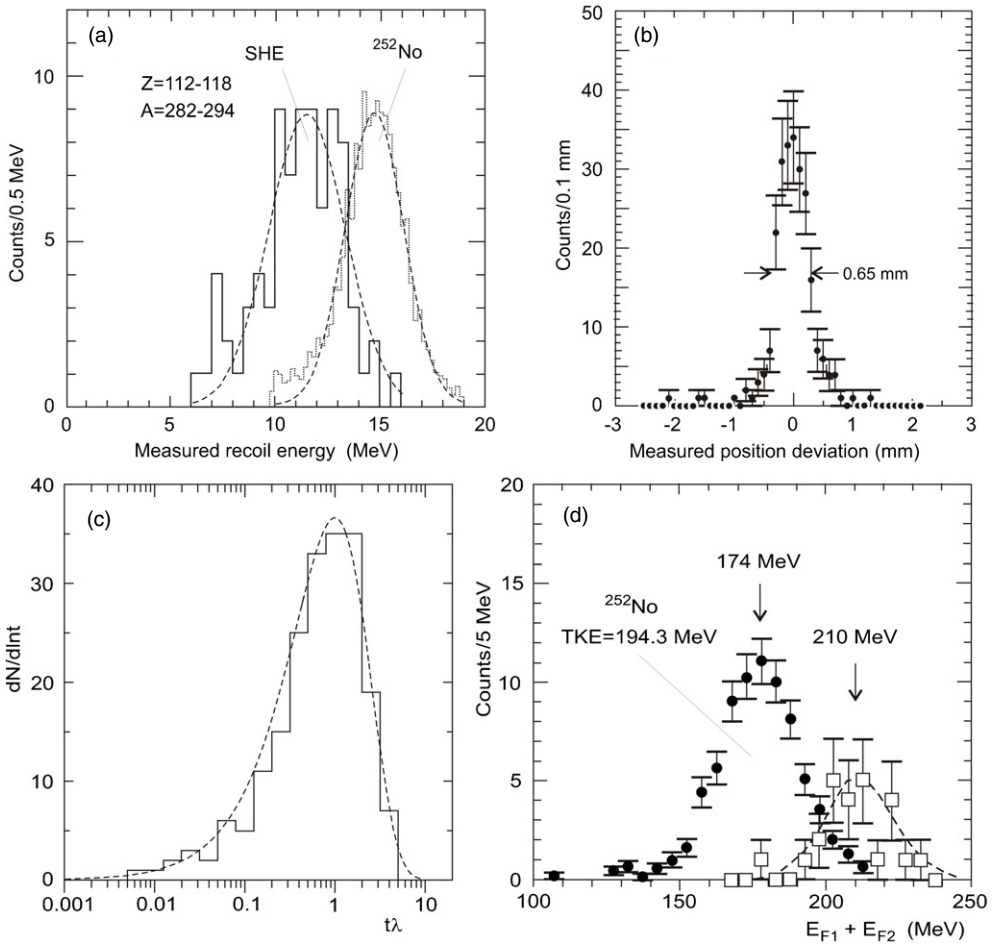

Figure 16. (a) Energy spectrum of recoil nuclei, registered by the front detector, for which consecutive decays have been observed (see the text). The dotted histogram presents the case of No nuclei—the evaporation products of the ^{206}Pb(^{48}Ca, $2n$)^{252}No reaction. The solid line denotes the evaporation products from the Act. + ^{48}Ca reactions. The dashed curves are drawn to guide the eye. (b) Position deviations of all signals (EVRs, α-particles and SF-fragments) in the observed decay chains of the Act. + ^{48}Ca reactions. The position of the α-particle deviates from the average value by more than 1 mm, caused by the low energy, $\Delta E_\alpha \leqslant 2.0$ MeV, deposited in the focal-plane detector resulting in a deteriorated position resolution. (c) Relative time intervals of all events in the observed decay chains compared with the average half-lives ($\lambda = \ln 2/T_{1/2}$) assigned to the particular nuclides (see table 3). The dashed curve is the calculated distribution. (d) Spectrum of the summed energy of the SF-fragments, registered for the isotope ^{252}No and the nuclei with $Z \geqslant 110$ (see the text). The value of $\overline{\text{TKE}}$ given for ^{252}No is from [136].

The average decay time $\bar{t}_\alpha$ and the half-life T_α ($\ln 2 \cdot t_\alpha = T_\alpha$) were determined from the time distributions of the α-particles with a given energy E_α. The decay time of the parent nucleus was estimated once the recoil nucleus was registered, whereas the decay time of the daughter nuclei from the time of registering the preceding α-particle. The assumption that in the decay with energy $Q_\alpha \pm \Delta Q_\alpha$ and half-life $T_\alpha \pm \Delta T_\alpha$, within the experimental error, there is no other α-transition with close values of Q_α and T_α is actually an approximation. As can

be seen from figure 16(c) such an assumption looks defensible for all nuclei in the observed decay sequences.

Finally, from the theory of α-decay it follows that for allowed α-transitions the energy and probability of decay (or half-life) are connected with each other by means of the well-known Geiger–Nuttall relation. This relation of the measured quantities Q_α and T_α serves as an additional verification that the observed signals pertain to α-particles emitted in radioactive decay. Moreover, as will be shown below, from the experimental values of Q_α and T_α we may, with high reliability, identify the atomic numbers of all nuclei constituting a given decay chain.

4.1.3. Spontaneous fission. As already mentioned above, all the observed decay chains, obtained in ^{48}Ca-induced reactions, terminate by spontaneous fission. Actually, as it will follow from further considerations, spontaneous fission is present as a competing process to the α-decay of some nuclei from the middle of the sequence. According to calibrations, the front and side detectors with a probability of about 40–45% simultaneously register both fission fragments; in about 25%, both fragments are absorbed by the front detector. In all other cases only one fragment is measured (by the front detector) with an energy $E_F \geqslant 130$ MeV. In 37 out of 86 decay chains, both SF-fragments were registered. With the exception of five events with $E_{\rm tot} = 200$–240 MeV, related to the symmetric fission of nuclei with $Z = 104$–106 (see below), the remaining 32 SF-events ($Z \geqslant 110$) are presented in figure 16(d). In this figure, the spectrum of summed energies of the SF fission fragments of ^{252}No, observed at DGFRS in the ^{206}Pb(^{48}Ca, $2n$)^{252}No reaction, is also shown. Comparing the experimental spectrum $E_{\rm tot}$(^{252}No) with the spectrum of the total kinetic energy (TKE) of this nucleus, measured in [136], it follows that the detector practically does not distort the shape of the TKE distribution, but shifts it by about 20 MeV. As previously mentioned, this happens due to the energy loss by the fragment emitted in the backward direction in the dead layers of the front and side detectors. In spite of the low statistics, the shape of the $E_{\rm tot}$ distribution of the SF-fragments from the decay chains, obtained in the fusion reactions from U to Cf + ^{48}Ca, differs insignificantly from that of ^{252}No. However, the average energy is about 35 MeV higher than for the ^{252}No nuclei. Unfortunately, when the DGFRS detector array registers the pair of SF-fragments from the implanted nuclei, the mass (or energy) asymmetry of the fragments is strongly distorted by the geometry of the detectors and does not reflect the fission mode of SF-nuclei. The SF characteristics of the synthesized nuclei will be presented and discussed below.

4.2. Even-Z nuclei

We may achieve the largest neutron excess in the compound nuclei and in the evaporation products by using heavy isotopes of even-Z actinides—^{244}Pu, ^{248}Cm and ^{252}Cf—as target material. With the exception of the highly radioactive ^{252}Cf (in the experiments we used the ^{249}Cf isotope), all the mentioned long-living isotopes ($T_{1/2} \geqslant 3 \times 10^5$ years) were used in our long-term irradiations by intense ^{48}Ca beams. Another advantage of the targets with even atomic numbers is that a few other isotopes with shorter half-lives ($T_{1/2} \geqslant 5 \times 10^3$ years) are also available. With a reliable safety system and control during the irradiation, they also work for the experiments aimed at the synthesis of the heaviest nuclei. There is a definite meaning in this.

By changing the mass of the isotope, it is possible to produce compound nuclei and respectively, evaporation residues with the same number of protons, but with different neutron numbers.

In fact, the evaporation residue with $Z = Z_{CN}$ and $N = N_{CN} - x$ with a given mass number can be produced in fusion reactions of ^{48}Ca with different isotopes of the target nuclei by ensuring the evaporation of the relevant number of neutrons. The change in the neutron number may be achieved by varying the excitation energy of the compound nucleus. In other words, in cross reactions with different target isotopes by varying the mass and/or the excitation energy of the compound nucleus, it becomes possible to determine the number of evaporated neutrons, leading to the formation of an evaporation residue with given decay characteristics. On the other hand, the looked-for nuclide may also be obtained by varying the charge (and mass) of the target nucleus; this allows the given nuclide to be obtained in different ways: either directly as a neutron evaporation residue or as a daughter or even granddaughter nucleus, the latter being the α-decay products of yet heavier nuclei. As will be shown below, all these methods were used in our experiments for the identification of the atomic and mass numbers of the evaporation residues in the fusion reactions of ^{48}Ca with actinide targets.

In connection with the following summary of the experimental results we shall make some explanations. In columns 1–5 of table 1, the conditions of the performed 23 experiments at DGFRS and of the two types of chemical experiments are presented. In the sixth column are given the final results—number of events—of the evaporation products, obtained in the various xn-evaporation channels. This information comes from the analysis of the results of all experiments. The events differ from each other by their decay mode. Events of the same type (decay mode, energy and time of correlated decays), observed in one and the same reaction, are put together and are shown in figures 17, 19, 20, 21 and 23. As mentioned previously, they are denoted by different symbols: $\boldsymbol{k}, \boldsymbol{l}, \boldsymbol{m}, \ldots, \boldsymbol{x}, \boldsymbol{y}, \boldsymbol{z}$ (the ^{283}113 decay sequence is shown in figure 23(a) without a symbol). The number of observed events with a given decay mode and the reaction channel leading to the parent nucleus are also presented (they are given in table 1 once more). At the same time, for each reaction the cross sections of all observed nuclides obtained at the different excitation energy of the compound nucleus (excitation functions) are also shown. The decay properties of the nuclei in the decay sequences (decay energy, lifetimes, etc), as well as the identification of decay chains produced in different reactions, are described in the text. The reader can find more specific information for each reaction with all the observed sequences, the determination of the probability for random correlations and other details in the original publications (see the references given in table 1).

4.2.1. Synthesis of isotopes of element 114. In order to produce isotopes of element 114, fusion reactions of ^{242}Pu and ^{244}Pu with ^{48}Ca-projectiles of different energies were chosen. The conditions of performing the experiments and the observed decay events of the new nuclides are collected in table 1.

In the ^{244}Pu + ^{48}Ca reaction at $E_L = 236$ MeV, corresponding to an excitation energy of the ^{292}114 compound nucleus $E_x \approx 35.2$ MeV (here and further the average values E_x are given, the energy ranges ΔE_x being shown in table 1), two identical decay chains were observed. They look like sequential decays of the type R-α_1-α_2-SF with total decay time of about 40 s (figure 17(a), sequence $\boldsymbol{k}$). The yield of these nuclei grows by a factor of about 5 when the energy is increased to $E_x \approx 41$ MeV, but at further rise of the energy to $E_x \approx 47$ MeV, the yield decreases. At the highest energy $E_x \approx 52.6$ MeV not a single nucleus with the given decay properties was detected. For the five observed events, the difference in energy of two correlated α-particles with $E_{\alpha 1} = 9.83$ MeV and $E_{\alpha 2} = 9.17$ MeV does not exceed the energy resolution of the detector. The time distributions of the signals, arising from the decays of the parent and daughter nuclei, indicate sequential radioactive decay with average decay times $\bar{t}_{\alpha 1}$, $\bar{t}_{\alpha 2}$ and $\bar{t}_{SF}$ also shown in the figure. The experimental values of the cross sections of nuclei

with $t_{\rm tot} = t_{\alpha 1} + t_{\alpha 2} + t_{\rm SF} \approx 40$ s at different excitation energies E_x are denoted by squares in the lower part of figure 17(a). In the same figure, the calculated excitation functions for the evaporation channels of the reaction ^{244}Pu(^{48}Ca, xn)$^{292-x}$114 are also shown [74, 137].

At the same time, in this reaction at $E_x \geqslant 41$ MeV, other short-lived nuclei, undergoing correlated R-α-SF decays within a time interval of about 1 s (figure 17(a), sequence $\boldsymbol{l}$), were also observed. These nuclei were not found at $E_x = 35.2$ MeV (the upper limit of the cross section was found to be about 0.4 pb). However, at an excitation energy $E_x = 41$ MeV seven similar decays were registered. Four other such sequences were also observed at $E_x \approx 47$ MeV and, finally, at the highest energy $E_x = 52.6$ MeV one more event was detected. All 12 events corresponding to short-lived nuclei are characterized by a strictly defined energy of the α-transition, $E_\alpha = 9.95$ MeV and mean time $\bar{t}_\alpha \approx 0.9$ s. After the second α-transition in all decay chains, spontaneous fission ($t_{\rm SF} \approx 0.14$ s) was observed. The production cross sections for the nuclei with $t_{\rm tot} = t_\alpha + t_{\rm SF} \approx 1$ s at different excitation energies E_x are shown by circles in the lower panel of figure 17(a).

Besides the above-mentioned two types of decays, at the maximum excitation energy $E_x = 52.6$ MeV, another event was detected as a new decay chain of the type R-α_1-α_2-SF with total decay time of about 6 s (figure 17(a), sequence $\boldsymbol{m}$). In this event, the two sequentially emitted α-particles with $E_{\alpha 1} = 10.03$ MeV and $E_{\alpha 2} = 9.54$ MeV, and $t_{\alpha 1}$, $t_{\alpha 2}$ and $t_{\rm SF}$ differ in energy and time from the five R-α_1-α_2-SF chains, observed at the lower energy. Obviously, this event belongs to the decay of another nucleus, which is formed only at the higher excitation energy $E_x > 47$ MeV (in the lower panel of figure 17(a), it is denoted by a triangle). We shall come back to the interpretation of this event later.

The experiment with the ^{242}Pu-target was also performed at four different beam energies, corresponding to the excitation energy range from 32.5 MeV to 45 MeV.

At the minimum energy of the compound nucleus ^{290}114, $E_x = 32.5$ MeV, six correlated decay chains were registered. In five of them, the decay chains are of the R-α_1-α_2-SF type with $t_{\rm tot} \approx 6$ s (figure 17(b), sequence $\boldsymbol{o}$). In one case, a short sequence R-α-SF with $t_\alpha + t_{\rm SF} \approx 4$ s (sequence $\boldsymbol{n}$) was observed. When the beam energy was increased by 3 MeV ($E_x = 35.2$ MeV), five other decay chains R-α_1-α_2-SF were detected. In addition, five more events were observed at the higher energy $E_x = 40.2$ MeV. However, already at the energy $E_x = 45.1$ MeV no event of the given type was detected. In all 15 R-α_1-α_2-SF events, when the α-particle energy was measured by the front detector the deviation of the α-particle energy of the first decay from the average value $E_{\alpha 1} = 10.02$ MeV did not exceed 0.07 MeV, which was practically defined by the energy resolution of the front detector. For the most part of the second decay with $E_{\alpha 2} = 9.53$ MeV, a similar situation took place. However, in three decays, correlated with the first decay, α-particles with energies 9.34 MeV (two times) and 8.94 MeV (not shown in figure 17(b)) were registered. In these events, as will be discussed below, the α-transition leads to the $\approx$0.2 MeV and $\approx$0.6 MeV excited states of the daughter nucleus.

In 1 out of the 15 mentioned R-α_1-α_2-SF sequences, the granddaughter nucleus instead of SF undergoes α-decay with $E_{\alpha 3} = 9.70$ MeV, $t_{\alpha 3} = 0.28$ s; after that another α-decay follows with $E_{\alpha 4} = 9.30$ MeV, $t_{\alpha 4} = 0.42$ s, and finally spontaneous fission occurs with $E_{\rm tot} = E_{F1} + E_{F2} = 228$ MeV, $t_{\rm SF} = 381$ s. In the figure, these decays are shown as a continuation of the sequence $\boldsymbol{o}$.

In addition to the R-α_1-α_2-SF decays, at the energy $E_x = 40.2$ MeV seven shorter 0.2 s decay sequences were registered. In three cases, after the detection of the recoil nuclei, α-decay with $E_\alpha = 10.21$ MeV, $\bar{t}_\alpha \approx 0.10$ s was observed, which was shortly followed by SF ($\bar{t}_{\rm SF} \sim 0.8$ ms). In the other four cases, the implanted nuclei undergo spontaneous fission with $\bar{t}_{\rm SF} \approx 0.17$ s. At the higher energy $E_x = 45.1$ MeV, the yield of nuclei, experiencing short decay, decreased: only one decay chain of type R-α-SF and another R-SF were registered.

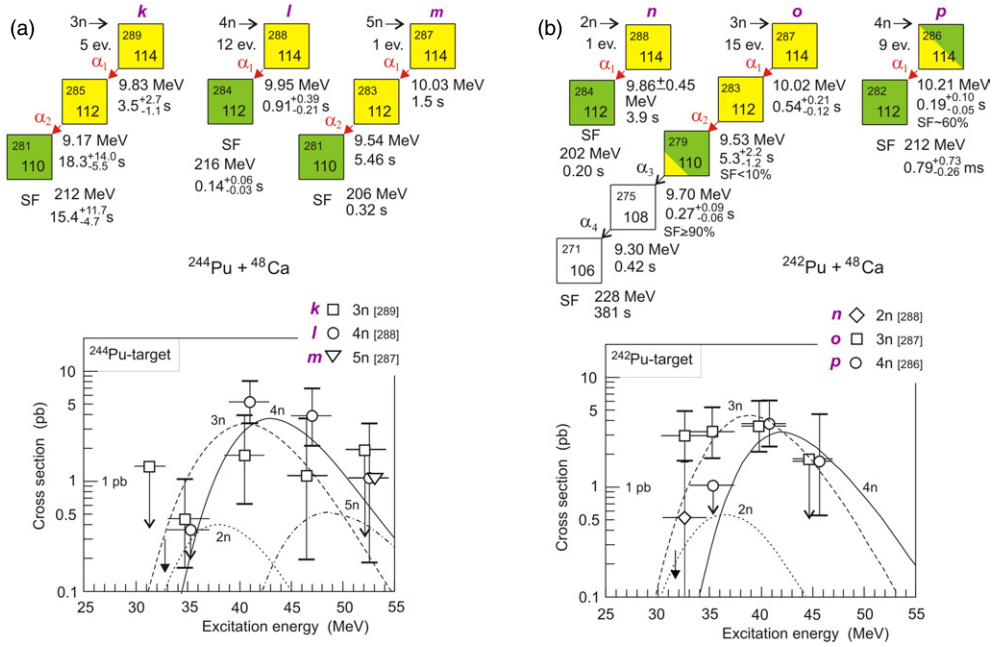

Figure 17. (a) Upper panel: sequences of correlated decays in the ^{244}Pu + ^{48}Ca reaction. The one-type chains are shown as one decay sequence and are denoted by $\boldsymbol{k}$, $\boldsymbol{l}$ and $\boldsymbol{m}$. Indicated are the number of events of a specific type, the average α-particle energy and the average summed energies of the SF-fragments, obtained in the given experiment. The decay times with errors (68% CL) are for the observed number of events. Lower panel: production cross sections of nuclei having the shown decays (denoted by letters) at different excitation energies of the compound nucleus. The lines denote the calculated excitation functions of the xn-evaporation channels in the ^{244}Pu + ^{48}Ca reaction. The black arrow shows the excitation energy of the compound nucleus ^{292}114 at the Coulomb barrier ($B_C = B_{\rm Bass}$). (b) As (a) for the ^{242}Pu + ^{48}Ca reaction (sequences $\boldsymbol{n}$, $\boldsymbol{o}$ and $\boldsymbol{p}$).

Given the decay times of all nine events and the dependence of the yield on the excitation energy, it is most probable that both decay chains R-α-SF and R-SF belong to the same nucleus. As shown in figure 17(b), sequence $\boldsymbol{p}$, this isotope undergoes with almost equal probability both types of decays: α-decay and SF. It is noteworthy that in the case of α-emission, the daughter nucleus decays by spontaneous fission within a short time, $\bar{t}_{\rm SF} \approx 0.8$ ms. Excitation functions for nuclei with two decay modes, R-α_1-α_2-SF and R-α/SF–SF, are shown in the lower panel of figure 17(b). Also here, the cross section for the one R-α-SF event (sequence $\boldsymbol{n}$), observed only at the low energy $E_x = 32.5$ MeV, is shown.

Now we can summarize the results of the two experiments, carried out with the ^{244}Pu- and ^{242}Pu-targets at different ^{48}Ca energies.

In each experiment, we observe nuclei, which undergo different types of decays. This difference manifests itself in the energies E_α and decay times t_α of nuclei comprising correlated decay sequences of the types R-α_1-α_2-SF, R-α-SF or R-α/SF–SF. All 43 detected events in our experiments belong to decay chains, which end by spontaneous fission. According to the efficiency of the detector array, in 20 cases both SF fission fragments were detected with total measured energy $E_{\rm tot}$ from 199 MeV to 230 MeV ($\bar{E}_{\rm tot} = 213.8$ MeV). Correcting for the energy loss of the fragments in the detector dead layers (see above), the measured value $\bar{E}_{\rm tot}$ corresponds to $\overline{\rm TKE} \approx 230$ MeV.

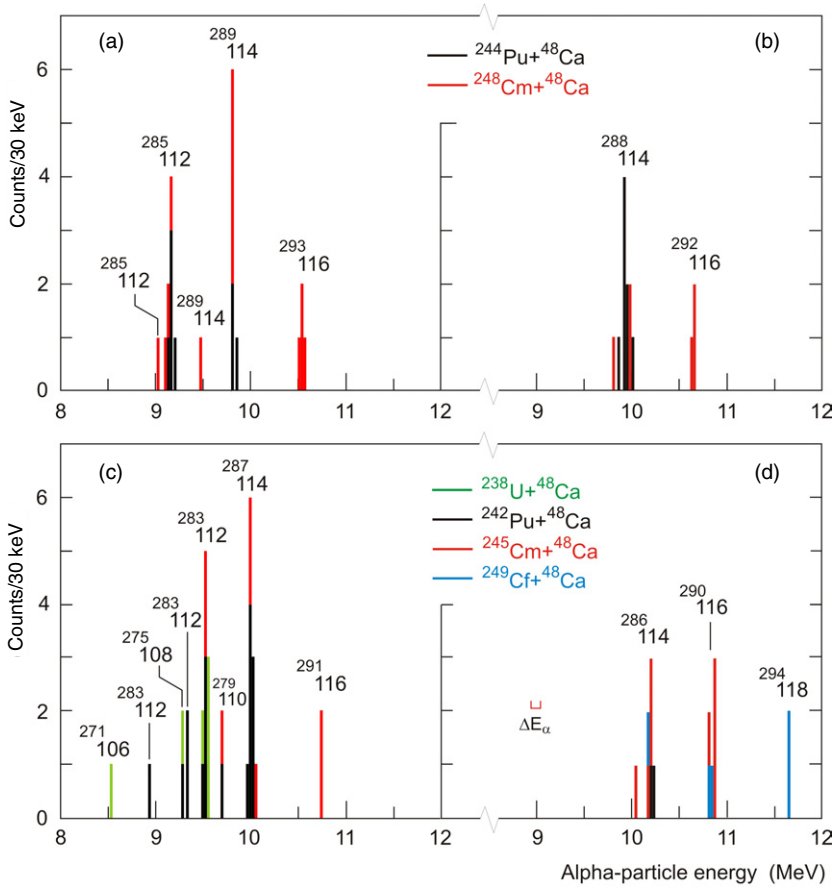

Figure 18. Energy spectra of α-particles of the decay chains, observed in reactions Act. + ^{48}Ca (marked by different colours). (a) Decay chains $\boldsymbol{k}$ and $\boldsymbol{r}$ from the reactions ^{244}Pu + ^{48}Ca (black) and ^{248}Cm + ^{48}Ca (red), respectively (figures 17(a) and 19(a)). (b) Decay chains $\boldsymbol{l}$ and $\boldsymbol{s}$ from the same reactions (figures 17(a) and 19(a)). (c) Decay chains $\boldsymbol{o}$, $\boldsymbol{t}$ and $\boldsymbol{v}$, observed in the reactions ^{242}Pu + ^{48}Ca (black), ^{245}Cm + ^{48}Ca (red) and ^{238}U + ^{48}Ca (green) (see figures 17(b), 19(b) and 20(a)). (d) Decay chains $\boldsymbol{p}$, $\boldsymbol{u}$ and $\boldsymbol{x}$, observed in the reactions ^{242}Pu + ^{48}Ca, ^{245}Cm + ^{48}Ca (red) and ^{249}Cf + ^{48}Ca (blue), respectively (see figures 17(b), 19(b) and 21(a)).

The spectra of the α-particles in the sequences with indices $\boldsymbol{k}$, $\boldsymbol{l}$, $\boldsymbol{o}$ and $\boldsymbol{p}$ are shown in black in figure 18, graphs (a), (b), (c) and (d), respectively.

Let us consider the sequences R-α_1-α_2-SF at $E_x = 52.6$ MeV for the ^{244}Pu + ^{48}Ca reaction and at $E_x \approx 35$ MeV in the case of ^{242}Pu + ^{48}Ca. As seen in figures 17(a) and (b) in the decay chains $\boldsymbol{m}$ and $\boldsymbol{o}$, all measured decay parameters—the α-particle energies $E_{\alpha 1}$, $E_{\alpha 2}$, as well as the decay times, are equal within the accuracy of the measurements.

When this nucleus is formed as an evaporation product in the two fusion reactions ^{48}Ca + ^{242}Pu,^{244}Pu, the difference in mass of the compound nuclei, $\Delta N_{\mathrm{CN}} = 2$, is compensated by emission of two more neutrons ($\Delta x = 2$), due to the increased excitation energy of the compound nucleus ^{292}114 by $\Delta E_x \sim 17$ MeV.

From these data and from the excitation function $\sigma(E_x)$, measured for nuclei which decay by the sequences R-α_1-α_2-SF in the reaction ^{242}Pu + ^{48}Ca (figure 17(b)), we can come to the

conclusion that they belong to the isotope ^{287}114, which is produced after the evaporation of three and five neutrons from the excited compound nuclei ^{290}114 and ^{292}114, respectively. Then, the short decays R-α-SF and R-α/SF–SF refer correspondingly to the neighbouring even–even isotopes ^{286}114 and ^{288}114. Finally, the decay chains R-α_1-α_2-SF, lasting about 40 s and observed only in the ^{244}Pu + ^{48}Ca reaction, belong to the decay of the odd isotope ^{289}114. The same conclusion can be drawn if the two other chain pairs $\boldsymbol{n}$ and $\boldsymbol{l}$ are considered, although the energy of the α-particle in the chain $\boldsymbol{n}$ is determined with poor accuracy. In any other versions of isotope identification, strong contradictions arise both in the decay properties and in the cross sections (excitation functions).

At the same time, the identification of Z, A, as well as the decay characteristics of the isotopes of element 114, obtained in the reactions ^{242}Pu, ^{244}Pu + ^{48}Ca, can be checked independently. There are two ways to do so.

The observed isotopes $^{286–289}$114, in principle, can be produced as daughter nuclides after the α-decay of heavier ones—the isotopes of element 116. Conversely, the daughter products of the α-decay of the isotopes of element 114 (nuclei with $Z = 112$) can also be produced as evaporation products. In the first case, in the fusion reaction ^{248}Cm + ^{48}Ca, the compound nucleus ^{296}116 ($N = 180$) has two protons and two neutrons more than the compound nucleus ^{292}114, which is formed in the ^{244}Pu + ^{48}Ca reaction. At a beam energy corresponding to the Coulomb barrier, the compound nuclei ^{296}116 and ^{292}114 have excitation energies $E_x^{\min} =$ 30.4 MeV and 32.9 MeV [138], respectively (here and further, the estimation of $E_x^{\min}$ is done for spherical nuclei). Then, after α-decay of the isotopes of element 116, produced in the ^{248}Cm + ^{48}Ca reaction, the daughter nuclei must reproduce the scenario of the decay of the isotopes of element 114 in the same evaporation channels as in the ^{244}Pu + ^{48}Ca reaction. A similar picture is expected when the results of the two reactions ^{246}Cm + ^{48}Ca and ^{242}Pu + ^{48}Ca are compared. If the lighter isotope ^{245}Cm were used as a target (as was in our case) then identical decay sequences should be found in the daughter nuclei—the evaporation products with $Z = 114$, formed in the $(x-1)n$-channels of the ^{242}Pu + ^{48}Ca reaction.

In contrast, the compound nuclei ^{286}112 from the fusion reaction ^{238}U + ^{48}Ca ($E_x^{\min} =$ 31.7 MeV) have two protons and two neutrons less than the compound nuclei ^{290}114, formed in the ^{242}Pu + ^{48}Ca reaction. Thus, when the number of evaporated neutrons is the same ($x =$ 3 or 4), the evaporation products of the reaction ^{238}U + ^{48}Ca will be the same isotopes ^{283}112 and ^{282}112, which are daughter nuclei after the α-decay of the isotopes ^{287}114 and ^{286}114 from the ^{242}Pu + ^{48}Ca reaction.

The following experiments were dedicated to the investigation of these two cases.

4.2.2. Synthesis of isotopes of element 116. For producing the isotopes of element 116, two targets made of the enriched isotopes ^{245}Cm and ^{248}Cm were used.

It is remarkable that the compound nucleus ^{296}116, produced in the fusion of ^{248}Cm and ^{48}Ca nuclei, has the maximum neutron excess ($N_{CN} = 180$). At present, the investigation of this reaction has been done at the two energies $E_x \approx 33$ MeV and 39 MeV (we plan to continue the measurements for higher energies).

In this reaction two new nuclides were observed. They underwent sequential decay as R-α_1-α_2-α_3-SF and R-α_1-α_2-SF, considerably differing in decay time (figure 19(a), sequences $\boldsymbol{r}$ and $\boldsymbol{s}$). Presenting in more detail the results of this experiment, we have to underline that at the energy $E_x \approx 33$ MeV three events were registered, evidencing the production of nuclei, which decayed in about 1.5 min by the four steps: R-α_1-α_2-α_3-SF. Two other events with similar properties were registered at the higher energy, $E_x \approx 39$ MeV. Let us compare the decay chains $\boldsymbol{r}$, figure 19(a), and sequence $\boldsymbol{k}$, figure 17(a). It can be seen that after the emission of the first α-particle with $E_{\alpha 1} = 10.54$ MeV and $\bar{t}_{\alpha 1} \approx 90$ ms the subsequent decay

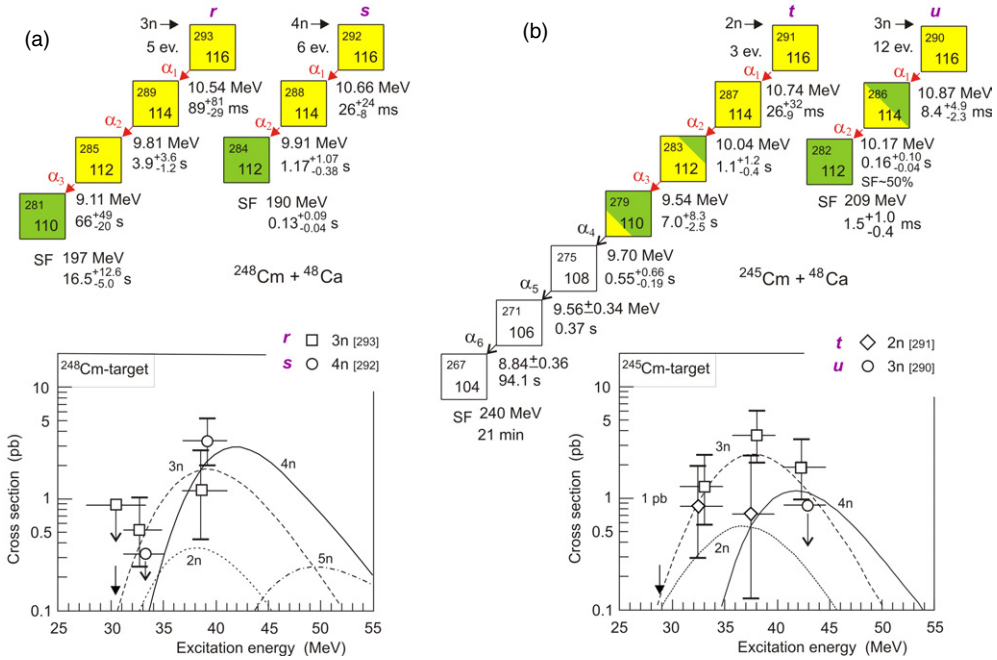

Figure 19. As figure 17 for the decay chains of nuclei, observed in the reactions (a) ^{248}Cm + ^{48}Ca and (b) ^{245}Cm + ^{48}Ca.

of the nuclei, produced in the ^{248}Cm + ^{48}Ca reaction, completely reiterates the chain, observed for the ^{289}114 isotope that was synthesized in the reaction ^{244}Pu(^{48}Ca, $3n$)^{289}114. Thus, the observed decay sequence R-α_1-α_2-α_3-SF is governed by the decay of the nucleus ^{293}116, an evaporation residue from the ^{248}Cm(^{48}Ca, $3n$)^{293}116 reaction. It should be noted that the rise of the cross section of the isotope ^{293}116, connected with the increase of the excitation energy of the compound nucleus ^{296}116 from 33 MeV to 39 MeV, is consistent with the expected excitation function for the $3n$-evaporation channel of the fusion reaction ^{248}Cm + ^{48}Ca.

Other sequences R-α_1-α_2-SF with shorter decay times of about 1 s were not observed at the minimum excitation energy $E_x \approx 33$ MeV. Six decay events of this type were registered at $E_x \approx 39$ MeV. From the comparison of the sequences s and l shown in figures 19(a) and 17(a), it follows that after the emission of the first α-particle with $E_{\alpha 1} = 10.66$ MeV and $\bar{t}_{\alpha 1} \approx 26$ ms the subsequent decay completely corresponds to the chain, observed for the ^{288}114 isotope, synthesized in the reaction ^{244}Pu(^{48}Ca, $4n$)^{288}114. The significant increase in the production cross section of the isotope ^{292}116, which is due to increase in the excitation energy from 33 MeV to 39 MeV, also agrees with the expected excitation function for the $4n$-evaporation channel of the fusion reaction ^{248}Cm + ^{48}Ca (lower panel in figure 19(a)). We presume that the further increase in the ^{48}Ca-beam energy by about 5 MeV can lead to a rise in the production cross section of the isotope ^{292}116.

In the experiment with the ^{248}Cm + ^{48}Ca reaction, the α-particle spectra of the daughter nuclei—the isotopes ^{289}114 and ^{288}114—coincide, as expected, with the spectrum of the parent nuclei, obtained earlier in the same evaporation channels of the reaction ^{244}Pu(^{48}Ca; $3n$, $4n$)$^{289,\,288}$114 (see figures 18(a) and (b), red and black colours, respectively). An exception is only one decay sequence of the odd isotope $^{293}116 - \alpha_1 \rightarrow {}^{289}114 - \alpha_2 \rightarrow {}^{285}112 - \alpha_3 \rightarrow$

^{281}110 (SF). In this decay chain, the energy $E_{\alpha 2} = 9.48$ MeV, possibly also $E_{\alpha 3} = 9.03$ MeV, differs from the energies $E_{\alpha 2} = 9.82$ MeV and $E_{\alpha 3} = 9.15$ MeV, observed in nine other sequences, registered in the ^{244}Pu, ^{248}Cm + ^{48}Ca reactions. Given the energy resolution FWHM ≈0.06 MeV in this experiment, the difference $\Delta E_{\alpha 2} \sim 0.35$ MeV could find an explanation as a transition to an excited state of the daughter nucleus ^{285}112.

The next experiment with the other reaction ^{245}Cm + ^{48} Ca was performed at several beam energies that corresponded to excitation energies of the compound nucleus ^{293}116 from 33 MeV to 43 MeV. A total of 15 correlated decay chains of two types were registered (figure 19(b)). Both decay modes were observed at the minimum energy $E_x = 33$ MeV as two chains R-α_1-α_2-α_3-SF with total decay time of about 10 s and as three shorter chains R-α_1-α_2/SF–SF lasting 0.5–0.9 s. At a higher energy, $E_x \approx 38$ MeV, only one event of the first type was registered. However, in this case, the granddaughter nucleus instead of spontaneous fission underwent α-decay (similarly to what was seen in one decay event of the isotope ^{287}114 in the reaction ^{242}Pu + ^{48}Ca, see figure 17(b), sequence ***o***). In this chain, after emission of the fourth α-particle with $t_{\alpha 4} = 0.7$ s, two more α-decays with $t_{\alpha 5} = 0.37$ s and $t_{\alpha 6} = 94.1$ s followed. After this, spontaneous fission was observed with $t_{\mathrm{SF}} = 21$ min and summed energy of the two fragments $E_{\mathrm{tot}} = 240$ MeV.

At the excitation energy $E_x \approx 38$ MeV five additional short R-α_1-α_2-SF chains were observed. Finally, at the maximum energy $E_x \approx 43$ MeV, long chains were not seen. Here four events, corresponding to short R-α_1-α_2/SF–SF sequences, were registered. The energy E_α and the average time $\bar{t}_\alpha$ of all nuclei in the decay chains shown in figure 19(b) give evidence of the production of two new isotopes (***t*** and ***u***) with different decay properties. Their production cross sections at different excitation energies of the compound nucleus ^{293}116 are presented in the lower panel of figure 19(b).

For the nuclei, which undergo R-α_1-α_2-α_3-SF decay, after the emission of the first α-particle with $E_{\alpha 1} = 10.74$ MeV, all subsequent decays reiterate the decay chains of the ^{287}114 isotope, formed in the ^{242}Pu(^{48}Ca, $3n$)^{287}114 reaction (see sequence ***o***, figures 17(b) and 19(b), as well as the α-particle spectrum in figure 18(c)). It follows from here that the first α-decay with $E_{\alpha 1} = 10.74$ MeV, $\bar{t}_{\alpha 1} \approx 26$ ms comes from the isotope ^{291}116, which was observed in the ^{245}Cm(^{48}Ca, $2n$)^{291}116 reaction at $E_x \approx 33$ MeV with the cross section $\sigma_{2n} = 0.9^{+2.0}_{-0.7}$ pb. In the decay of the ^{291}116 nucleus, similarly to the isotope ^{287}114, a long decay sequence R-α_1-α_2-. . .-α_6-SF was once more registered. The difference between them lies in that the spontaneous fission, which terminated the six sequential α-transitions from the nucleus ^{291}116, belongs to the isotope ^{267}Rf ($t_{\mathrm{SF}} = 110$ min), whereas in the decay of ^{287}114 spontaneous fission originated from the descendant—the isotope ^{271}Sg ($t_{\mathrm{SF}} \approx 2.8$ min).

In 12 decay sequences of another nucleus, after the emission of an α-particle with $E_{\alpha 1} = 10.87$ MeV, $\bar{t}_{\alpha 1} \approx 10$ ms, the daughter nucleus undergoes practically in equal shares either α-decay with $E_{\alpha 2} = 10.17$ MeV or spontaneous fission with $\bar{t}_{\alpha/\mathrm{SF}} \approx 0.16$ s. In the case of α-decay, the granddaughter nucleus undergoes spontaneous fission with $\bar{t}_{\mathrm{SF}} \approx 1.5$ ms.

As can be seen from figure 19(b) chains ***u*** of type R-α_1-α_2/SF–SF and from figure 18(d) (α-particle spectra), the decay of the daughter nucleus α_2/SF–SF reiterates the scenario and the decay properties of the even isotope ^{286}114, produced in the ^{242}Pu(^{48}Ca, $4n$)^{286}114 reaction. This implies that the first α-transition with $E_{\alpha 1} = 10.87$ MeV, $\bar{t}_{\alpha 1} \approx 8.5$ ms belongs to the decay of the even–even isotope ^{290}116, which is formed in the ^{245}Cm(^{48}Ca, $3n$)^{290}116 reaction. Indeed, the maximum cross section of the isotope ^{290}116 is observed at $E_x \approx 38$ MeV (figure 19(b), lower panel) in agreement with the expected $3n$-evaporation channel of the ^{245}Cm + ^{48}Ca reaction.

Summarizing the results of the experiments with the ^{245}Cm and ^{248}Cm targets, we may conclude that all four synthesized isotopes of element 116 are α-emitters. In the consecutive

α-transitions, they fully reiterate the decay sequences of the daughter nuclei—the isotopes of element 114, synthesized in the reactions ^{242}Pu and ^{244}Pu + ^{48}Ca. Also, for all the four isotopes, the energies Q_α and half-lives T_α were determined.

4.2.3. Evaporation residues with $Z = 112$. Five isotopes $^{233–236}$U and ^{238}U can be, in principle, used as target material for the synthesis of the isotopes of element 112 in fusion reactions with the projectile ^{48}Ca. We have performed experiments only with the two isotopes ^{233}U and ^{238}U.

The choice of the target ^{233}U is, in fact, an advance to the neutron-deficient nuclei. In the ^{233}U(^{48}Ca, 3–4n)^{278,277}112 reaction, the evaporation residues have altogether 166 and 165 neutrons. The decay characteristics of the isotope ^{277}112, which was synthesized in the cold fusion reaction ^{208}Pb(^{70}Zn, n)^{277}112 [139, 140], are known. The properties of the neighbouring even–even nucleus ^{278}112, as it follows from predictions and from the experimental data, obtained for nuclei with $Z < 112$, can be estimated quite correctly. This isotope, the product of the reaction ^{233}U(^{48}Ca, 3n)^{278}112, should be reliably detected by our setup.

The experiment was performed at the ^{48}Ca-beam energy, corresponding to the excitation energy range $32.7 \leqslant E_x \leqslant 37.1$ MeV, where almost equal cross sections are expected for the 3n- and 4n-evaporation channels. In a lengthy irradiation of the ^{233}U target by a beam dose 7×10^{18}, not a single event was observed. With the fast mode of detection at the DGFRS, it is practically improbable that such result could be due to the short decay time of the isotope ^{278}112. Therefore, the upper limit of the cross section of the looked-for isotopes of element 112 was determined at a level of 0.6 pb.

The reaction with the isotope ^{238}U was performed at three energies: $E_x = 31.4$, 35.0 and 39.8 MeV. At the lowest energy, $E_x = 31.4$ MeV, one event was registered, corresponding to an R-SF decay with $t_{SF} = 4.84$ s. At the energy $E_x = 35$ MeV, six other events were observed: two R-SF chains (as in the previous case) and three R-α-SF chains with total decay time of about 3 s. The sixth event represents a long chain of sequential α-decays, R-α_1-α_2-α_3-α_4-SF, lasting about 3.3 h (see figure 20(a), sequence v). In this decay, the spontaneous fission of the daughter nucleus competes with α-decay, which, in turn, prolongs the decay by two more α-transitions and leads to a SF-emitter with $t_{SF} = 3.33$ h. The energies of the α-particles in all R-α-SF decay chains coincide with each other and are equal to $E_\alpha = 9.54$ MeV. The time of the sequences R-α-SF, R-SF and the two first α-transitions in the long R-α_1-α_2-α_3-α_4-SF chain agree with each other within the statistical time distribution of the decay events with $T_{1/2} \sim 4$ s. Most probably, all seven registered events can be assigned to the decay of one nucleus that undergoes R-α-SF decay ($E_\alpha = 9.54$ MeV, $\bar{t}_\alpha \sim 5$ s, $\bar{t}_{SF} \sim 0.1$ s). However, it should be noted that the three-fold loss of an α-particle in the R-α-SF decay chain amounts to about 4.5%. It can be that because of the large difference in the half-lives of ^{283}112 ($T_\alpha \approx 4$ s) and the neighbouring even–even isotopes ^{282}112 ($T_{SF} \approx 0.5$ ms) and ^{284}112 ($T_{SF} \approx 0.1$ s), the even–odd nuclide, formed as an evaporation product in the ^{238}U + ^{48}Ca reaction, with small probability may also undergo spontaneous fission (see below).

At the maximum energy, $E_x = 39.8$ MeV, the above-mentioned chains were not observed. Here, only one short R-SF decay chain with $t_{SF} = 0.21$ ms (figure 20(a), sequence w) was registered. The energy spectra of the α-particles, obtained in the reaction ^{238}U + ^{48}Ca in the chain v, are shown in figure 18(c) in green. From the comparison of the decay characteristics of the nuclei, shown in figures 20(a) and 17(b), as well as in figure 19(b), it follows that the sequences, observed in the ^{238}U + ^{48}Ca reactions, reiterate the decay of the daughter nuclei ^{287}114 and ^{286}114 (or of the granddaughters of the nuclei ^{291}116 and ^{290}116). From the excitation functions of the isotopes ^{283}112 and ^{282}112 (lower panel of figure 20(a)), it is also

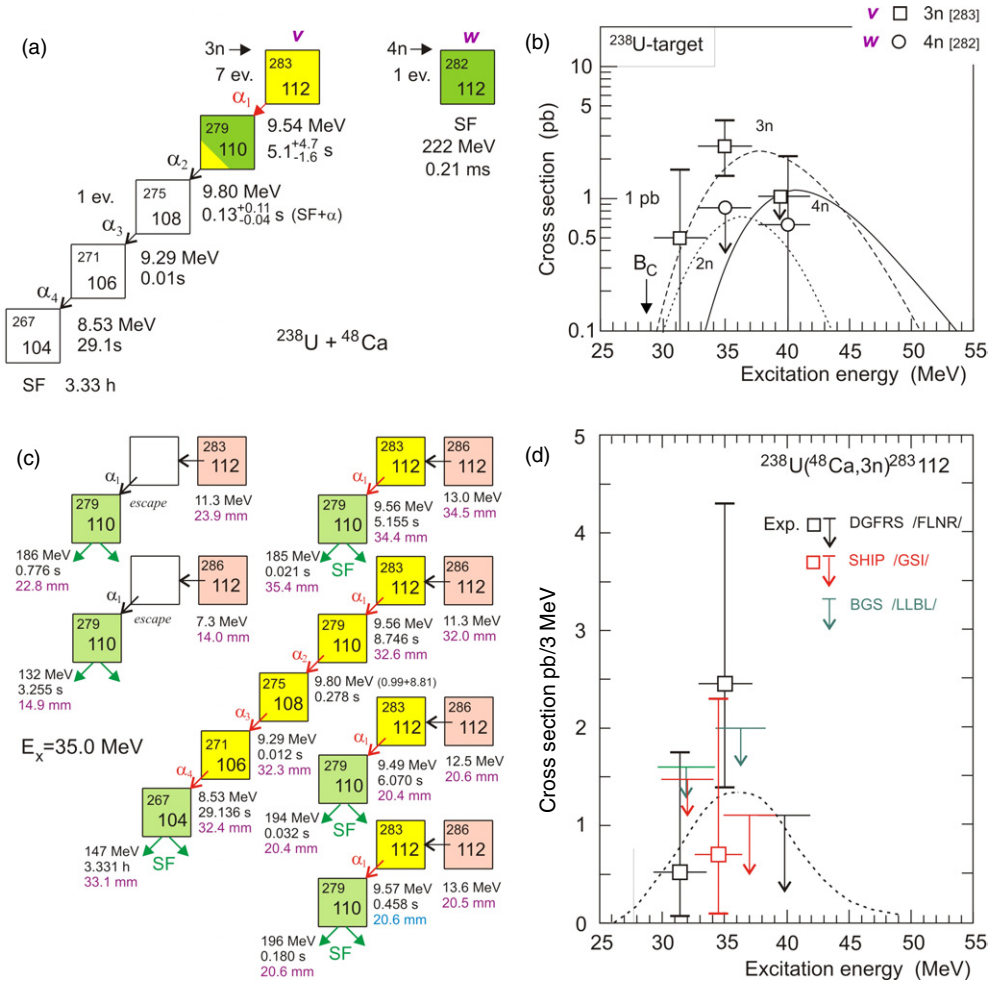

Figure 20. (a) Decay chains v and w, observed in the ^{238}U + ^{48}Ca reaction. (b) Calculated excitation functions for the 2n-, 3n- and 4n-evaporation channels of the ^{238}U + ^{48}Ca reaction; squares and circles—experimental cross sections correspond to v and w decay chains. (c) All decay sequences registered by the detector array of DGFRS at the ^{48}Ca-beam energy of 234 MeV ($E_x = 32.9$–37.2 MeV). For each nucleus in the sequences shown are: the energy, time and position of the signals due to the emitted particles; for the recoil nuclei implanted in the front detector the energy and position are given. (d) Cross sections (and upper limits) of the production of the ^{283}112 isotope in the ^{238}U + ^{48}Ca reaction, measured at different setups (indicated in the figure) in the experiments of [121, 141, 142]. The dashed line reflects the width of the excitation function of the 3n-evaporation channel according to statistical calculations and observations in other Act. + ^{48}Ca reactions. See also the Note on page R237.

seen that these nuclides are formed in the 3n- and 4n-evaporation channels of the ^{238}U + ^{48}Ca reaction.

What concerns the ^{238}U + ^{48}Ca experiments, it is necessary to make a few remarks.

The experiments Act. + ^{48}Ca were started in 1998 (they were continued in 2002–2003) as an attempt to synthesize element 112 in the ^{238}U + ^{48}Ca reaction [143] with the VASSILISSA separator. In these experiments at the excitation energy $E_x \approx 33$–36.5 MeV, corresponding to

the maximum of the $3n$-evaporation channel, spontaneous fission was observed with $T_{SF} \sim$ 3–5 min. At $E_x \approx 39$ MeV, the effect was not seen. However, the results were not confirmed at DGFRS (see above). Not excluding *a priori* the possibility of various ways of decay of the even–odd nucleus $^{283}112$—the evaporation residue of the $^{238}U + ^{48}Ca$ reaction, we plan to investigate the reason for this evident inconsistency separately after the programme at DGFRS is fulfilled. Meanwhile the attempts to observe the isotope $^{283}112$ in experiments at BGS (LBL, Berkeley) gave no result. The upper limit of observation of $^{283}112$, as estimated by the authors, was $\sigma_{3n} \leqslant 2.0$ pb (84% CL) [141].

Finally, at the SHIP separator (GSI, Darmstadt) in the same reaction $^{238}U + ^{48}Ca$ at $E_x \approx$ 34.5 MeV one spontaneous-fission event was observed with $t_{SF} = 7.57$ s with the two fragments registered with $E_{tot} = 206$ MeV (TKE ≈ 242 MeV) [142]. At the higher energy $E_x \approx 37$ MeV, as well as at the lower energy $E_x \approx 31.8$ MeV, an upper limit of the cross section was determined as $\sigma \leqslant 0.6$ pb and $\sigma \leqslant 0.9$ pb, respectively. All cross sections, obtained in the mentioned experiments, together with the data from DGFRS are presented in figure 20(d). In the left part of the figure (panel c) are shown all events, registered at the separator DGFRS in the $^{238}U + ^{48}Ca$ reaction at $E_x \approx 35$ MeV (the beam dose being 7.1×10^{18}) [121]. Four out of six decay sequences in all details (including the α-decay of ^{279}Ds and subsequent decays) reiterate the decay of the daughter and granddaughter nuclei, namely $^{287}114$ and $^{291}116$, produced in the $3n$-channel of the reaction $^{242}Pu + ^{48}Ca$, in the $5n$-channel of the $^{244}Pu + ^{48}Ca$ reaction and the $2n$-channel of the reaction $^{245}Cm + ^{48}Ca$, respectively. As it will be shown later, these sequences are completely adequate to the decay of the isotope $^{283}112$ in the experiment aimed at the chemical identification of element 112 (see below).

At the same time, as it follows from the experiments $^{233}U + ^{48}Ca$ ($N_{CN} = 169$) and $^{237}Np + ^{48}Ca$ ($N_{CN} = 172$), the latter will be described below and the former considered reactions $^{242,244}Pu$, $^{245,248}Cm + ^{48}Ca$ ($N_{CN} = 176$–180), the cross sections of the xn-channels of the reaction $^{238}U + ^{48}Ca$ ($N_{CN} = 174$) are smaller than for nuclei with higher Z_{CN} and greater neutron excess. This question will be discussed later in connection with the mechanism of fusion and survival of nuclei in Act. $+ ^{48}Ca$ reactions.

4.2.4. Synthesis of element 118. Decay properties of the isotopes of element 118 are of interest as a test for the predictive power of microscopic models. As mentioned earlier, practically all model calculations of nuclear masses point to the existence of the closed neutron shell $N = 184$, whereas for the position of the proton shell there are different versions. We may suppose that the differences in the predicted closed proton shell will manifest themselves in the decay properties of the isotopes of the elements with $Z \geqslant 120$ [40–42]. Meanwhile the heaviest nuclei, which may be produced with ^{48}Ca-projectiles, are the isotopes of element 118—a product of the reaction $^{249}Cf + ^{48}Ca$.

For instance, the even–even nucleus with $Z = 118$, $A = 294$ according to the MM-model ($Z_{SHELL} = 114$) [144] will undergo α-decay with $Q_\alpha = 12.11$ MeV and $T_\alpha \sim 0.1$ ms. In the HFB-model [27, 145], the values $Q_\alpha = 11.31$ MeV, $T_\alpha \sim 7$ ms are predicted, whereas in the RMF-model [146] they are $Q_\alpha = 11.03$ MeV, $T_\alpha \sim 35$ ms. The uncertainty in the decay energy, predicted in the different models, amounts to more than 1.0 MeV and the half-lives vary by about three orders of magnitude.

The variations in the heights of the barriers of the isotopes of element 118, predicted in the different models, mean different survivability of the compound nuclei and, consequently, different cross sections of the evaporation residues. In the MM-model, the expected cross section for producing nuclei with $Z = 118$ ($Z > Z_{SHELL}$) is less than for the isotopes of element 114 ($Z = Z_{SHELL}$). At the same time, in the microscopic models ($Z < Z_{SHELL}$), the advance

to the proton shell $Z_{\mathrm{SHELL}} = 120$, 122 or 124 can, in contrast, bring forth an increase of the survivability of the compound nuclei with $Z = 118$.

The first attempt to synthesize element 118 was done in 1999 in the cold fusion reaction ^{208}Pb(^{86}Kr, n)^{293}118. The expected enhanced probability of fusion of the magic nuclei ^{208}Pb and ^{86}Kr [147] compared to the ^{208}Pb + ^{70}Zn reaction was not observed; from the data of several experiments, an upper limit of the cross section, $\sigma_n \leqslant 0.2$ pb, was obtained [148–151]. As it follows from calculations (figure 7(a)) and from the data shown above (see figure 9(c)), this result could be explained in terms of factors that hinder the fusion of such massive nuclei and, for this reason, by small formation cross section of the compound nucleus ^{294}118.

In our experiments, we used a more asymmetric reaction: fusion of ^{249}Cf and ^{48}Ca.

In this reaction, the compound nucleus ^{297}118 is by 2p and 2n (or by an α-particle) heavier than the nucleus ^{293}116, produced in the reaction ^{245}Cm + ^{48}Ca. In the two reactions, the compound nuclei ^{297}118 and ^{293}116 have, at the Coulomb barrier, almost equal excitation energy: 26.6 MeV and 28.9 MeV, respectively. In the case of α-decay of the isotopes of element 118, their daughter nuclei must completely reiterate the scenario of the decay of the isotopes of element 116, which are formed in the same evaporation channels of the ^{245}Cm + ^{48}Ca reaction.

The experiment was carried out at two ^{48}Ca-beam energies, corresponding to excitation energies of the compound ^{297}118 nucleus: $E_x \approx 29.2$ MeV and 34.4 MeV.

During the 2300 h irradiation (dose 2.5×10^{19}) of the ^{249}Cf-target (0.23 mg cm^{-2} thick), at the beam energy corresponding to $E_x \approx 29.2$ MeV only one R-α_1-α_2-SF decay chain, lasting 0.56 s, was observed [130]. In the search for R-SF correlations, we analysed all 18 signals from fission fragments, observed in this experiment, and found only one event as a possible candidate for SF-decay. In this event, after detection of the recoil nucleus, 3.2 ms later, the front and side detectors registered spontaneous fission with summed energy of the two fragments $E_{\mathrm{tot}} = 223$ MeV (TKE ≈ 245 MeV). In the second experiment, performed 3 years later with a thicker target (0.34 mg cm^{-2}) and at a higher energy $E_x \approx 34.4$ MeV and with a beam dose 1.6×10^{19}, we observed two other decay chains: R-α_1-α_2-SF and R-α_1- α_2-α_3-SF with $t_{\mathrm{tot}} \sim 0.16$ s [152]. No R-SF correlations were observed in this run. Considering all three α-decay chains together, it was determined that the energies of the α-particles from the first two decays are in agreement with each other. They are $E_{\alpha 1} = 11.65$ MeV and $E_{\alpha 2} = 10.82$ MeV, respectively. In one of the three cases, in the third decay, instead of spontaneous fission, α-decay with $E_{\alpha 3} = 10.16$ MeV and $t_{\alpha 3} = 0.15$ s was observed, after which 2.7 ms later spontaneous fission occurred. The energies and decay times of the nuclei in the decay chains show that all three events belong to the decay of the same nucleus. The decay properties of this nuclide are shown in figure 21(b) by the chain $\boldsymbol{x}$.

The latter can be compared with two other chains from the decay of the nuclei ^{291}116 and ^{290}116 (see chains $\boldsymbol{t}$ and $\boldsymbol{u}$ in figure 21(a)). From the α-particle spectra, presented in figure 18(d), it is seen that after the α-decay of the nucleus ($E_{\alpha 1} = 11.65$ MeV), produced in the reaction ^{249}Cf + ^{48}Ca, all its subsequent α_2-SF/α_3-SF decays coincide with the properties of the isotope ^{290}116 and differ (especially in the daughter products) from the decay characteristics of the neighbouring isotope ^{291}116. Therefore, the observed decay sequence R-α_2-SF/α_3-SF results from the decay of the even–even nucleus ^{294}118, produced in the reaction ^{249}Cf(^{48}Ca, $3n$)^{294}118. Having three events of α-decay of the nucleus ^{294}118 and only the one above-mentioned R-SF event, we can point to the insignificant limit relative to spontaneous fission $b_{\mathrm{SF}} < 50\%$. The production cross section of the isotope ^{284}118, $\sigma_{3n} = 0.5^{+1.6}_{-0.3}$ pb at $E_x \approx 34.4$ MeV, is consistent with the expected excitation function for the $3n$-evaporation channel in the reaction ^{249}Cf + ^{48}Ca (see the lower panel in figure 21(b)).

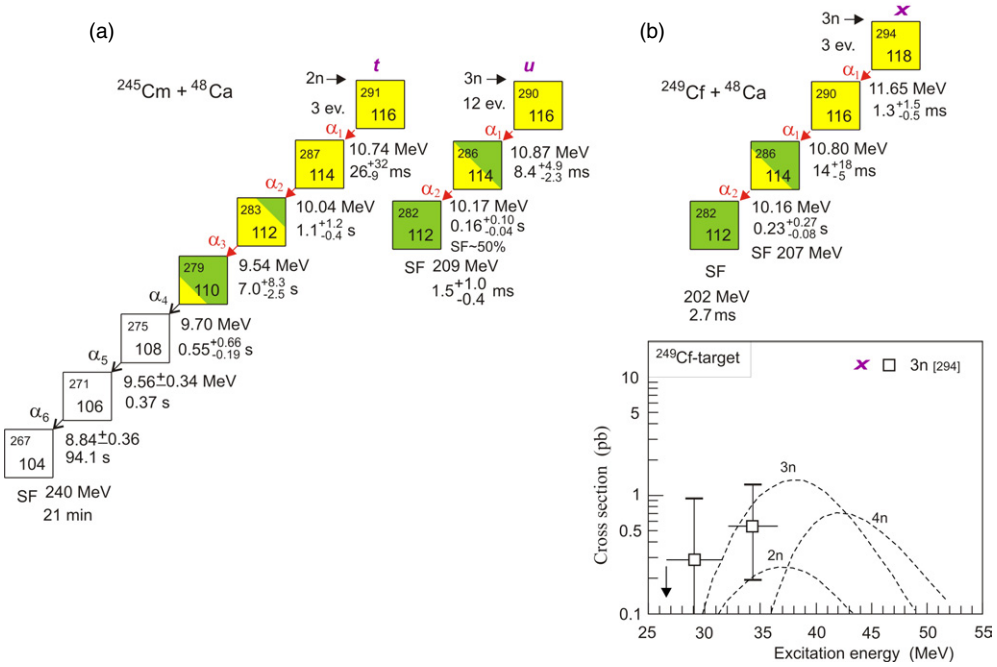

Figure 21. (a) Decay chains of the isotopes $^{291}116$ and $^{290}116$, obtained in the ^{245}Cm + ^{48}Ca reaction. The α-particle energies and mean decay times of the daughter nuclei, the isotopes with $Z = 114, 116, 112, \ldots$, are determined from all events and in all reactions, where these nuclides have been observed (see table 3). (b) The chain of sequential decays of the $Z = 118$, obtained on the basis of three events in the reaction ^{249}Cf + ^{48}Ca at $E_{\mathrm{Lab}} = 245$ MeV and 251 MeV (see table 1). The comparison of the decay properties of the nuclei shown in both figures allows making a conclusion that all chains observed in the reaction ^{249}Cf + ^{48}Ca pertain to the decay of the even–even isotope of element 118, produced in the reaction ^{249}Cf(^{48}Ca, $3n$)^{294}118. In the lower panel, the calculated excitation functions of the reaction ^{249}Cf(^{48}Ca, xn)$^{297-x}$118 are compared with the experimental data.

The question of the low cross section for producing the isotope ^{284}118 we shall discuss below together with all experimental results.

In this way, in the fusion reactions ^{238}U, ^{242,244}Pu, ^{245,248}Cm and ^{249}Cf + ^{48}Ca 15 formerly unknown, even-Z heaviest nuclei with mass from 279 to 294 and atomic number from 110 to 118 were synthesized. All four isotopes of element 116 with mass $A = 290$–293 decay by emission of α-particles with a half-life from 7 ms to 60 ms (figure 19). Their daughter products,four isotopes of element 114, are also α-emitters with $T_{1/2} = 0.13$–2.6 s (an exception is the light even–even isotope ^{286}114 with a branch $b_{\mathrm{SF}} \approx 50\%$). Spontaneous fission is the basic mode of decay of the even isotopes of element 112: ^{282}112 ($T_{\mathrm{SF}} \approx 0.8$ ms) and ^{284}112 ($T_{\mathrm{SF}} \approx 0.1$ s); for them, in all the observed 12 and 19 events, respectively, not a single α-decay was observed. These nuclei end the chains of the α-decays of the heavier precursors—the even isotopes with $Z \geqslant 114$. In contrast, the odd isotopes ^{283}112 ($T_{1/2} \approx 3.8$ s) and ^{285}112 ($T_{1/2} \approx 30$ s) undergo α-decay. Spontaneous fission becomes the main mode of decay of the daughter products—the odd isotopes with $Z = 110$: ^{279}110 ($T_{\mathrm{SF}} \approx 0.2$ s) and ^{281}110 ($T_{\mathrm{SF}} \approx 11$ s). About 10% of the events correspond to α-decay of the isotope ^{279}110. During the experiment, in the reactions ^{238}U, ^{242}Pu and ^{245}Cm + ^{48}Ca, only three α-decays of the nucleus ^{279}110 were observed. However, these three events open a unique possibility of obtaining new

neutron-rich isotopes of the already known elements, such as ^{267}Rf ($N = 163$) or ^{271}Sg ($N = 165$). They contain 4–5 neutrons more than the heaviest known isotopes of these elements, obtained in hot fusion reactions with ^{22}Ne [153] or ^{26}Mg ions [154]. The new isotopes of the first trans-actinides are situated near the closed shells $Z = 108$, $N = 162$. High stability relative to different radioactive decay modes is expected for them. These expectations, as it will be shown below, are now confirmed by the experiment. Altogether, this is a wide region for studying the effects of nuclear shells on the decay properties of heavy nuclei.

Unfortunately, the ways to such neutron-rich nuclei are blocked by spontaneous fission of the heavier predecessors. In order to avoid this constraint, it is reasonable to obtain nuclei with an odd number of protons (or, even better, with an odd number of neutrons). As is known, the odd nucleon in the nucleus reduces the probability of α-decay on the average by about a factor of 3–10 and that of spontaneous fission by more than three orders of magnitude. Because of this, if isotopes with an odd number of protons, such as ^{237}Np, ^{243}Am or ^{249}Bk, are used as targets, then, in fusion reactions with ^{48}Ca, it may become possible to obtain isotopes of the odd elements 113, 115 and 117, which will undergo sequential α-decays, leading to nuclei with $Z = 103$–105. We used two of these reactions to synthesize isotopes of elements 113 and 115.

4.3. Odd-Z nuclei

4.3.1. Synthesis of isotopes of elements 115 and 113. According to the calculations [74, 137] and the experimental cross sections $\sigma_{xn}(E_x)$ of evaporation residues, measured in the ^{238}U, ^{242,244}Pu, ^{245,248}Cm and ^{249}Cf + ^{48}Ca reactions, the $3n$- and $4n$-evaporation channels of the ^{243}Am + ^{48}Ca reaction, leading to the isotopes ^{288}115 and ^{287}115, should be observed with the highest yields.

The $3n$-evaporation channel results in the odd–odd isotope of element 115 with mass 288. The expected decay scenario of this isotope according to macro-microscopic calculations [39, 144] is shown in figure 22. The decay chain of the odd–odd isotope of element Rg ($Z = 111$) with mass 272, produced in the cold fusion reaction ^{209}Bi(^{64}Ni, $1n$)^{272}Rg [139, 155, 156], is shown for comparison. For the first five α-transitions in the decay of ^{288}115, with α-decay energies varying from $Q_\alpha = 10.95$ MeV for ^{288}115 [144] to $Q_\alpha = 9.08$ MeV for ^{272}Bh [39], one would expect a total time interval of about 10 s. The probability of spontaneous fission for these isotopes is rather low (taking into account the decay properties of neighbouring even-Z nuclei and the hindrance factors for fission of odd isotopes).

A considerable increase in lifetime could be expected for the following nuclei, ^{268}Db ($Q_\alpha = 7.80$ MeV, $T_\alpha \geqslant 5$ h) and ^{264}Lr ($Q_\alpha = 6.84$ MeV, $T_\alpha \geqslant 100$ d) [39]. For these nuclei, the competition of spontaneous fission or electron capture (EC) with α-decay could be larger. The electron capture of the odd–odd isotopes ^{268}Db or ^{264}Lr leads to the even–even isotopes ^{268}Rf or ^{264}No; for them, spontaneous fission with a short lifetime is expected (e.g., $T_{SF} = 1.4$ s is predicted for ^{268}Rf [25]). Thus, the decay chain of the parent nucleus ^{288}115 should terminate by spontaneous fission after a time interval essentially exceeding the total decay time for all preceding α-decays. A comparable decay pattern is expected for the neighbouring isotope ^{287}115.

The Coulomb barrier in the ^{243}Am + ^{48}Ca reaction is about 236 MeV. With 248 MeV ^{48}Ca-projectiles, the excitation energy of the compound nucleus ^{291}115 is $E_x \approx 40$ MeV, corresponding to the maximum for the $3n$-evaporation channel, resulting in production of the isotope of element 115 with neutron number $N = 173$. During a 270 h run, a beam dose of 4.3×10^{18} projectiles was delivered to the target. In this run, three R-α_1-α_2-α_3-α_4-α_5-SF sequences that lasted for about 1 d were registered. This experiment was already described

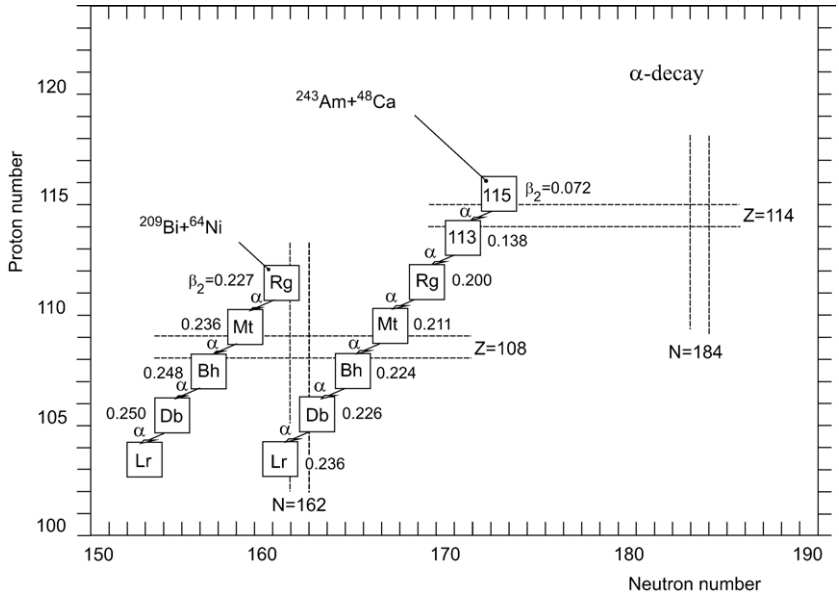

Figure 22. Expected decay chain for ^{288}115 [39, 144] and the decay chain observed for the parent nucleus ^{272}Rg [139, 155, 156]. The calculated deformation parameters β_2 [39, 144] are shown for each isotope.

in detail as an example for the performance of DGFRS when registering long-lasting decay sequences (see figure 15).

The R-α_1-α_2-α_3-α_4-α_5 sequences were detected in total time intervals of 15–29 s; the SF-decays of the final nuclei in the chains were detected 17–29 h after the last α-decay. The α-particle energies for each isotope in all observed decay chains are equivalent within the energy resolution of the detectors. One can conclude that in all three cases we observed decays originating from the same parent nucleus, most probably from the isotope ^{288}115 (see chain $\boldsymbol{y}$ in figure 23(b)). The corresponding cross section at 248 MeV ^{48}Ca-ion energy amounts to $\sigma_{3n} = 2.7^{+4.8}_{-1.6}$ pb.

This conclusion may get support through application of the systematic behaviour of the cross sections $\sigma_{xn}(E_x)$ of complete-fusion reactions shown in figure 23(b), right graph. Indeed, if the 3n-evaporation channel was observed at $E_x = 40$ MeV, then a small increase of the bombarding energy (by about 5 MeV or 2%) should result in decreasing the production cross section. That is why the next experiment was performed at the energy $E_x \approx 44.5$ MeV, close to the expected maximum for the cross section of the 4n-evaporation channel.

During the second 250 h run, the same beam dose of 4.3×10^{18} was delivered to the target. One decay chain only, consisting of four α-decays and a spontaneous-fission event, was registered at $E_x \approx 44.5$ MeV (chains $\boldsymbol{z}$, figure 23(b)). The beam was switched off after the detection of an EVR signal followed 46.6 ms later by an α-particle with $E_\alpha = 10.59$ MeV. Three other α-decays were detected during a time interval of 0.4 s. The first of them ($E_{\alpha 2} = 10.12$ MeV) was registered in 0.147 s; after 0.245 s, the next α-particle with $E_{\alpha 3} = 10.37$ MeV (1.30 MeV + 9.07 MeV) was detected by both the front and a side detector. The last α-particle ($E_{\alpha 4} = 10.33$ MeV) was observed after 14.0 ms, and 106 min later, a SF-event was detected in the same position on the strip with a summed energy $E_{\rm tot} = 170 + 36 = 206$ MeV.

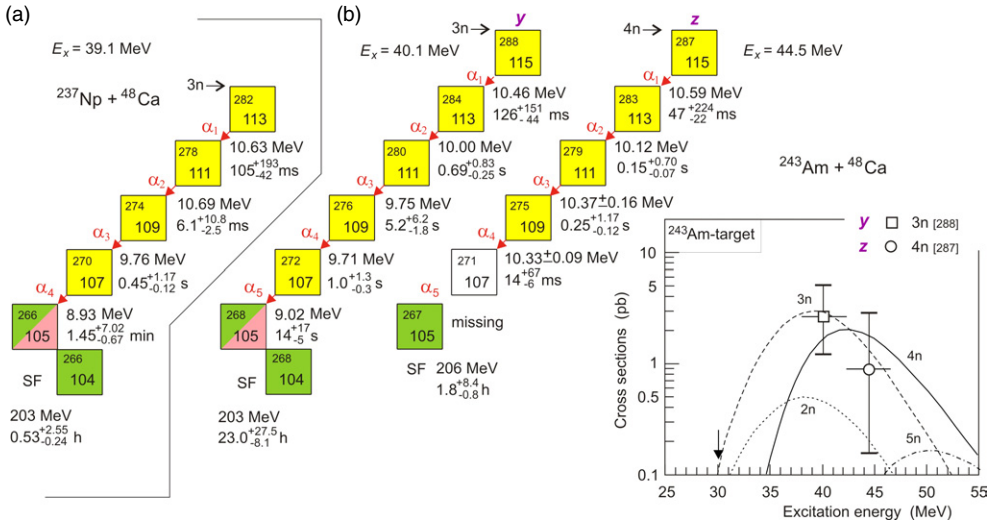

Figure 23. (a) Decay chains, observed in the reaction ^{237}Np + ^{48}Ca at excitation energies of the compound nucleus ^{285}113 E_x = 36.9–41.2 MeV, corresponding to the maximum of the 3*n*-evaporation channel (see the text). (b) Correlated decay chains ***y*** and ***z***, obtained in the reaction ^{243}Am + ^{48}Ca at two excitation energies of the compound nucleus (indicated in the figure). For the odd–odd isotopes ^{266}Db and ^{268}Db the data t_{SF}(exp) are comparable with the expected values t_{EC}. Because of this, the experimentally observed spontaneous fission can be assigned to the even–even isotopes ^{266}Rf and ^{268}Rf, respectively. On the right-hand side of the chains the calculated excitation functions of the *xn*-evaporation channels of the ^{243}Am + ^{48}Ca reaction are shown. The points with error bars are the experimental cross sections.

As can be seen from figure 23(b), the decay pattern of these nuclei is similar to that in the previous three chains observed at $E_x \approx 40$ MeV. However, the decay properties are significantly different. The total decay time of this chain is about ten times shorter, and the α-decays are characterized by higher α-particle energies and shorter lifetimes; in particular, the α-particle energies of the third and fourth nuclei in the last chain are larger by about 0.6 MeV. Therefore, this short-lived decay chain originates from another parent nucleus.

The aforementioned R-α_1-…-α_5-SF decay chains, observed at $E_x \approx 40$ MeV, corresponding to the expected maximum for the yield of the 3*n*-evaporation channel, were not seen at $E_x \approx 44.5$ MeV. That is in agreement with expectations for the 3*n*-evaporation channel. Consistent with this observation, the shorter lived decay chain was not observed at $E_x \approx 40$ MeV. It is most probable that this shorter lasting decay originates from the parent odd–even isotope ^{287}115, produced in the reaction ^{243}Am(^{48}Ca, 4*n*) at the higher excitation energy, $E_x = 44.5$ MeV. The corresponding cross section amounts to $\sigma_{4n} = 0.9^{+3.2}_{-0.8}$ pb.

In the single decay chain originating from ^{287}115, we assume that we have missed the α-decay of ^{271}Bh. Indeed, in four decay chains, in total 19 α-particles were registered, using a detector with 87% efficiency. Thus, the loss of one α-particle seems rather probable. Because of the high energies and relatively long decay times of the four observed α-particles, they could not be assigned to the decays of nuclei with $Z \leqslant 107$. The expected T_α value for ^{271}Bh is ∼10 s ($Q_\alpha = 9.07$ MeV [39], $T_\alpha \approx 5$ s for an allowed transition). This is much shorter than the interval between the last observed α-particle and the terminating SF-event, but is much longer than the intervals between the observed correlated α-particles. The assignment of SF to ^{271}Bh would result in a Q_α upper limit for this isotope at 0.7 MeV lower than the calculated

value [39] (applying a hindrance factor of 5). Therefore, we assume that an unobserved α-decay of ^{271}Bh occurred in the time interval between the fourth α-particle and the spontaneous fission.

In this decay chain, the SF occurs directly in the decay of ^{267}Db, since the calculated α-decay and EC-decay energies for this nucleus are rather low ($Q_\alpha = 7.41$ MeV [39], $T_\alpha \sim 10$ d; $Q_{EC} = 0.79$ MeV [157], $T_\beta \sim 1$ d [158]) and its expected partial half-lives significantly exceed the observed time interval of 106 min.

4.3.2. Elements 113 as an evaporation product. Having synthesized the isotopes with $Z = 113$ as α-decay products in the ^{243}Am + ^{48}Ca reaction, we also tried to synthesize element 113 as an evaporation residue of the ^{237}Np + ^{48}Ca reaction. According to calculations and all earlier investigations with ^{48}Ca-induced reactions, the highest cross section is expected for the $3n$-evaporation channel leading to the formation of the odd–odd nucleus ^{282}113 ($N = 169$). The data of this experiment are at present being analysed and the results shown below are only preliminary.

During a 970 h run, a beam dose of 1.1×10^{19} projectiles was delivered to the ^{237}Np-target. In the given experiment, at the beam energy $E_{Lab} = 244$ MeV (the excitation energy interval of the compound nucleus ^{285}113 is $E_x = 36.9$–41.2 MeV), two events were observed. The experimental conditions (see table 1) and the properties of the nuclei in the decay chains (figure 23(a), it is shown without a symbol) imply that most probably these events can be assigned to the evaporation product of the reaction ^{237}Np(^{48}Ca, $3n$)^{282}113.

In the first event, the registration of the recoil nucleus and the α-particle with an energy $E_{\alpha 1} = 10.62$ MeV and decay time $t_{\alpha 1} = 88.9$ ms switched the beam off. All the following decays were observed without background from the projectiles coming from the separator. The second α-particle with an energy $E_{\alpha 2} = 10.69$ MeV was registered after $t_{\alpha 2} = 6.2$ ms. The third α-particle with an energy $E_{\alpha 3} = 10.02$ MeV was detected after $t_{\alpha 3} = 472.6$ ms only by the side detector (without a position signal). The probability of random registration of this α-particle is $\sim 10^{-3}$. After $t_{\alpha 4} = 87.98$ s, a fourth α-particle was observed with $E_{\alpha 4} = 8.93$ MeV. In 31.74 min after the emission of the fourth α-particle, spontaneous fission was registered as two fission fragments with $E_{tot} = 174$ MeV.

For the second event, the first three α-transitions, $E_{\alpha 1} = 10.64$ MeV, $t_{\alpha 1} = 122.7$ ms; $E_{\alpha 2} = 10.80 \pm 0.76$ MeV (the side detector), $t_{\alpha 2} = 5.8$ ms and $E_{\alpha 3} = 9.76$ MeV, $t_{\alpha 3} = 810.1$ ms, are consistent with those observed for the first event. Unfortunately, the high registration threshold for the third α-particle ($E_{\alpha 3} \geqslant 9.9$ MeV) did not prolong the beam-off time. This switched the beam on, which increased the probability of random coincidences in the last two long decays (the fourth α-particle and the single SF-fragment). At the same time, the probability of random correlation of the first three decays R-α_1-α_2-α_3 lasting <1 s amounts to 4×10^{-6}. This event may be used for clarifying the parameters of the first decay chain and determining the cross section of the reaction ^{237}Np(^{48}Ca, $3n$)^{282}113. The corresponding cross section at 244 MeV ^{48}Ca-ion energy amounts to $\sigma_{3n} = 0.9^{+1.6}_{-0.6}$ pb.

4.4. Chemical experiments

The chemical studies on the superheavy elements comprise a new field in the setting up of experiments aimed at the synthesis and investigation of the properties of the heaviest nuclei. The sophisticated methods successfully applied for the actinides and the first trans-actinide elements turned out to be useless as soon as the half-lives of the heavier nuclei reached $T_{1/2} \leqslant 1$s. It should be noted that the majority of the trans-actinide nuclei and all nuclides, produced in cold fusion reactions, were synthesized and identified by means of physical

methods determined by the short half-lives. At the same time, one of the direct methods of atomic-number identification is based on classical chemical methods, which were long ago used in the first identification and characterization of many of the artificial elements heavier than uranium (see, e.g., [159] and references therein). Obviously, the investigation of the chemical properties of the new nuclides is of separate interest in connection with the study of the structure of superheavy atoms and of the chemical behaviour of the heavy and superheavy elements.

Such a possibility is now opened for a series of neutron-rich relatively long-lived nuclei synthesized in Act. + ^{48}Ca reactions. As it follows from the results presented above, such nuclei are the ones with odd proton number and/or odd neutron number, formed in the α-decay sequences of isotopes with $Z \geqslant 114$. It is seen from table 3 that some of them have half-lives ranging from several seconds to $\sim$1 d, times reachable by radiochemical methods. Further below we shall describe the setting up of the experiments and shall present the results on the chemical isolation of two nuclides: ^{268}Db ($T_{SF} \approx 1.2$ d) and ^{283}112 ($T_{\alpha} \approx 4$ s). These results are compared with the data from DGFRS.

4.4.1. Chemical separation of ^{268}Db. As shown above, the longer lived R-α_1-...-α_5-SF decay chains terminated by a SF-nuclide ($T_{SF} = 16^{+19}_{-6}$ h) were associated with the decay of the odd–odd isotope ^{288}115, produced in the 3n-evaporation channel of the ^{243}Am + ^{48}Ca reaction. Since all consecutive α-decays and SF are strongly correlated with each other and the order of occurrence of the nuclei in the decay chains is determined, *the identification of the atomic number of any nucleus in this chain* would independently prove the synthesis of the previously unknown elements 115 and 113.

According to the atomic configuration in the ground state, Db should belong to the 5th group of the periodic table, as a heavier homologue of Nb and Ta. The chemical behaviour of Db has been investigated through the study of the 34 s ^{262}Db both in a solution as chloride or fluoride and in the gas phase as volatile bromides and chlorides [160, 161]. For the purpose of chemical identification, Db can be separated, along with the members of chemical group 5, from the other elements. For this purpose, we developed a method of sorption extraction for the group-5 elements as anionic fluoride complexes. Keeping in mind that the $Z = 105$ isotope of interest undergoes spontaneous fission, special attention was paid to separating the group-5 elements from the actinides and, most important, from SF-isotopes, e.g., ^{252}Cf and ^{254}Cf. Here, we shall not give details of the chemical method used for separation of the elements of group 5 (they can be found in the original papers [126–128]), but rather we shall describe the setup of the experiment and shall give the main results.

The 32 cm^2 rotating target consisted of the enriched isotope ^{243}Am (99.9%) in the oxide form. The target material was deposited onto 1.5 μm Ti foils to a thickness of about 1.2 mg cm^{-2} of ^{243}Am. It is noteworthy that in comparison with the experiment at DGFRS, the target thickness is three times bigger. On leaving the target, the recoiling products stopped in a 50 mm diameter copper block positioned on the beam axis, 100 mm downstream from the target. The collection efficiency of EVRs (angular acceptance $\pm 12.5^{\circ}$) was close to 100%. The range of recoils in the catcher did not exceed 3–4 μm. After the end of the irradiation, a 7 to 10 μm layer (120–180 mg of Cu) was cut from the catcher surface using a micro-lathe and dissolved in 10 ml of concentrated HNO_3.

The final nitric acid solution contained a large amount of copper (the catcher material), unwanted reaction products from transfer, fusion–fission and induced fission reactions with the ^{243}Am target, as well as products of the reactions of ^{48}Ca with Cu. To monitor the performance of the chemical procedure for the isolation of the group-5 elements and for determination of the suppression factor for actinides, aliquots of nitrate tracer solutions, containing ^{92m}Nb, ^{177}Ta

and the rare earth isotopes ^{169}Yb and ^{167}Tm, were added to the dissolved reaction products. The trans-actinides ($Z \geqslant 104$) were separated by sorption onto Dowex 50 × 8 cation-exchange resin with subsequent desorption using 1 M HF, which forms anionic fluoride complexes of groups 4 and 5 elements. It was determined that ^{92m}Nb and ^{177}Ta—the group-5 elements—were isolated with efficiency of about 80%, and the actinides were suppressed by a factor higher than 10^5. As the final step of the chemical procedure, the column eluant (∼0.1 ml) was deposited onto a 0.4 μm polyethylene foil. All procedures starting from the end of irradiation until the beginning of detector measurements took 2–3 h.

For the registration of α-particles and spontaneous-fission fragments, the sample was placed between two 6 cm^2 silicon detectors. Four chambers with detectors were located inside a neutron detector for the registration of spontaneous-fission neutrons. The neutron detector had 72 ^{3}He-counters distributed in a polyethylene moderator as three concentric rings at different distances from the chambers with the counting samples. The detector array was calibrated with ^{248}Cm and ^{252}Cf sources. The efficiency for detection of fission fragments was about 90%, for neutrons the average efficiency was about 40%. In the course of the 330 h test run, performed before the experiment, not a single SF-event was detected.

In June 2004, a total of eight similar irradiations of duration between 20 and 45 h each were performed. The target was bombarded by ^{48}Ca ions with an energy corresponding to 247 MeV in the middle of the target. The resulting excitation energy of the compound nucleus ^{291}115 was $E_x = 35.0$–43.8 MeV, practically covering the entire energy interval of the $3n$-evaporation channel of the ^{243}Am + ^{48}Ca reaction, leading to the isotope ^{288}115. A total beam dose of 3.4×10^{18} was collected in this experiment.

In eight irradiations of the ^{243}Am target with ^{48}Ca ions, 15 spontaneous-fission events were detected. The measurements were carried out for 957 h. All SF-events appeared in a 174 h interval following the start of the measurements. No events were detected in the next 783 h. Run conditions and results of measurements (fission fragment energies corrected for losses in the source and backing layer, numbers of neutrons detected by the ^{3}He-counters for every fission event and SF-events registration times from the beginning of the measurement) are given in [126, 127].

A ninth irradiation was carried out under the same conditions, at the same beam energy as in the previous eight runs, but *without chemical separation* of the reaction products. The goal of this experiment was to determine the background of SF-nuclei (mainly Cf isotopes) implanted into the catcher. After the end of the irradiation (the beam dose was 2.9×10^{17}), the detection rate of about 2 SF/day was virtually unchanged throughout the duration of counting. The separation factor of group-5 elements from the actinides being $\geqslant 10^5$, the spontaneous fission of all actinide isotopes including ^{252,254}Cf and ^{264}Lr could yield no more than 0.02 events in 174 h.

It should be noted that in the given method two elements with $Z = 104$ and 105 are separated. At the same time, the reaction mechanism, as well as the decay properties of even-Z nuclei, excluded the assumption that the observed SF activity belonged to the decay products of element 114. Indeed, the isotopes of element 114 can be obtained only in (p, xn)-channels of the reaction ^{243}Am + ^{48}Ca. Reactions with the emission of protons and α-particles were not observed neither in cold nor in hot fusion reactions, induced by projectiles with $A > 40$ and leading to heavy nuclei in numerous previous experiments (see, e.g., [60, 139, 140, 148–156]). They have a lower probability in comparison with xn-evaporation channels. The data from our experiments are additional direct illustration of this. Among the 48 decay sequences from the decay of even-Z nuclei, obtained in the reactions ^{238}U, ^{242}Pu, ^{245}Cm and ^{249}Cf + ^{48}Ca, not a single one could be attributed to the decay of the isotopes of elements 115, 113 or 111, which were seen in the experiments using the ^{243}Am + ^{48}Ca reaction. On the other hand, in

Table 2. Results obtained with DGFRS and in the chemical experiments in the ^{243}Am + ^{48}Ca reaction.

Separation method	Recoil separator	Radiochemical separation
Separation efficiency	35%	80%
Detection method	Decay chains of nuclei with $Z = 115$	SF of nuclei with $Z = 105$
^{48}Ca-beam energy in the middle of the target layer	246 MeV	247 MeV
Total ^{48}Ca-beam dose	4.3×10^{18}	3.4×10^{18}
Thickness of the ^{243}Am target	0.36 mg cm^{-2}	1.2 mg cm^{-2}
Number of detected SF-events	3	15
Formation cross section for the nuclei with $Z = 115$	$2.7^{+4.8}_{-1.6}$ pb	$4.0^{+1.4}_{-1.1}$ pb
Half-life	16^{+19}_{-6} h	32^{+11}_{-7} h
Total kinetic energy of fission fragments	≈225 MeV	≈230 MeV
Average neutron multiplicity per fission	–	≈4.2
Identification method of SF-decaying nuclei in the reaction ^{243}Am + ^{48}Ca	Excitation functions and decay properties ($Z = 115$)	Isolation of group-5 elements ($Z = 105$)

the on-line ^{243}Am + ^{48}Ca experiment, at the total beam dose of 9×10^{18}, we observed no isotopes of element 114 that could be the products of (p, xn)-reaction channels for $1 \leqslant x \leqslant 4$. According to decay characteristics, among all the synthesized isotopes of element 114, only the nucleus ^{287}114, with a probability of about 8%, decays into the final nucleus ^{267}Rf ($T_{SF} \sim$ 1.3 h). In the chosen time schedule for irradiation (20–45 h), chemical separation (2–3 h) and measurement (960 h), the probability to register the decay of the ^{287}114 nucleus is negligibly small. Therefore, all 15 SF-events, observed in the chemical experiment, pertain to decay of the group-5 nuclide ($Z = 105$).

Nevertheless, the chemical experiments, with separation of the isotope ^{268}Db in the ^{243}Am + ^{48}Ca reaction, were continued. In the second experiment, a more sophisticated method was used. It made it possible to completely separate the elements of group 5 (Nb, Ta, Db) from the elements of group 4 (Zr, Hf, Rf), as well as to separate the homologues Nb and Ta. In this experiment five events, corresponding to the decay of ^{268}Db, were observed, all of them in the group-5 fraction, in agreement with its relationship to the closest homologue—Ta [128].

The parameters of both the DGFRS and the chemistry experiments and the decay properties of the final SF-nuclide, observed after five consecutive α-decays in the ^{243}Am + ^{48}Ca reaction, are presented in table 2. Over the course of the two chemistry experiments, 20 decays of a SF-nuclide were observed with $T_{1/2} = 28^{+11}_{-4}$ h and a total deposited energy $E_{tot} \approx 230$ MeV [126–128]. The production cross section for SF-nuclei, produced in the ^{243}Am + ^{48}Ca reaction, was $4.2^{+1.6}_{-1.2}$ pb. These results agree with the original element-115 synthesis experiment with DGFRS, where the same SF activity was first observed as the terminating isotope, following the five consecutive α-decays from the ^{288}115 parent nucleus.

Thus, the data from the chemistry experiment give independent identification of the atomic number of all nuclei in the correlated decay sequence: $Z = 115 - \alpha \rightarrow 113 - \alpha \rightarrow 111 - \alpha \rightarrow 109 - \alpha \rightarrow 107 - \alpha \rightarrow$ **105** (SF). Moreover, it gives evidence of the synthesis of two new elements 115 and 113 in the reaction ^{243}Am + ^{48}Ca.

4.4.2. Chemistry of element 112. The above-discussed case concerning the chemical identification of the long-living nuclide ^{268}Db can also be applied for another SF-nuclide, namely ^{267}Rf ($T_{SF} \approx 1.3$(h)), which terminates the long decay sequence of even-Z nuclei: $^{291}116(\alpha) \rightarrow {}^{287}114(\alpha) \rightarrow {}^{283}112(\alpha) \rightarrow {}^{279}110(\mathrm{SF}/\alpha) \rightarrow {}^{275}108(\alpha) \rightarrow {}^{271}106(\mathrm{SF}/\alpha) \rightarrow {}^{271}104(\mathrm{SF})$, see figure 25. Unfortunately, the high probability for spontaneous fission of the preceding nuclei ^{279}110 and ^{271}106 reduces by more than one order of magnitude the effective production cross section of this nucleus. In order to surpass this limitation, it is reasonable to study heavier nuclei with $Z > 110$ applying express radiochemical techniques. We should note that such methods were widely used in earlier studies of the chemical properties of short-lived isotopes of elements 104–108 [154, 160–162].

As is seen from the properties of nuclei in the observed decay chains, the most suitable for this purpose are the odd isotopes of element 112: ^{283}112 ($T_{1/2} \approx 4$ s) and ^{285}112 ($T_{1/2} \approx 30$ s), undergoing α-SF decay. Below we shall discuss the experiment aimed at the study of the chemical properties of the ^{283}112 isotope; in a similar way, the longer lived isotope ^{285}112 could be investigated.

According to the atomic configuration in the ground state, element 112 should belong to the 12th group of the periodic table as a heavier homologue of Hg, Cd and Zn. From Monte Carlo calculations follows that at room temperature the behaviour of Hg atoms is evidence of their high volatility. As it has been shown in the experiments [163], the Hg atoms in neutral gaseous atmosphere (e.g., in He or Ar at atmospheric pressure) can be transported together with the buffer gas to a significant distance (∼30 m) with a velocity of up to 5 m s^{-1}. The elements that are lighter than Hg (Au, Pt, . . . , down to Xe) and their chemical homologues, the elements with $Z < 112$ down to Rn, are not volatile. Because of this, a system that uses a capillary tube as means of transport to a rather long distance (during the motion through the capillary an atom experiences more than 10^5 collisions with the internal surface) has extremely high selectivity when separating the volatile elements such as Hg and 112.

The chemical behaviour of Hg and element 112 is a different question. To what extent element 112 is a homologue of Hg depends on the so-called relativistic effect in the electronic structure of the superheavy atom. According to some relativistic calculations, the chemical behaviour of element 112 (as well as of the other atoms with higher atomic number) will somewhat differ from that of its light homologue. The predictions claim an increased chemical stability of the elemental atomic state for element 112 and a noble-gas-like inertness similar to radon [164]. In contrast, other calculations of the full electronic structure of the element-112 atom predicted its chemical behaviour like a noble transition metal [165]. Recently, relativistic density functional calculations of the stability of molecules between element 112 and a noble metal (interaction of element 112 with gold clusters) predicted a behaviour close to Hg [166]. Will element 112 as actively as Hg interact with Au or just the opposite—will it be closer to the chemically neutral Rn?

The simultaneous study of the chemical behaviour of Hg, Rn and element 112 makes it possible to get an answer to this question and experimentally check the theoretical predictions. In this sense, the commissioning of such an experiment is aimed not only to the identification of the atomic number 112, but is rather broader, because for the first time simultaneously the chemical properties of the superheavy element are investigated.

Both characteristics, the high volatility and the ability to form inter-metallic compounds, defined the experimental setup for the chemical identification of element 112. The first experiments were carried out with the reaction ^{238}U + ^{48}Ca. The method aimed at registering a long-living isotope ($T_{SF} \sim 3$ min) [143]; however, its properties, as was mentioned above, were not confirmed in the following experiments at DGFRS. The relatively low cross section of this reaction and slow transport, as well as the technical difficulties in the measurement of rare

SF-events by registration of only one fission fragment during the long-running experiment, did not allow making confident conclusions about the chemical behaviour of element 112 [167]. In the third experiment, which will be outlined in the following, a faster and more sophisticated technique was used to study element 112 in different assumptions concerning its chemical properties.

The reaction ^{242}Pu(^{48}Ca, $3n$)^{287}114-α $\rightarrow$ ^{283}112 was used to produce the isotope ^{283}112. Its cross section, as it follows from experiment (see above), is higher than for the ^{238}U(^{48}Ca, $3n$)^{283}112 reaction.

The recoil nuclei leaving the ^{242}Pu-target stopped in a high-purity gaseous medium: He(70%) + Ar(30%). The energy of the ^{48}Ca beam at the middle of the target was $E_{\mathrm{Lab}} =$ 245 MeV, which for a 1.4 mg cm^{-2} thick target corresponded to the maximum yield of the isotope ^{287}114 ($T_{1/2} \approx 0.5$ s)—the product of the $3n$-evaporation channel of the fusion reaction ^{242}Pu + ^{48}Ca (see figure 17(b), sequence ***o***). To the ^{242}Pu-target (99.93%) about 15 μg cm^{-2} of $^{\mathrm{nat}}$Nd was added; this allowed to simultaneously produce the neutron-deficient short-lived α-radioactive ^{185}Hg isotope having a half-life of 49 s, which served to monitor the production and separation processes.

The recoiling nuclei, which stopped in the He/Ar medium, were transported to the detectors by means of a 8 m capillary tube (the inner diameter was 1.5 mm). The total transport time from the reaction chamber to the detectors was 3.6 s. This time is long enough for the decay ^{287}114(0.5s)-α $\rightarrow$ ^{283}112. Also, only about 50% of the daughter nuclides ^{283}112 reached the detector chamber.

The setup COLD [168] consists of 32 pairs PIPS (passivated ion-implanted planar silicon) detectors, about 1 cm^2 each, placed one opposite the other with a 1.5 mm gap in between, through which the He/Ar gas flows. One of the detectors of each pair was covered with a 30–50 nm gold layer. The temperature gradient along the whole length of the detectors spanned a range from -24 °C to -184 °C in the first experiment and from +35 °C to -180 °C in the second one. The energy resolution for α-particles' decay amounted to 120 keV. The SF fission fragment energy was calibrated using a thin ^{248}Cm source.

In the control experiments, only α-particles from the decay of $^{181-188}$Hg (the fusion $^{\mathrm{nat}}$Nd + ^{48}Ca reaction), ^{211}At and ^{219,220}Rn were observed. As it was expected, only nuclei with high volatility were transported to the detectors. It was shown that all Hg atoms are registered by the first detectors with the Au coating. This can be explained by the strong adsorption on the detector Au-surface, which is due to the chemical reaction leading to the production of the Hg/Au compound (adsorption enthalpy $-\Delta H_{\mathrm{ads}} \approx 98$ kJ mol^{-1} [168]). In contrast, the decay of the chemically neutral Rn atoms is observed in the region of the last detectors, which are at the lowest temperatures (figure 24), consistently with the adsorption enthalpy of Rn ($-\Delta H_{\mathrm{ads}} \approx 30$ kJ mol^{-1} on gold and $\approx$20 kJ mol^{-1} on ice [169, 170]). In these conditions, the atoms of element 112 must be between these two extreme cases, their position (detector number) depending on their chemical properties.

Two events from the decay of ^{283}112 were observed in the detector chamber (figure 24). In the first case, the sequence α-SF with $E_\alpha = 9.38 \pm 0.12$ MeV and then 0.59 s later the two fragments with total kinetic energy TKE = 231 MeV were registered by the second pair of detectors with the Au-surface at temperature -28 °C (the temperature conditions for detectors 1–32 were in the range -24 °C to -184 °C). In the second case, the same α-SF sequence ($E_\alpha = 9.47 \pm 0.12$ MeV, $t_{\mathrm{SF}} = 0.54$ s, TKE = 232 MeV) was registered by the seventh detector pair again on the Au-surface, which was at -5 °C (the temperature conditions for detectors 1 to 32 were in the range +35 °C to -180 °C). Both events are consistent with the properties of the decay of the ^{283}112 nucleus (see the sequences ***o*** in figure 17(b) and table 3). While the first event practically follows the location of the Hg atoms, the second one

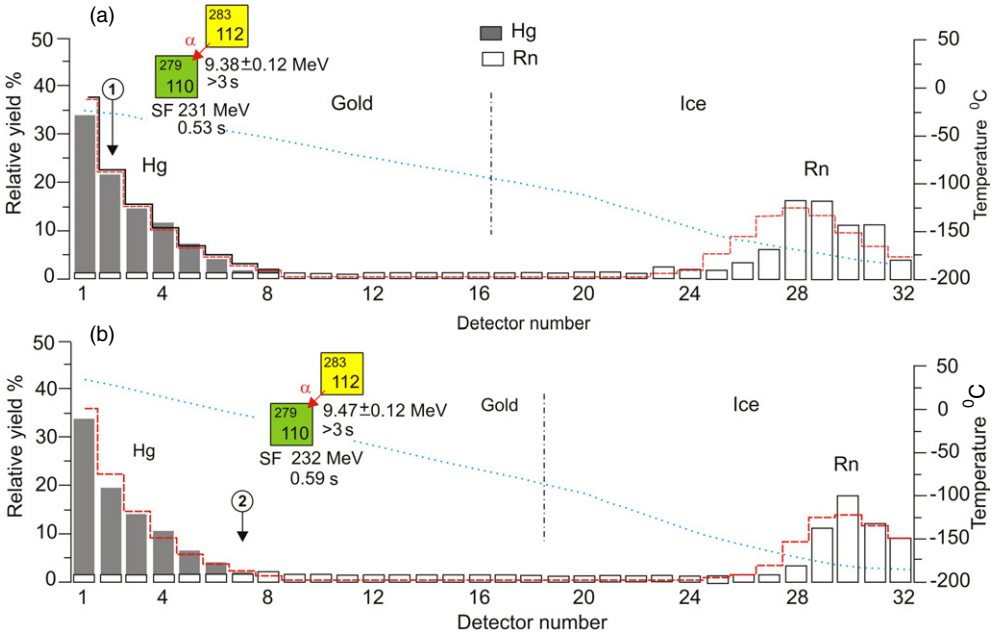

Figure 24. Results of thermo-chromatographic separation of element 112, produced in the reaction ^{242}Pu(^{48}Ca, 3n)^{287}114-$\alpha \rightarrow {}^{283}$112. The dotted blue lines (right-hand axis) denote the temperature distribution along the 32 detectors from the two experiments. The relative yields of the 49s-^{185}Hg and 3.7s-^{219}Rn are shown together with the observed decays of 3.8s-^{283}112 (black arrows) as a function of the detector number. (a) The Monte Carlo simulation [171] of the adsorption process of Hg and Rn on the gold surface and ice is shown by the red dashed line. The temperature gradient is −24 °C to −184 °C. (b) Same as (*a*) at the temperature gradient +35 °C to −180 °C. Figure and numbers are taken from [172].

somewhat differs (the probability of Hg hitting the 7th detector is about 3%). This may mean weaker adsorption of element 112 with gold compared to Hg, but it is obviously stronger than expected for noble-gas-like behaviour. Avoiding the details, they will be given in a separate publication [172] (experiments with the isotopes ^{283}112 and ^{285}112 will be continued), even now from the obtained data a conclusion can be drawn that the isotope ^{283}112 by its chemical properties is related to the group 12 elements. The production cross section of ^{283}112 in the reaction ^{242}Pu(^{48}Ca, 3n)^{287}114-$\alpha \rightarrow {}^{283}$112 is estimated as 2–4 pb depending on the adsorption properties of the parent nucleus ^{287}114 at room temperature (from the DGFRS measurements $\sigma_{3n} = 3.6^{+3.4}_{-1.7}$ pb [121]).

The results of the given experiment in an independent way confirm the identification of the atomic numbers of the nuclides in the even-Z nuclear decay chain $^{291}116 \rightarrow {}^{287}114 \rightarrow$ **^{283}112** $\rightarrow {}^{279}110 \rightarrow {}^{275}108 \rightarrow {}^{271}106 \rightarrow {}^{267}104$.

The luminosity of the chemical experiment can be improved several times by means of increasing the beam intensity (rotating target) and the velocity of transporting the recoiling ions to the detectors. At the same time, in the same experimental conditions, it is possible to investigate another long-lived isotope, ^{285}112 ($T_{1/2} \approx 30$s), produced in the ^{244}Pu + ^{48}Ca reaction. Finally, the evaporation residue—the isotope ^{289}114 ($T_{1/2} \approx 3$s)—can be used for setting up experiments on the chemistry of element 114. All this demonstrates the perspectives provided by Act. + ^{48}Ca for the study of the chemical properties of superheavy elements.

5. Discussion of the results

5.1. Decay properties of superheavy nuclei

The decay properties of the 34 new nuclides, produced in experiments with ^{48}Ca-projectiles, are given in table 3. Here the total number of events corresponding to the decay of nuclides of given Z and A is shown, independent of how they were produced: as evaporation residues or as daughter nuclei after the α-decay/s of heavier precursors. The modes of decay, shown in the fourth column of table 3, mean that all observed events are identical for the given decay mode. In those cases, where two decay modes (α, SF) were observed, an approximate branching ratio, governed by the statistical error of registered events, has been estimated. The values of T_α expected for the measured Q_α (see below) are presented in the sixth column.

The identification of the atomic numbers of the nuclides was performed in several independent ways based on

- the mechanism of fusion reactions (excitation functions and cross bombardments ensuring variation of the proton and neutron numbers in the compound nucleus);
- the decay properties of the nuclei in the decay sequences (half-lives T_α and α-decay energies Q_α of even–even (and for many even–odd) isotopes;
- the radiochemical identification of the atomic number of the nuclides ^{268}Db and ^{283}112 in correlated α-decay chains of the nuclei 115 $\rightarrow$ 113 $\rightarrow$ Rg $\rightarrow$ Mt $\rightarrow$ Bh $\rightarrow$ (Db) and 116 $\rightarrow$ 114 $\rightarrow$ (112) $\rightarrow$ Ds $\rightarrow$ Hs $\rightarrow$ Sg $\rightarrow$ Rf.

All methods give the same identification of the atomic number of the synthesized nuclei. When the atomic numbers of the parent nuclei are determined (showing that they are the products of xn-evaporation channels of complete-fusion reactions), the identification of the mass of an isotope with given decay characteristics (as well as that of the neighbouring nuclei) comes to determination of the number of evaporated neutrons by the compound nuclei formed in the investigated reaction at various excitation energies. This is achieved

- by means of the measured excitation functions ensuring variation of the neutron number in the compound nucleus;
- by producing the same nuclei in different ways: as evaporation residues and as α-decay products of heavier nuclei.

The adjoining four isotopes of the elements with $Z = 112$, 114 and 116, genetically connected with the daughter nuclei by consecutive α-decays, are shifted in mass according to the mass and the excitation energy of the compound nucleus and give a self-consistent determination of the atomic and mass numbers of all nuclides, synthesized in the ^{48}Ca-induced experiments (figure 25).

Further verification of the identification of the mass number of the isotopes follows from the decay properties. Because of the high suppression of spontaneous fission of nuclei with odd neutron numbers, their decay chains are longer and the total decay time is noticeably higher than in the neighbouring even-N isotopes. This tendency is well seen for all known isotopes with $Z \leqslant 112$, it also takes place for the synthesized new nuclides with $Z = 112$–116 (figure 25).

Now we shall discuss the decay properties of the synthesized nuclei.

5.1.1. Alpha decay. As can be seen from table 3, the odd isotopes of element 112 and all isotopes (even and odd) with $Z \geqslant 113$ predominantly undergo α-decay. The spectra of the α-particles in most cases are characterized by well-defined decay energy (the α-lines, see figure 18). This is generally the situation for allowed ground-to-ground-state transitions at

Table 3. Decay properties of nuclei.

Z	A	Number of observed[a]	Decay mode, branch (%)[b]	Half-life[c]	Expected half-life[d]	E_α (MeV)	Q_α (MeV)
118	294	3 (3/3)	α	$0.89^{+1.07}_{-0.31}$ ms	0.4 ms	11.65 ± 0.06	11.81 ± 0.06
116	293	4 (4/4)	α	61^{+57}_{-20} ms	80 ms	10.54 ± 0.06	10.69 ± 0.06
	292	5 (4/5)	α	18^{+16}_{-6} ms	40 ms	10.66 ± 0.07	10.80 ± 0.07
	291	3 (3/3)	α	18^{+22}_{-6} ms	20 ms	10.74 ± 0.07	10.89 ± 0.07
	290	10 (10/10)	α	$7.1^{+3.2}_{-1.7}$ ms	10 ms	10.84 ± 0.08	11.00 ± 0.08
115	288	3 (3/3)	α	87^{+105}_{-30} ms	60 ms	10.46 ± 0.06	10.61 ± 0.06
	287	1 (1/1)	α	32^{+155}_{-14} ms	30 ms	10.59 ± 0.09	10.74 ± 0.09
114	289	10 (9/9)	α	$2.6^{+1.2}_{-0.7}$ s	2 s	9.82 ± 0.05	9.96 ± 0.05
	288	18 (16/16)	α	$0.80^{+0.27}_{-0.16}$ s	0.9 s	9.94 ± 0.06	10.08 ± 0.06
	287	16 (16/16)	α	$0.48^{+0.16}_{-0.09}$ s	0.5 s	10.02 ± 0.06	10.16 ± 0.06
	286	24 (19/12)	α: 50 SF: 50	$0.13^{+0.04}_{-0.02}$ s	0.2 s	10.19 ± 0.06	10.33 ± 0.06
113	284	3 (3/3)	α	$0.48^{+0.58}_{-0.17}$ s	0.3 s	10.00 ± 0.06	10.15 ± 0.06
	283	1 (1/1)	α	100^{+490}_{-45} ms	140 ms	10.12 ± 0.09	10.26 ± 0.09
	282	2 (2/2)	α	73^{+134}_{-29} ms	6 ms	10.63 ± 0.08	10.78 ± 0.08[e]
112	285	10 (10/10)	α	29^{+13}_{-7} s	50 s	9.15 ± 0.05	9.28 ± 0.05
	284	19 (17/–)	SF	97^{+31}_{-19} ms			$\leqslant 9.80$
	283[f]	22 (19/19)	α: 100 SF: $\leqslant 10$	$3.8^{+1.2}_{-0.7}$ s	3 s	9.54 ± 0.06	9.67 ± 0.06
	282	12 (12/–)	SF	$0.82^{+0.30}_{-0.18}$ ms			$\leqslant 10.69$
111	280	3 (3/3)	α	$3.6^{+4.3}_{-1.3}$ s	0.4 s	9.75 ± 0.06	9.87 ± 0.06
	279	1 (1/1)	α	170^{+810}_{-80} ms	7 ms	10.37 ± 0.16	10.52 ± 0.16
	278	2 (2/1)	α	$4.2^{+7.5}_{-1.7}$ ms	1 ms	10.69 ± 0.08	10.85 ± 0.08[e]
110	281	10 (10/–)	SF	$11.1^{+5.0}_{-2.7}$ s			$\leqslant 9.00$
	279	26 (22/3)	α: 10 SF: 90	$0.20^{+0.05}_{-0.04}$ s	0.2 s	9.70 ± 0.06	9.84 ± 0.06
109	276	3 (3/3)	α	$0.72^{+0.87}_{-0.25}$ s	0.1 s	9.71 ± 0.06	9.85 ± 0.06
	275	1 (1/1)	α	$9.7^{+46.}_{-4.4}$ ms	2 ms	10.33 ± 0.09	10.48 ± 0.09
	274	2 (2/1)	α	445^{+810}_{-176} ms	20 ms	9.76 ± 0.10	9.90 ± 0.10[e]
108	275	3 (3/3)	α	$0.19^{+0.22}_{-0.07}$ s	0.8 s	9.30 ± 0.06	9.44 ± 0.06
107	272	3 (3/3)	α	$9.8^{+11.7}_{-3.5}$ s	3 s	9.02 ± 0.06	9.15 ± 0.06
	270	1 (1/1)	α	61^{+292}_{-28} s	5 s	8.93 ± 0.08	9.06 ± 0.08[e]
106	271	3 (3/2)	α: 70 SF: 30	$1.9^{+2.4}_{-0.6}$ min	0.8 min	8.54 ± 0.08	8.67 ± 0.08
105	268	18 (18/–)	SF/EC	29^{+9}_{-6} h			$\leqslant 7.83$
	267	1 (1/–)	SF	$1.2^{+5.8}_{-0.6}$ h			$\leqslant 8.15$
	266	1 (1/–)	SF/EC	22^{+105}_{-10} min			$\leqslant 8.24$[e]
104	267	2 (2/–)	SF	$1.3^{+2.3}_{-0.5}$ h			$\leqslant 8.21$

[a] Number of observed decays and number of events used for calculations of half-lives/α-particle energies, respectively.
[b] Branching ratio is not shown if only one decay mode has been observed.
[c] Error bars correspond to 68% confidence level if more than one event has been observed. For only one registered event, the error bars correspond to 95%.
[d] Half-lives calculated using the Viola–Seaborg formula (see the text) for α-decay energies, given in the last column.
[e] Preliminary data from the ^{237}Np + ^{48}Ca reaction (see the text).
[f] See also the Note on page R237.

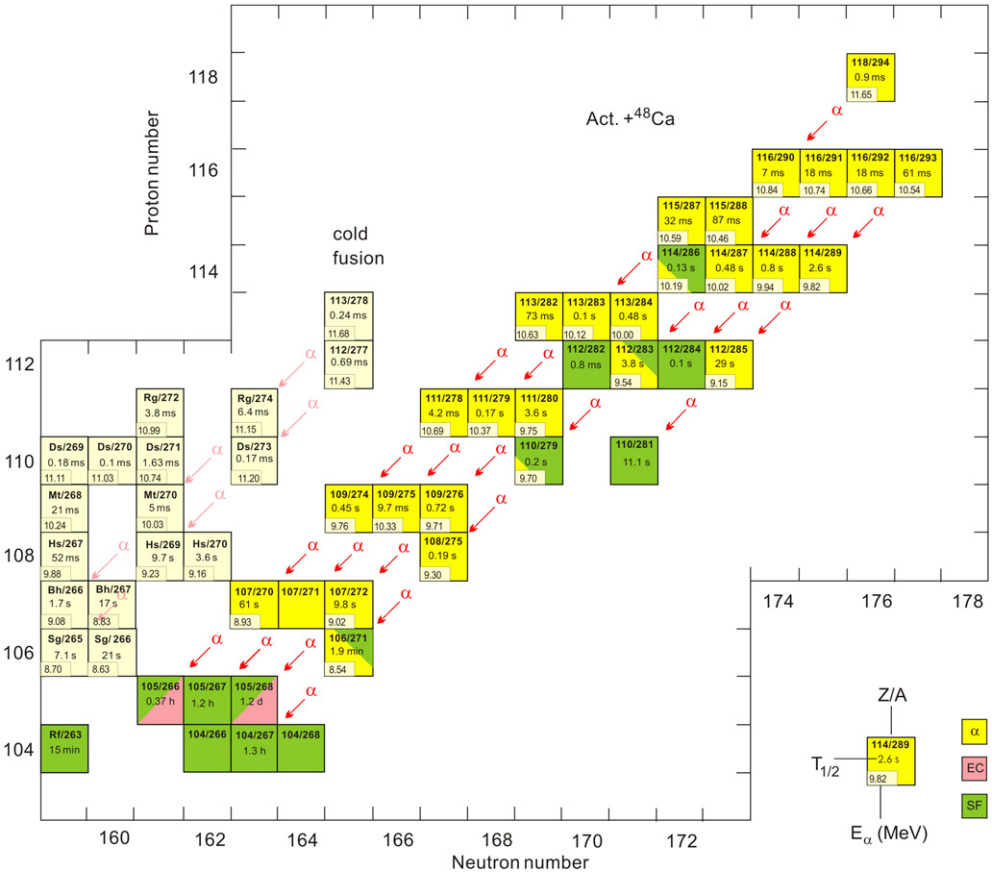

Figure 25. Chart of the heaviest nuclides with $Z \geqslant 104$ and $N \geqslant 159$. The symbols are given in the right lower corner of the figure. To avoid making the figure too complicated, the squares contain the half-lives (without errors) and the maximum α-transition energy (E_α in MeV). For the nuclei synthesized in cold fusion reactions the values of $T_{1/2}$ and E_α are taken from the compilation of [183]; for the products of the reaction Act. + ^{48}Ca (including ^{282}113 and its daughter nuclei) the data are taken from table 3.

$J = 0$ in the α-decay of even–even nuclei. As known from α-decay theory, in this case the probability for the decay (or the half-life T_α) is directly connected to the decay energy Q_α and the atomic number of the nucleus. The Geiger–Nuttall relation [173], connecting these quantities (in the version of Viola–Seaborg [174] or any other version [175–179]), well describes all 65 known even–even nuclei heavier than Pb, for which both partial half-life and decay energies have been measured. The experimental values obtained earlier in hot and cold fusion reactions and belonging to the α-decay of even–even nuclei with $100 \leqslant Z \leqslant 110$ are shown in figure 26. The data for all isotopes with even proton numbers from $Z = 106$ to 118, produced in ^{48}Ca-induced reactions, are presented in the same figure.

The experimental values Q_α(exp) and T_α(exp) with their errors, given in table 3, can be used for the calculation of the atomic numbers of nuclei comprising the chains of correlated decays. For instance, the probability that the consecutive α-transitions observed in the ^{245}Cm, ^{248}Cm + ^{48}Ca reactions take place in the nuclei with atomic numbers $116 \rightarrow 114 \rightarrow 112 \rightarrow 110$ amounts to 0.992. The probability that these chains for some reason can be attributed to the decay of the parent nucleus with $Z = 114$ is $\leqslant 0.005$.

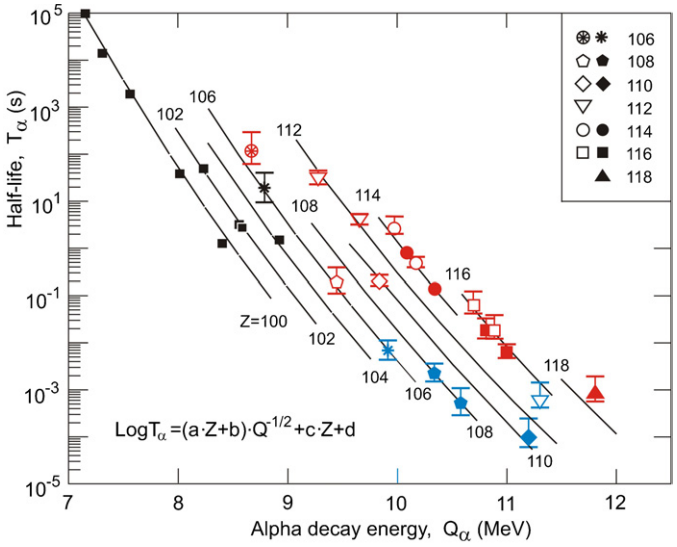

Figure 26. Half-lives T_α as a function of the α-decay energy Q_α for nuclei with even atomic numbers $Z \geqslant 100$ (indicated in the figure). The solid lines represent calculations using the Viola–Seaborg formula (given in the figure) with the parameters $a = 1.787$, $b = -21.40$, $c = -0.2549$, $d = -28.42$ [7]. The filled symbols refer to even–even nuclides, the open ones are for even–odd. Blue symbols refer to the nuclides, obtained in cold fusion, red symbols in Act. + ^{48}Ca reactions.

The half-lives T_α(exp) at measured decay energies Q_α(exp) of the new nuclides, as seen from figure 26, agree well with the calculated values for a given Z. Quantitatively this is seen in the comparison of the data, presented in the fifth and sixth columns of table 3, where the ratio T_α(exp)/T_α(calc) determines the hindrance factor. The agreement for the even–even isotopes is expected and can be explained by the ground-to-ground-state transitions. For odd isotopes, the situation differs slightly from the previous case. In fact, for two isotopes, ^{283}112 and ^{289}114, transitions to excited states of the daughter nuclei ^{271}Ds ($E_x \approx 0.2$ MeV, two events; ≈0.6 MeV, one event) and ^{289}114($E_x \approx 0.35$ MeV, one event), respectively, have been observed. One more event might probably be added to them—it has been registered in the ^{244}Pu + ^{48}Ca reaction as an $\alpha_1 \rightarrow \alpha_2 \rightarrow \alpha_3 \rightarrow$ SF decay sequence and was considered a candidate for the possible decay of the isotope ^{289}114 [180] (scenarios of such a decay were discussed in [27, 181, 182]). The mentioned individual cases do not let us draw a reliable picture of the decay of odd isotopes and determine the characteristics of the low-lying levels of superheavy nuclei, although the population of excited states in α-decay of the parent nucleus depends on the way of its production: as an evaporation residue or as a daughter of a heavier α-precursor. However, it should be noted that these events comprise only a small part ($\leqslant$15%) of the intensity of the main α-transition shown in table 3. Because of this, we may assume that the experimentally observed main decay modes (the corresponding energies Q_α(exp) are given in table 3) are also connected with transitions between ground states. This suggestion is necessary for the comparison with the theoretical models in which the values of Q_α are calculated from the ground-state nuclear masses.

The values of Q_α(th), obtained in the framework of the MM-model in the version of [39, 144] for the isotopes of all elements with even atomic numbers from $Z = 100$ to 118 and with odd atomic numbers from $Z = 103$ to 115, are presented in figures 27(a) and (b), respectively. The experimental values Q_α(exp) for all known α-emitters in the given Z and N

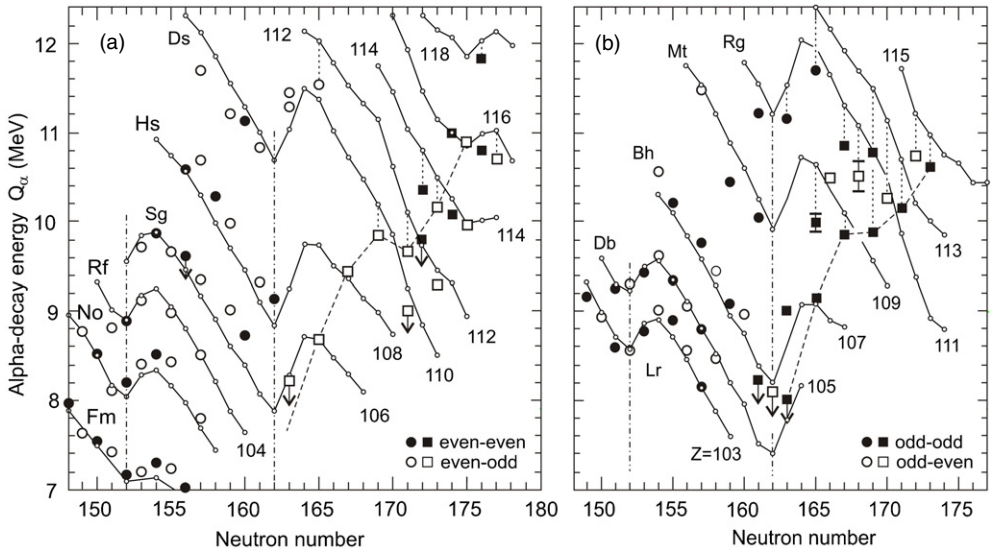

Figure 27. Alpha-decay energy versus neutron number of trans-fermium nuclei. (a) Isotopes of even-Z elements with $Z \geqslant 100$. (b) Isotopes of odd-Z elements with $Z \geqslant 103$. Circles denote nuclei synthesized in hot fusion reactions with light ions (^{22}Ne, ^{26}Mg, ^{36}S) and in cold fusion with massive projectiles; squares correspond to the nuclei, produced in ^{48}Ca-induced reactions. Dashed lines represent long sequences of correlated decays of the nuclei ^{288}115 and ^{291}116, observed in the reactions ^{243}Am + ^{48}Ca and ^{245}Cm + ^{48}Ca (see panel (a)), respectively. The solid lines are drawn through the values of Q_α (small open circles), calculated in the MM-model [39, 144]. The closed neutron shells $N = 152$ and $N = 162$ are shown by the vertical dashed-dotted lines.

intervals, as well as those obtained in reactions with ^{48}Ca, are also shown. It should be noted that for even-Z isotopes the agreement between theory and experiment, which was observed earlier for deformed nuclei located between the closed shells $N = 152$ and $N = 162$, also takes place for the new neutron-rich nuclei with neutron number $N > 162$. According to predictions of the MM-model, at crossing the shell and increasing the neutron number in the region of $N > 162$, the nuclear deformation significantly decreases. Thus, nuclei with neutron numbers $N \geqslant 175$ are close to being spherical ($\beta_2 \approx 0.09$) [144]. The data we have obtained are for nuclei with $Z = 106$–116 and $N = 165$–177, which fall into this transitional region of deformation and, as can be seen from figure 27(a), in general agree with the predictions of the model.

For odd-Z nuclei the data are scarce and the statistics is poor. The parent and daughter nuclei, ^{288}115 ($N = 173$) and ^{284}113 ($N = 171$), are quite away from the deformed shell $N = 162$. Thus, their relatively long half-lives could be caused by the influence of the next, spherical shell $N = 184$. The comparison of the decay properties of the odd–odd isotope ^{278}113 ($N = 165$), observed in two decay chains produced recently in the cold fusion reaction ^{209}Bi(^{70}Zn, $1n$)^{278}113 [73], with those for ^{284}113 ($N = 171$) reveals a reduction of the α-decay energy by 1.7 MeV and a corresponding increase in the half-life by a factor of 2×10^3. The odd–odd isotopes ^{272}Rg ($T_{1/2} = 3.1$ ms) [139, 155, 156], ^{274}Rg ($T_{1/2} = 6.4$ ms) [73], ^{278}Rg ($T_{1/2} = 4.2$ ms) and ^{280}Rg ($T_{1/2} = 3.6$ s) demonstrate comparable behaviour.

For the isotopes $^{278\text{–}280}$Rg and $^{282\text{–}284}$113, the difference between theoretical and experimental Q_α values is 0.6–0.9 MeV. Some part of this energy can be accounted for by γ-ray emission from excited levels, populated during α-decay. For the even-Z nuclei as

well, the agreement between theory and experiment becomes somewhat worse as one moves away from the deformed nuclei in the vicinity of the neutron shells $N = 152$ and $N = 162$ to the more neutron-rich nuclides with $N \geqslant 169$.

The measured T_α(exp) values closely reproduce the calculated ones for the first two nuclei of these chains; thus element 115 and its daughters—the isotopes of element 113—have rather low hindrance factors, if any, for α-decay. For the isotopes of elements Rg, Mt and Bh, the difference between measured and calculated T_α values results in hindrance factors of ∼3–20. These match the hindrance factors that can be extracted for the deformed odd–odd nuclei ^{272}Rg and descendants, produced in experiments with cold fusion reactions [139, 155, 156]. One can assume that in this region of nuclei, a noticeable transition from spherical to deformed shapes occurs at $Z = 109$–111, resulting in a change of the level structures of these nuclei and in an increased probability of α-transitions going via excited states. Another sign of such a change in nuclear shape might be the significant increase in the difference of α-decay energies of the neighbouring isotopes, observed as the decay chains reach $Z = 111$, see figure 27(b). This assumption is in agreement with macroscopic–microscopic calculations [39, 144]. The deformation parameter β_2 was calculated to be 0.072 and 0.138 for ^{288}115 and ^{284}113, respectively. As the decay chain recedes from the shell closure at $Z = 114$ and $N = 184$, β_2 increases to 0.200, 0.211 and 0.247 for ^{280}Rg, ^{276}Mt and ^{272}Bh, respectively. In the decay chain $^{291}116 \rightarrow {}^{287}114 \rightarrow \cdots \rightarrow {}^{267}$Rf we observed a similar variation in α-decay energies (see figure 27(a)). The slope of Q_α versus N remains practically the same for elements 112–116, but increases significantly for the nuclides with $Z = 111$ and 110. Again, such an effect might be caused by the transition from spherical to deformed nuclear shapes during successive α-decays, if we discuss the experimental data from the point of view of MM-models and compare them to the numerical calculations of [39, 144].

As a whole, the predicted Q_α values for the heaviest nuclei, observed in our experiments, are systematically larger than the experimental data. At the same time, the trends of the predictions are in good agreement for the 27 nuclides with $Z = 106$–118 and $N = 163$–177, especially considering that the theoretical predictions match the experimental data over a broad, previously unexplored region of nuclides.

The trend of the $Q_\alpha(N)$ systematics, predicted by theory and confirmed by experimental data for odd-Z isotopes of Mt and Bh along with even-Z isotopes of Ds, can be considered *as direct experimental evidence for the deformed neutron shell closure at $N = 162$*. The stabilizing effect of the $N = 162$ shell can be observed for the Db isotopes. The relatively small change in the half-lives of the known lighter mass isotopes ^{260}Db ($T_{1/2} = 1.5$ s), ^{261}Db ($T_{1/2} = 1.8$ s), ^{262}Db ($T_{1/2} = 34$ s) and ^{263}Db ($T_{1/2} = 27$ s) [135] contributes to the prediction of a considerable increase in T_α for the new heavier isotopes ^{266}Db, ^{267}Db and ^{268}Db with $T_\alpha \geqslant 5 \times 10^2$ s, $T_\alpha \geqslant 5 \times 10^3$ s and $T_\alpha \geqslant 3 \times 10^5$ s, respectively.

The comparison of Q_α(exp) with the values Q_α(th), calculated within the Skyrme-Hartree–Fock–Bogoliubov [27, 181, 182, 184, 185] and the relativistic mean field models [146, 186], is presented in figure 28 for even–even isotopes of elements 112, 114, 116 and 118. In the figure, we have added data for Q_α(th), obtained in two versions of the macro-microscopic model [144, 187]. It can be seen that the best agreement between theory and experiment is achieved in the MM-model, especially in the version of [187]. In the HFB-model, a better agreement is obtained with masses from [184] calculated with 18 parameters. Finally, in the RMF-model in the two versions shown in figure 28, the agreement between theory and experiment is least satisfactory. It cannot be excluded that a better agreement can be achieved in this model too, if a different set of parameters is used.

As a whole, the measured values of Q_α(exp) are in agreement with theory, because the model calculations do not claim to be more precise in determining Q_α(th) than 0.4–0.6 MeV.

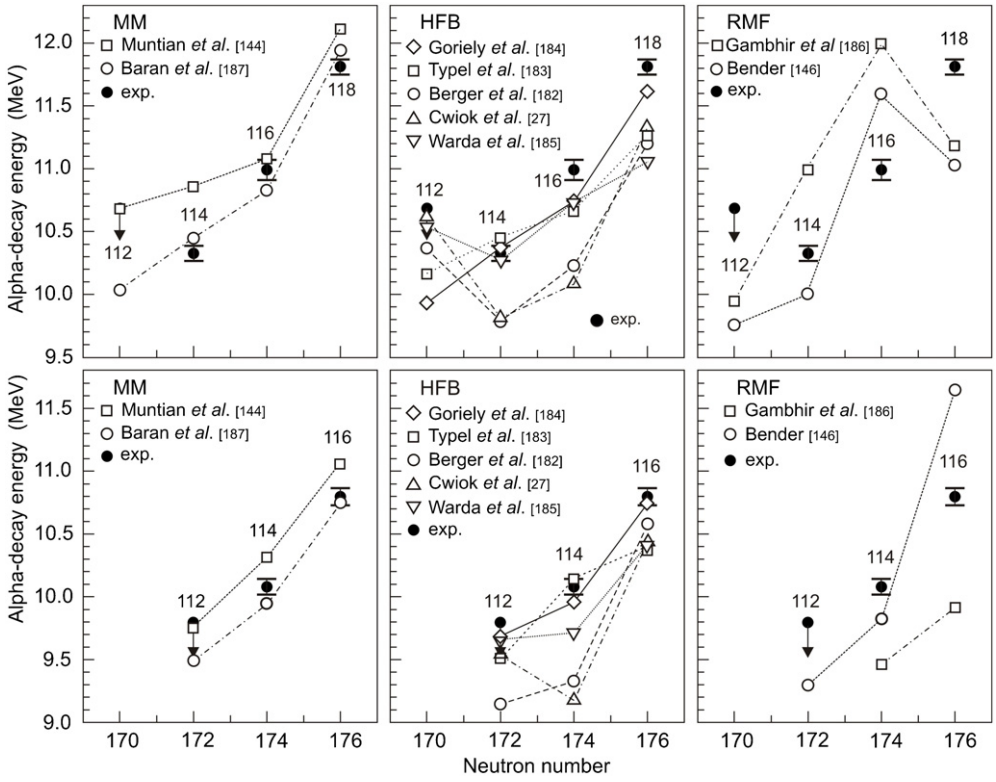

Figure 28. Alpha-decay energy versus neutron number of the even–even isotopes with $Z = 112$–118 and $N = 170$–176. The open symbols are values of Q_α(th), obtained in different versions of ground-state nuclear mass calculations in the framework of the MM-, HFB- and RMF-models. The black points with error bars are experimental data from table 3.

We must recall that all three models predict the same spherical neutron shell at $N = 184$, but different proton shells, $Z = 114$ (MM) and $Z = 120$, 124 or 126 (HFB, RMF). Yet, all describe the experimental data equally well. Such insensitivity with respect to the various models in this region of Z and N can be explained either by the remoteness of the nuclei under consideration from the closed shell at $N = 184$ or by the weaker influence of the proton shells at $Z = 114$ or higher, compared to that of the neutron shell at $N = 184$.

5.1.2. Spontaneous fission. For 8 out of the 34 synthesized nuclei spontaneous fission is the predominant mode of decay (see table 3). In two more nuclei, ^{271}Sg and ^{286}114, spontaneous fission competes with α-decay. For the remaining nuclides spontaneous fission was not observed. The partial SF-half-lives of nuclei with $N \geqslant 163$, produced in fusion reactions with ^{48}Ca, together with the half-lives of SF-nuclides with $N \leqslant 160$, are shown in figure 29(a). Four isotopes of element 112 with $N = 170$–173 are located in a region, where a steep rise of $T_{SF}(N)$ is expected. Indeed, in the even–even isotopes ^{282}112 and ^{284}112 the difference of two neutrons increases the partial half-life T_{SF} by two orders of magnitude. The neighbouring odd isotopes ^{283}112 and ^{285}112 undergo α-decay. For them, only lower limits of T_{SF} can be determined (shown in the figure). From the measured SF-half-lives for the even–even isotopes ^{282}112 and ^{284}112 it follows that the odd neutron in the ^{283}112 nucleus imposes a hindrance to

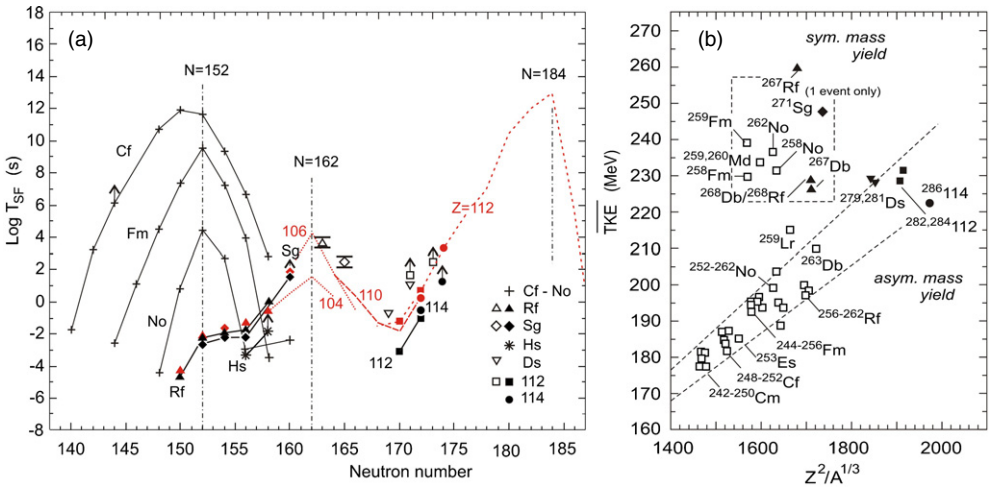

Figure 29. (a) Partial half-lives for spontaneous fission T_{SF} versus N for nuclei with even atomic numbers $Z = 98$–114. Solid symbols and crosses denote even–even nuclei, whereas open symbols denote even–odd nuclei. Black are the experimental data, red the calculated T_{SF} values. Solid black lines are drawn through the experimental points T_{SF}(exp) of even–even nuclei, the red lines through T_{SF}(th), obtained in calculations [25, 188] for even–even isotopes with $Z = 104$–112. (b) Systematics of mean total kinetic energies of fission fragments ⟨TKE⟩ versus the parameter $Z^2/A^{1/3}$. The open squares are experimental data for the isotopes with $Z = 96$–104 [189], the black symbols are the data for SF-isotopes with $Z \geqslant 104$, observed in Act. + ^{48}Ca reactions. The dashed lines conditionally separate the zones of mass-asymmetric and mass-symmetric fission modes.

spontaneous fission of the order of $\geqslant 3 \times 10^3$. Given such a large hindrance factor, it cannot be excluded that one or two decay events of the ^{283}112 nucleus, registered as R-SF chains (see figure 20), can be attributed to the spontaneous fission of the even–odd isotope ^{283}112.

Such a picture is also observed for the even–even isotopes of element 114: the additional two neutrons in the nucleus ^{286}114 ($T_{SF} \approx 0.13$ s) lead to significant increase of the stability of the nucleus ^{288}114 relative to spontaneous fission. In fact, α-decay was registered in 17 out of 18 decay events of the nucleus ^{288}114 ($T_\alpha \approx 0.8$ s), which was produced in the ^{244}Pu(^{48}Ca, $4n$) ^{288}114 and ^{248}Cm(^{48}Ca, $4n$)^{292}116-$\alpha \rightarrow$ ^{288}114 reactions.

It is significant that the rise of stability relative to spontaneous fission is observed for the heavy nuclei with $Z \geqslant 110$ (figure 29(a)), which are 10–12 neutrons further from the closed neutron shell $N = 184$. On moving to the nuclei with $Z < 110$ and $N < 170$ (in the experiments, spontaneous fission was observed for the seven odd nuclides ^{279,281}Ds, ^{271}Sg, ^{267}Db, ^{266,268}Db [SF/EC] and ^{267}Rf), the probability for spontaneous fission decreases again when the closed deformed shell $N = 162$ is approached. The stabilizing effect of the $N = 162$ shell manifests itself in the properties of the even–even isotopes of Rf, Sg and Hs with $N \leqslant 160$, which, as seen from figure 29(a), are also well described by the mentioned model calculations. The odd SF-isotopes with $Z = 104$–110, produced in the ^{48}Ca-induced reactions, are located in the transition region, where the larger the neutron number the smaller the effect of the $N = 162$ shell. In this region, the $N = 184$ shell comes into effect. Such a behaviour of T_{SF}(exp) as a function of Z and N correlates with the SHE fission barrier heights and has been predicted by all models, MM, HFB and RMF.

Given these considerations, several scenarios can be chosen for the decay of the investigated heavy nuclei. For the isotopes with $Z \geqslant 112$ and $N > 172$, the main mode

is α-decay. This is due to the high stability of neutron-rich nuclei relative to spontaneous fission ($T_{SF} \gg T_\alpha$). As a result of the successive α-decays, the neutron number in the daughter nuclei decreases and this, in turn, leads to a significant increase of the probability of their spontaneous fission. The competition T_{SF}/T_α is seen already in the even–odd effects in the isotopes of element 112 with neutron numbers $N = 170$–173. But already the odd isotopes of element 110 with $N \leqslant 171$ practically all undergo spontaneous fission ($T_{SF} < T_\alpha$). However, if we burst through the limit of SF-nuclei, similarly to what we saw for the rare α-decay branch of the isotope ^{279}110, the daughter products—the isotopes ^{275}Hs ($N = 167$) and ^{271}Sg ($N = 165$)—will decay again mainly by emission of α-particles ($T_{SF} > T_\alpha$). The competition with spontaneous fission will arise only very close to the $N = 162$ shell, where the partial half-life relative to α-decay strongly increases and $T_{SF} < T_\alpha$ in spite of the hindrance caused by the odd neutron numbers. It is noteworthy that this very complex decay pattern agrees on the whole with the predictions of the macro-microscopic theory (see figure 3). For the isotopes of element 115, due to the strong hindrances to spontaneous fission of nuclei with odd proton (or/and neutron) number, α-decay predominates as far as the $N = 162$ shell, where, similarly to the previous case, the decay sequence terminates by spontaneous fission.

The systematics of the total kinetic energies of spontaneous-fission fragments from all known even–even isotopes with $Z \geqslant 96$ are shown in figure 29(b). Two groups can be distinguished and are marked with dashed lines. They correspond to the mass-asymmetric and mass-symmetric fission modes. These are characterized by a different dependence of TKE on $Z^2/A^{1/3}$ [189]. All SF-nuclei with $Z = 110$–114 are in the region of asymmetric fission. This complies with the data, obtained for the fission of excited nuclei (see figure 10(b)). The experimental values of TKE for the lighter nuclides—the isotopes ^{267}Rf ($N = 163$), ^{267,268}Db ($N = 162$, 163) and ^{271}Sg ($N = 165$)—are found to be in the range of values for nuclei undergoing bimodal fission (here we have also shown the known nuclei $^{258–260}$Fm, ^{259,260}Md and some others [57, 90]) for which the mass-symmetric component is characterized by a high value of the fission fragment total kinetic energy. As was mentioned earlier, the detector array of the DGFRS does not allow direct measurements of the mass or energy of individual fission fragments. As a result, the information on the fission modes is deduced indirectly from the measured summed energies of two fission fragments and this is done at low statistics. However, in the ^{243}Am + ^{48}Ca reaction, after the chemical separation of group-5 elements and the measurement of the energy of each fragment from a thin source, in all the 15 SF-decays of the ^{268}Db nucleus (or ^{268}Db-EC $\rightarrow$ ^{268}Rf) symmetric fission with TKE $\approx$ 230 MeV and emission of about four neutrons per fission have been registered [126]. The measured values of TKE and $\overline{\nu}$ are in agreement with the expected total energy $Q_F \approx 280$ MeV, realized in the symmetric fission mode of the ^{268}Db/^{268}Rf nuclei. It was mentioned that the appearance of the mass-symmetric fission mode of nuclei close to the $N = 162$ shell is due to the same reasons that manifest themselves in the fission of the isotopes of the actinides—the shell effects at $Z = 50$ and $N = 82$, which play an important role in the process of fission of a heavy nucleus with large neutron excess.

5.2. General comparison with theory

The given analysis of the data on the properties of nuclei, produced in Act. + ^{48}Ca reactions, from the point of view of different models allows a general conclusion to be drawn about the consistency of theoretical predictions and experimental results.

As was mentioned above, according to theoretical expectations, the stability of nuclei with $Z \geqslant 112$ and $N \geqslant 172$ with respect to spontaneous fission steeply increases with neutron number. The odd isotopes of element 112 with $N \geqslant 171$ and all isotopes of element 114

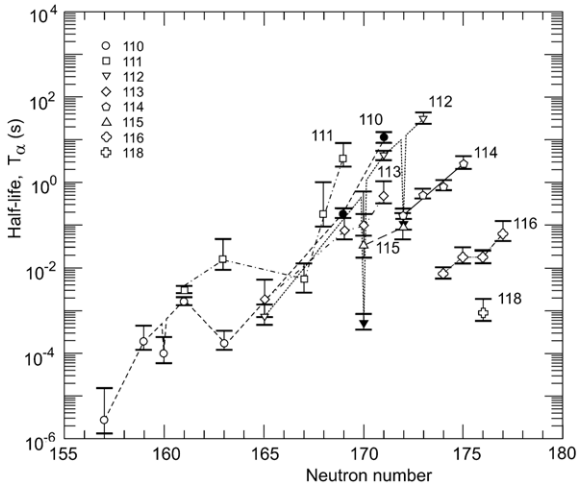

Figure 30. Experimental half-lives (in seconds) of the isotopes with atomic numbers Z $\geqslant$ 110 as a function of the neutron number. The open symbols denote nuclei undergoing α-decay, the solid symbols SF-decay. All nuclides with $N \leqslant 165$ shown in the figure have been synthesized in cold fusion reactions, nuclei with $N > 165$ in Act. + ^{48}Ca reactions. The curves are drawn through the points to guide the eye.

with $N \geqslant 173$ undergo α-decay. Nuclides with odd proton number $Z = 115$–107, present in the decay sequence of the isotopes $^{287,288}115$ and $^{282}113$, are also α-emitters. For most of the synthesized nuclei, the measured energies of α-decay with accuracy better than 5% are consistent with predictions of theory. Best agreement is found with the calculations in the framework of the MM-model ($\Delta Q_\alpha \leqslant 0.5$ MeV), and probably better agreement can also be found in self-consistent microscopic models.

The main conclusion of theory, connected with the significantly increased stability in the region of the heaviest neutron-rich nuclei, due to the shell effect ($N = 184$), is confirmed by the properties of the synthesized nuclei. A simple comparison of the half-lives of the isotopes of element 112, produced in cold fusion and in Act. + ^{48}Ca reactions, indicates that the increase of the neutron number in the nucleus $^{277}112$ ($N = 165$) by 6–8 units leads to an increase of T_α(exp) by a factor of 10^4 and 10^5, respectively. Similar is the situation with the isotopes of elements 110, 111 and 113 (figure 30).

The decay energies Q_α(exp) for all nuclei with $Z \leqslant 108$ and $N \leqslant 167$, measured in the ^{48}Ca-induced reactions, also agree with the theoretical values Q_α(th). Together with the earlier data for the lighter isotopes of these elements, obtained in cold fusion reactions, they confirm the existence of the closed neutron shell $N = 162$.

The half-lives of the spontaneously fissioning even–even nuclei $^{272}112$, $^{274}112$ and $^{276}114$ are in agreement with T_{SF}(th) within the uncertainties of the calculations of the tunnelling process through the fission barrier. The agreement of the measured and calculated values T_α and T_{SF} of nuclei with different proton/neutron numbers well reproduces the competition between the two decay modes, α-decay and spontaneous fission. As a consequence, the decay patterns also turn out to be very close to what has been expected (figure 3).

The above considerations show that the basic theoretical concept on the existence of closed nuclear shells in the region of the hypothetical superheavy nuclei and their decisive role in defining the limits of nuclear mass has received its experimental confirmation.

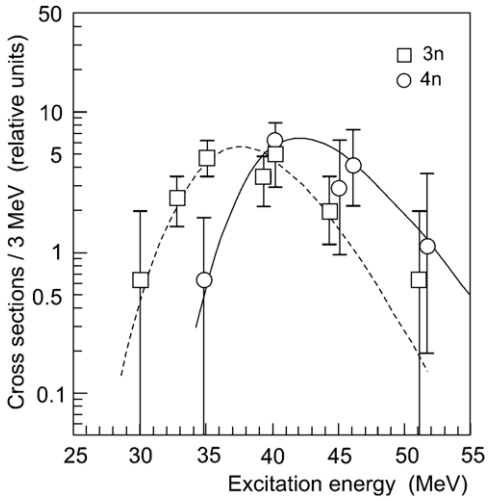

Figure 31. Experimental cross sections (in arbitrary units) of the isotopes of element 114, produced in the $3n$- and $4n$-evaporation channels of the ^{242,244}Pu + ^{48}Ca reactions at different excitation energies of the compound nucleus. The lines represent statistical calculations [137].

5.3. Reactions of synthesis

Some conclusions can be deduced about the mechanism of the Act. + ^{48}Ca reactions used to synthesize the listed new heaviest nuclides.

The two types of fission cross sections, $\sigma_{QF}(E_x)$ and $\sigma_{FF}(E_x)$, measured formerly in the reactions Act. + ^{48}Ca, can be now directly compared to the total cross sections for evaporation residues, defined as $\sigma_{EVR}(E_x) = \Sigma\sigma_{xn}(E_x)$. It should be noted that the evaporation residues from all the investigated reactions, observed in a relatively narrow energy interval ($E_x - E_x^{min} \leqslant 20$MeV), are mainly determined by the $3n$- and $4n$-evaporation channels. The excitation functions, measured in experiments with ^{48}Ca-projectiles and various targets, have bell-type shape with maxima at the excitation energy, corresponding to the emission of three or four neutrons and with full-width-at-half-maximum FWHM $\approx$ 10 MeV—typical for the process of neutron evaporation from a hot nucleus with a temperature $\sim$1.5 MeV (figure 31).

As a quantitative example we shall consider the ^{244}Pu + ^{48}Ca reaction; all other reactions practically reiterate this case.

The total cross sections for evaporation residues, measured in the fusion reaction ^{244}Pu + ^{48}Ca at different excitation energies of the compound nucleus ^{292}114, are presented in figure 32(b). For comparison, similar data for the evaporation residues (the No isotopes), produced in the ^{208}Pb + ^{48}Ca reaction, are given in figure 32(a).

As can be seen in figure 32(b), the maximum cross section for producing isotopes of element 114, $\sigma_{EVR} \approx$ 7pb, corresponds to the excitation energy $E_x \approx 42$ MeV. The cross section, measured with the CORSET setup for the same reaction at the same excitation energy, is $\sigma_{FF} \approx$4 mb. If we assume that at $E_x \approx 42$ MeV, $\sigma_{CN} \approx \sigma_{FF}$, then the ratio σ_{EVR}/σ_{FF} gives an estimate of the survivability factor of the compound nucleus ^{292}114 of the order of $P_{sur} \sim 2 \times 10^{-9}$. In the reactions ^{206,208}Pb + ^{48}Ca at $E_x = 42$ MeV, the survivability of the compound nuclei ^{254,256}No (see also graph (a)) is close to this value ($P_{sur} \sim 10^{-8}$).

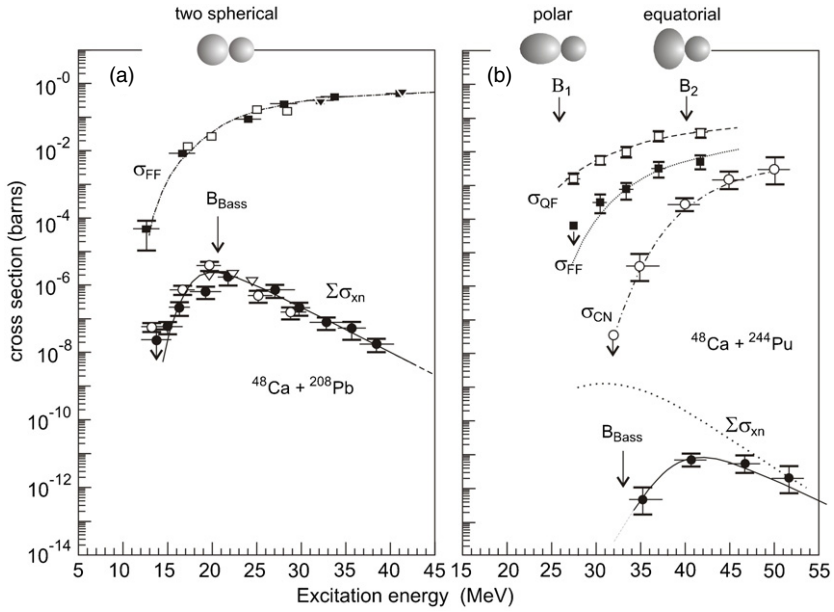

Figure 32. (a) Fission cross sections are denoted by squares (open [67], solid [68]) and evaporation-residue cross sections (summed cross section of all evaporation channels) by circles (open [62], solid [63]), measured in the ^{208}Pb + ^{48}Ca reaction at different excitation energies of the compound nucleus ^{256}No. (b) Cross sections σ_{QF} (open squares), σ_{FF} (solid squares [87]) and σ_{EVR} (solid circles [122, 123]) at different excitation energies E_x, obtained in the reaction ^{244}Pu + ^{48}Ca. The dotted curve is the cross section $\sigma_{EVR}(E_x)$ calculated assuming $\sigma_{FF} = \sigma_{CN}$ (see the text). The open circles denote the cross section $\sigma_{CN}(E_x)$ calculated on the basis of the experimental cross sections $\sigma_{EVR}(E_x)$ assuming equal probabilities $P_{surv}(E_x)$ for the excited nuclei ^{256}No and ^{292}114. In the upper part of the figure, the effect of the orientation of the target nucleus in the touching point is illustrated. The reaction Coulomb barrier, corresponding to the polar (B_1) and the equatorial (B_2) orientation of the target nucleus, as well as the Coulomb barrier for fusion of spherical nuclei (B_{Bass}) is indicated.

At the same time, at $E_x \approx 42$ MeV, the cross sections σ_{EVR} for the isotopes of element 114 are about 500 times smaller than the cross sections of No isotopes. This difference is explained by the fact that $\sigma_{FF}(E_x = 42$ MeV), measured in the ^{48}Ca + ^{244}Pu reaction, is almost by a factor of 100 less than that obtained for ^{48}Ca + ^{208}Pb. As it will be seen from the following, the cross section for the compound nucleus ^{292}114 may be even smaller. Then the probability of its survival should be higher than the estimate done by assuming $\sigma_{CN}(E_x) \approx \sigma_{FF}(E_x)$. Such a conclusion can be confirmed by using energies $E_x < 42$ MeV.

In the ^{48}Ca + ^{208}Pb reaction when the excitation energy is decreased, the cross section σ_{EVR} increases, due to the rise of the survivability of the compound nucleus ^{256}No, and reaches a maximum value at $E_x^{min} \approx 22$MeV, which corresponds to the Coulomb barrier of the reaction (figure 32(a)). The experimental excitation functions of the No isotopes from the $^{204,206–208}$Pb + ^{48}Ca reactions are well reproduced by various statistical calculations assuming, in first approximation, that $\sigma_{CN}(E_x) \approx \sigma_{FF}(E_x)$.

In the reaction ^{244}Pu + ^{48}Ca, the situation is different. When approaching the Coulomb barrier, the cross section for evaporation residues decreases significantly and, at $E_x^{min} \approx 33$MeV, σ_{EVR} becomes almost two orders of magnitude less than at $E_x \approx 42$ MeV. If in analogy to the reaction ^{48}Ca + ^{208}Pb we assume that $\sigma_{CN}(E_x) \approx \sigma_{FF}(E_x)$, then $\sigma_{EVR}(E_x)_{114}$

can be calculated similarly as for No. As can be seen in figure 32(b), in this case the calculated cross sections considerably differ from the experimental result. In the region of $E_x^{\min} \approx 33$ MeV, the cross section $\sigma_{\rm EVR}$(calc) is higher by a factor more than 10^4 than $\sigma_{\rm EVR}$(exp); such a discrepancy cannot be eliminated by any variation of the parameters of the statistical calculations. Obviously, the strong decrease of the evaporation-residue cross section close to the Coulomb barrier of the ^{244}Pu + ^{48}Ca reaction is due to the difference between the two seemingly connected processes—the formation of the compound nucleus and its fission.

The shift by about 8–10 MeV in the direction of higher energies of the maximum of $\sigma_{\rm EVR}$ relative to $E_x^{\min}$ is an extremely important circumstance, when it comes to choosing the incident energy of the ^{48}Ca ions for the SHE synthesis experiments. The shift of $\sigma_{\rm EVR}(E_x)$ relative to the Coulomb barrier $B_{\rm Bass}$ changes the ratio of the cross sections for xn-evaporation channels and shifts the maxima of the excitation functions (especially those for small neutron number, $x = 2, 3$) to the direction of higher compound nucleus excitation energies. This was seen in the first experiments with the reactions ^{244}Pu + ^{48}Ca and ^{248}Cm + ^{48}Ca at an excitation energy of the compound nuclei ^{292}114 $E_x = 35$ MeV and ^{296}116 $E_x = 33$ MeV close to the calculated cross section maximum $\sigma_{4n}(E_x)$. The experimentally measured values Q_α(exp) and T_α(exp) were close to the expected for the even–even isotopes ^{288}114 and ^{292}116 (see table 3 and figure 27). As a consequence, in the first (the most probable) interpretation of the data, the chains ***k*** (figure 17) and ***r*** (figure 19), observed in ^{244}Pu, ^{248}Cm + ^{48}Ca reactions, were assigned to decays of the isotopes ^{288}114 and ^{292}116 [122, 129]. However, only after measuring the excitation functions of all isotopes of elements 114 and 116, observed in the ^{242,244}Pu, ^{245,248}Cm + ^{48}Ca reactions, it was found out that they pertain to the even–odd nuclei ^{289}114 and ^{293}116, which are products of the $3n$-evaporation channel shifted to higher excitation energies.

An explanation of such a shift in $\sigma_{\rm EVR}(E_x)$ can be found in the shape of the interacting nuclei [121].

In the fusion of the two spherical nuclei ^{208}Pb and ^{48}Ca, the maximum $\sigma_{\rm EVR}$ at $E_x \approx E_x^{\min}$ corresponds to the optimal conditions for formation of the compound nucleus ^{256}No and its survival. In the fusion of the spherical ^{48}Ca with the deformed ^{244}Pu nucleus ($\beta_2 \approx 0.25$), the Coulomb barrier and the configuration of the heavy nucleus with summed mass at the moment of its formation depend on the orientation of the target nucleus at the touching point. In the case of '*polar*' orientation, corresponding at the touching point to the maximum distance between the centres of mass (charge) of the interacting nuclei, the Coulomb barrier is reduced relative to the fusion barrier for spherical nuclei. This makes it possible to produce a nucleus with lower excitation, but larger deformation in the initial stage of the fusion process. In contrast, in the case of '*equatorial*' orientation, corresponding to the minimum distance between the nuclear centres, the Coulomb barrier increases relative to the former example by about 20 MeV, but the produced nucleus has a more compact shape. All other configurations are intermediate between these two extremes.

The quasi-fission reaction channels most probably occur at the earliest stage of collective motion, when the heavy nucleus is still strongly deformed. The principal contribution to the quasi-fission cross section at lower excitation energies ($E_x \leqslant 30$–35 MeV) is from the 'polar' interactions of the colliding nuclei. Therefore, up to $E_x \approx 27$ MeV, the dependence $\sigma_{\rm QF}(E_x)$ or $\sigma_{\rm STICK}(E_x)$is relatively weak, see figure 32(b). In contrast, as shown in [190] and in the experimental studies of the reaction W(Ge, xn) [191], the more compact configuration in the '*equatorial*' collisions, with higher probability reaches the final spherical shape and, therefore, such collisions will be decisive for determining the fusion–evaporation cross section.

The observed dependence $\sigma_{\rm FF}(E_x)$ is steeper than that of $\sigma_{\rm QF}(E_x)$ and is shifted to higher values of E_x. If we assume that, compared with $\sigma_{\rm FF}(E_x)$, $\sigma_{\rm CN}(E_x)$ corresponds to certain

more strict selection of the target–nucleus orientation, we can obtain more realistic values of $\sigma_{CN}(E_x)$ and better agreement for all investigated Act. + ^{48}Ca reactions.

It should be noted that the significant decrease of the ratio σ_{EVR}/σ_{FF} in the low energy region means that the composite system, having acquired deformation close to the fission barrier, can undergo fission by-passing the stage of formation of a compound nucleus [91] (see figure 6(b)). In fact, this is a second limitation (of the quasi-fission type) on the path of collective motion of the composite system towards the final stage of formation of a spherical nucleus.

Continuing to consider the reaction ^{244}Pu + ^{48}Ca, we shall try, in first approximation, to deduce the dependence $\sigma_{CN}(E_x)$ based on the experimental cross sections $\sigma_{EVR}(E_x)$. At this, we assume that the survivability $P_{sur}(E_x)$ is the same for element 114 as for No. The resulting $\sigma_{CN}(E_x)$, obtained in this way, is shown in figure 32(b) by the dotted–dashed line. It is easy to see that the curve $\sigma_{CN}(E_x)$ is substantially steeper than $\sigma_{FF}(E_x)$. The 'effective' Coulomb barrier in this case corresponds to almost the strict orientation of the target nucleus ($\theta \approx 90^\circ$) with respect to the direction of the ^{48}Ca-projectile. Therefore, the dynamic hindrances to the formation of a heavy compound nucleus depend on the shape of the interacting nuclei and their orientation at the point of contact. In the Act. + ^{48}Ca reactions this effect plays an essential role (the influence of the different types of deformations on the fusion probability in Act. + ^{48}Ca reactions has been considered separately in [192]).

On the other hand, at any energy, including $E_x \geqslant 42$ MeV, σ_{CN} cannot exceed σ_{FF}. Since at $E_x \approx 42$ MeV, P_{sur} for the nuclei ^{256}No and ^{292}114 differ at most by a factor of 5 (at the level of $1/P_{sur} \sim 10^8$), it can be assumed that their fission barrier heights are almost the same. If in reality the cross section for the formation of the compound nucleus ^{292}114 is lower than shown in figure 32(b), this would mean that $P_{sur}(114) > P_{sur}(\text{No})$ and, hence, $B_f(114) > B_f(\text{No})$. Since in nuclei with $Z \geqslant 98$–100 the appearance of a fission barrier is almost completely due to shell effects, the presence of a high fission barrier in the ^{292}114 nucleus is evidence of the existence of the strong effect of the new shell in the deformation energy of the superheavy nucleus.

Another issue is the dependence of the survivability of heavy nuclei on the shell effect.

In figure 33, the maximum cross section σ_{EVR} for the evaporation residues in the reactions ^{233,238}U, ^{237}Np, ^{242,244}Pu, ^{245,248}Cm and ^{249}Cf + ^{48}Ca is presented as a function of the neutron number of the compound nucleus. It can be seen that increasing the number of neutrons from $N_{CN} = 169$ (^{233}U + ^{48}Ca) to $N_{CN} = 172$ (^{237}Np + ^{48}Ca) and then to $N_{CN} = 178$–180 (^{244}Pu, ^{248}Cm + ^{48}Ca) the cross section σ_{EVR} rises by more than one order of magnitude. As mentioned before, this change in $\sigma_{EVR}(N_{CN})$ in turn indicates an increase in the survivability of the heavy compound nucleus, which is mainly due to the increase of its fission barrier when approaching the closed neutron shell $N = 184$ (see figure 11). This conclusion also follows from the measured cross section ratios σ_{4n}/σ_{3n}, which increase with N_{CN} (for ^{292}114 $\sigma_{4n} > \sigma_{3n}$ and at $E_x \approx 54$ MeV an event corresponding to the $5n$-evaporation channel was observed [133]). Let us recall that for all studied nuclei the fission barrier height is completely determined by the nuclear shell effect. For this reason, the observed increase in the survivability of the excited nuclei with neutron number appears to be, to our opinion, evidence for the existence of the closed neutron shell in the region of $N \geqslant 180$.

But the advance towards neutron-rich nuclei in the reactions Act. + ^{48}Ca is connected with the increase of Z_{CN}. One may assume that the proton shell $Z = 114$ also contributes to the increase of the fission barrier (in the microscopic models HFB and RMF a similar effect is expected for the nuclei with $Z = 120$, 124 or 126). According to the calculations, the effect of the proton shell is substantially weaker than that of the neutron shell $N = 184$ and, moreover, is less localized [37]. At the same time, as can be seen from figure 33, the cross section for

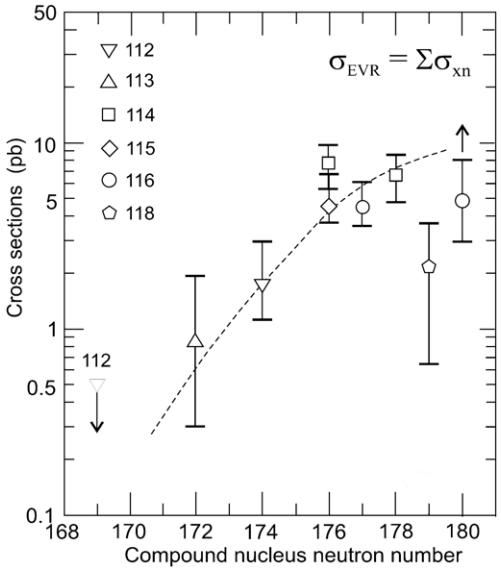

Figure 33. Maximum cross sections σ_{EVR} as a function of Z_{CN} and N_{CN}, obtained on the basis of the values of $\sigma_{xn}(E_x)$ measured in the reactions Act. + ^{48}Ca, accounting for the experimental and calculated widths of the excitation functions of the 3*n*- and 4*n*-evaporation channels (see figure 31).

nuclei of element 118 in the reaction ^{249}Cf(^{48}Ca, 3*n*)^{294}118 turned out to be by almost one order of magnitude less than that for elements 114 or 116 with close neutron numbers N_{CN}. This difference is due to the choice of the lower incident ^{48}Ca-projectile energy relative to the calculated maximum of the 3*n*-channel of the ^{249}Cf + ^{48}Ca reaction (we tried to observe both isotopes of element 118, which could be produced in the 2*n*- and 3*n*-channels).

It is also probable that the survivability of the compound nucleus ^{297}118 ($N_{CN} = 179$) is lower than that of the neighbouring nuclei—^{296}116 or ^{292}114—because of the farther distance from the shell $Z = 114$. Unfortunately, in this nuclear region and at poor statistics we cannot make whatever definite conclusions about the position and influence of the proton shell $Z_{SHELL} = 114$.

The results on the experimental investigation of the formation and of the decay properties of nuclei, produced in Act. + ^{48}Ca reactions, can be summarized as follows.

In the fusion reactions ^{238}U, ^{242,244}Pu, ^{243}Am, ^{245,246}Cm and ^{249}Cf + ^{48}Ca, the evaporation residues were observed with cross sections ranging from 0.5 to 5 pb depending on the mass and atomic number of the compound nucleus. In the ^{233}U + ^{48}Ca reaction only an upper limit of the cross section $\sigma \leqslant 0.6$ pb was obtained.

The small cross sections are connected with the competing quasi-fission channels and selection of compact shapes (orientation of the target nucleus) in the early stage of the fusion process. The excitation functions correspond to the evaporation of mainly three or four neutrons from the excited nucleus, the maximum cross sections for evaporation residues are observed at an excitation energy of about 40 MeV (hot fusion). The main loss is due to the low survivability of the compound nuclei. However, the survivability increases with the neutron number. This fact can be taken as a consequence of the rise of the fission barriers of the heaviest nuclei when approaching the $N = 184$ shell.

The atomic numbers of the heaviest elements with $Z \geqslant 112$ have been determined by physical and chemical methods. It has been shown that the final product of the consecutive five α-decays of element 115, and correspondingly four α-decays of element 113, is Db ($Z = 105$)—the chemical homologue of W; while element 112, which is the product of α-decay of element 114 (or consecutive two α-decays of element 116), is the chemical homologue of Hg. The mass numbers of the isotopes of each element are determined by identification of the evaporation reaction channels and the decay properties of the searched-for nuclei.

The evaporation residues undergo successive α-decays, which end by spontaneous fission. For all α-transitions the energies and half-lives, as well as for spontaneous fission—half-lives and fission fragment mean total kinetic energies, have been determined.

Together with the data from cold fusion reactions they evidence that the experimentally determined decay properties of the heaviest nuclei, in general, are in good agreement with modern microscopic nuclear models.

6. Perspectives

Relative to the 30-year old history of investigations on heavy nuclei in cold fusion reactions that have led to the discovery of six new elements, the results obtained in Act. + ^{48}Ca reactions are the next step in the synthesis and studies of the properties of new, heavier elements. Reproducing them in other experiments is, in our opinion, of great interest. The neutron-rich and rather long-lived nuclides, produced with cross sections of few picobarns in Act. + ^{48}Ca reactions, are unique objects whose nuclear structure, decay modes, spontaneous fission, atomic and chemical properties have to be studied. All fields of investigations can advance, if a way to increase the production rate of nuclei is found. This task is connected with the improvement of the experimental techniques and the search for new possibilities to produce and study the sought-for nuclei.

When the situation is considered from the point of view of the present state of art, we should note that it is technically possible to increase the intensity of the ^{48}Ca beam up to 5–10 pμA, a factor of 5–10 greater than the present value. Perhaps, this is also not the limit of modern accelerators. The targets used at DGFRS, with some modifications, are capable of accepting such beam intensities.

Another issue is the separation of the looked-for nuclei from all other reaction products. As can be seen from table 3, the half-lives of odd-N isotopes of elements 112–114 are of the order of $0.5\ \text{s} \leqslant T_{1/2} \leqslant 30\ \text{s}$. Therefore, super-fast 'in-flight' methods of separation are not necessary for them as was the case with short-lived EVRs of cold fusion reactions. For the separation of the volatile atoms with $Z \geqslant 112$ (see the experiments on the chemistry of element 112), not as fast, but more efficient 'on-line' mass separation methods can be used. In this way, it could become possible to increase the yield of the new nuclei by using targets up to 1.5 mg cm^{-2} thick (instead of the 0.35 mg cm^{-2} used now at DGFRS) and to improve the transmission of the separator. A setup of a new type based on this principle—MASHA (mass analyser for superheavy atoms [193])—is now being used for 'off-line' separation of heavy nuclides. In the 'on-line' mode of operation it will let us obtain evaporation residues with adjacent masses and will let us perform simultaneous separation of parent and daughter (granddaughter) nuclei with the measurement of their mass with accuracy better than 0.1 amu [194].

The separation of the isotopes with $T_{1/2} \geqslant 1$ s may also be carried out by means of express chemical methods. The experiments aimed at the study of the chemical properties of element 112, performed with the isotope ^{283}112 ($T_{1/2} \approx 3.5$ s) [172], will be continued with another longer lived nuclide—^{285}112 ($T_{1/2} \approx 30$ s), which is produced in the 3n-evaporation channel

of the ^{244}Pu + ^{48}Ca reaction. As was pointed above, such a technique with some modifications can also be used for the study of the chemical properties of element 114 (^{289}114, $T_{1/2} \approx 3$ s).

Of certain interest are the investigations of the spontaneous fission of the relatively long-living isotopes ^{267}Rf ($T_{SF} \approx 1.5$ h) and ^{268}Db ($T_{1/2} \approx 1$ d), and the isotopes of element ^{281}110 ($T_{SF} \approx 11$ s), which terminate the decay chains of ^{289}114 and ^{293}116 (see figure 25). Highly perspective from this point of view is the synthesis of element 117 in the ^{249}Bk(^{48}Ca, 3–4n)^{294,293}117 reaction. The products of successive α-decays of the evaporation products of this reaction—the isotopes of elements 105–115—have two more neutrons compared to the nuclei in the decay chains of the isotopes ^{287,288}115, obtained in the reaction ^{243}Am + ^{48}Ca.

All this in general, the increase of the luminosity of the experiments and the application of high-efficiency separation methods of evaporation products, will make it possible to increase the detection rate of observed nuclei with $Z = 110$–116 by almost two orders of magnitude. The increase in the yield will let start spectroscopic studies, including the measurement of the low-lying levels of odd isotopes, which can be directly compared to the predictions of various models.

As it seems to us, this is the closest perspective.

A long-term perspective, less clear, is connected with the production of long-lived nuclei and with the advance to the region of still heavier elements. At present, the reactions Act. + ^{48}Ca seem to be most efficient, if not the only ones, for the production of nuclei with highest mass.

However, the reactions Act. + ^{48}Ca have their own limitations—they cannot let us advance further than the isotopes of elements 114 and 116, situated 9–7 neutrons away from the $N = 184$ shell. At the same time, according to the theoretical expectations and the experimental data from the ^{48}Ca-induced reactions, we have every reason to assume that with the further increase of the neutron number in the isotopes of elements with $Z \geqslant 110$ their half-lives will substantially increase. Unfortunately, the limit on the neutron excess in the compound nucleus ($N_{CN} = 180$) and correspondingly in the products of the 3n- and 4n-evaporation channels of the fusion reaction ^{248}Cm + ^{48}Ca cannot be overcome since ^{249}Cf is the heaviest target material available for this purposes. In principle, the desired result can be reached in the isotopes with $Z > 118$, which are produced in the fusion reactions of ^{244}Pu and ^{248}Cm nuclei with heavier projectiles, such as ^{58}Fe or ^{64}Ni, leading to the formation of still heavier elements with $Z = 120$–124 and $N = 179$–183, respectively. However, the attractive possibility of obtaining nuclei close to the neutron $N = 184$ shell again requires studies of the reaction mechanism so as to provide realistic estimates of the probability of producing compound nuclei in such reactions.

At the same time, the setting up of such experiments, taking into account the mentioned possibilities to increase the experimental luminosity, seems to be very important as a test for theory, where the different predictions of the nuclear properties in the vicinity of the spherical neutron shell $N = 184$ are most striking. This is illustrated in figure 34 by the experimental values of Q_α(exp) for the Po isotopes ($Z = Z_{SHELL} + 2$) and the calculations in various models, performed for the isotopes of element 116 ($Z = Z_{114} + 2$). At crossing the neutron shell $N = 126$, the energy Q_α changes by $\Delta Q_\alpha \approx 4$ MeV, whereas the half-life T_α(exp) by a factor 10^{16}. In the MM-model, as can be seen from the figure $\Delta Q_\alpha \approx 1.1$ MeV [187], the expected T_α(th) change by a factor $\sim 10^3$. A considerably stronger neutron shell effect follows from the calculations within the HFB-model, where for $Z = 116$, $\Delta Q_\alpha \approx 2.2$ MeV [185]; here, when approaching $N = 184$, a significant increase of the half-lives is expected compared to the MM-model. It can be seen from the figure that the decay properties of the isotopes, produced in the reaction ^{245,248}Cm + ^{48}Ca ($N = 174$–177), are not sensitive to these variations in the expected properties of nuclei with $N \geqslant 180$.

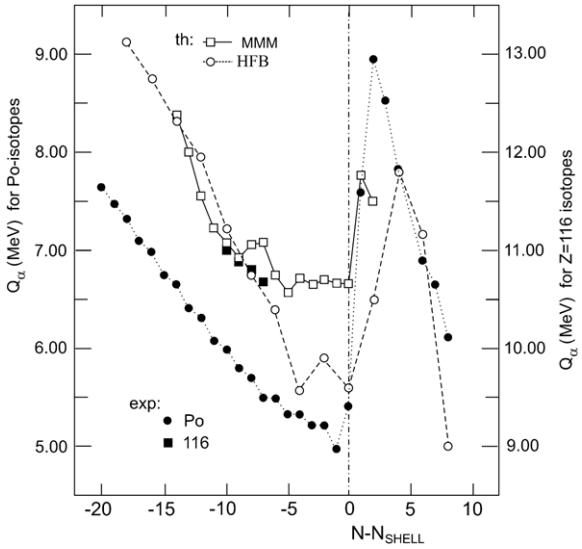

Figure 34. Decay energy Q_α as a function of the neutron number N in units of N–$N_{\rm SHELL}$. The black points denote Q_α(exp) on the left scale for the Po ($N_{\rm SHELL} = 126$) isotopes, the black squares denote Q_α(exp) on the right scale for the isotopes with $Z = 116$ ($N_{\rm SHELL} = 184$), produced in the reactions ^{245,248}Cm + ^{48}Ca [121, 123]. The open circles and squares are the calculated values Q_α(th), obtained in the framework of the MM- [187] and HFB- [185] models, respectively. The curves through the experimental and theoretical points are drawn to guide the eye.

Another possibility is the use of neutron-rich radioactive nuclei as beams. Among them of definite interest is the doubly magic nucleus ^{132}Sn ($T_{1/2} = 39$ s); in the fusion with stable nuclei, for instance with ^{174,176}Yb, it could lead to compound nuclei with $Z_{\rm CN} = 120$ and $N_{\rm CN} = 186, 188$. However, the ∼1.5-fold increase of the Coulomb repulsion in symmetric reactions, compared to the Act. + ^{48}Ca ones, will enhance the hindrance to the formation of a compound nucleus. As long as the calculation of these limitations is very uncertain, it seems reasonable to estimate them using test reactions with known nuclei. One of the symmetric reactions—^{136}Xe(^{136}Xe, xn)$^{272-x}$Hs—seems to be suitable for this purpose. More details on the motivation and the setting of such an experiment can be found in [195].

6.1. Search for superheavy elements in nature

The problem of reaching the very long-lived nuclei with high neutron excess is connected with of the issue of nucleosynthesis in the region of the heavy and superheavy elements. The possibility of elements heavier than ^{238}U to exist in nature has been the subject of discussions for many years within various theoretical concepts [196–204]. The search for heavy elements in natural samples and in cosmic rays in the 1970s and 1980s was one of the extensive experimental investigations (see the review papers [55, 205] and references therein). In all experiments only upper limits of the superheavy element concentration in the studied samples have been determined. We do not plan to discuss this topic in general (it can be the subject of a separate investigation). We shall consider only the basic ideas and the results of these investigations from the point of view of the expected nuclear properties, as given by the data from the artificial synthesis of the heaviest nuclides.

Since, in general, the mechanism of the nucleosynthesis of medium and heavier nuclear masses up to uranium has different interpretations, the model calculations of the *r*-process leading to the formation of nuclei with $Z > 92$, depends to a great extent on the strength of the neutron shell $N = 184$ and on the assumed temperature and density of the neutron flux [206–208]. For instance, calculations of the *r*-abundance of the heavy elements, analysed in [209] and based on the nuclear binding energies from models such as the extended Thomas–Fermi plus Strutinsky integral (ETFSI) [210] or HFB in various versions [211–213], point to the formation, together with Th and U, of nuclei with mass $A > 238$ (up to mass numbers $A \sim 290$). It is noteworthy that in the experiments, performed in the 1970s and 1980s and aimed at the search for superheavy elements in nature and in cosmic rays, with the exception of finding ultra-small quantities of ^{244}Pu in rocks [214], no long-lived nuclides with $Z > 94$ were found.

At that time, the experiments on the search of long-lived isotopes among the heaviest elements—the products of the nucleosynthesis—were motivated by the quite optimistic forecasts about their extremely high stability ($T_{1/2} \geqslant 10^9$ years). When choosing the objects of such studies, it was assumed that the most stable nuclei were located in the vicinity of the closed shells $Z = 114$ and $N = 184$ [55, 205], where the maximum shell effect was expected. However, as it follows from modern microscopic models (their agreement with the experimental data was demonstrated above), in this nuclear region the calculated values of T_α amount to only 10^3–10^5 s [7, 215–217]. A noticeable increase in T_α and T_{SF} may be expected in the region of nuclei with $Z \leqslant 110$, which has not yet been looked for. At the same time, in nuclides with $Z \leqslant 110$ the approaching of the closed $N = 184$ shell leads to loss of stability relative to β^--decay and the search for our objects—nuclei with longest half-lives—is determined by the probability of the three types of decays: α, β and SF. This situation is illustrated in figure 35 for the isotopes of element 108.

According to calculations [7], the partial half-lives T_α and T_{SF} for the magic nucleus ^{292}Hs are about 2×10^6 years and $T_{SF} \approx 3 \times 10^4$ years, respectively. However, as it follows from the same calculations, the neutron-rich nucleus ^{292}Hs is unstable with respect to β^--decay. When approaching the region of $N < 184$ (^{286}Hs is the heaviest β^--stable isotope), the stability of the nucleus relative to α-decay and SF is considerably reduced (figure 35), not leaving any chance to be observed.

At the same time, all above-mentioned arguments are based on the rather controversial different model predictions on the detailed decay properties of extremely neutron-rich nuclei. This concerns in the first place the spontaneous-fission half-lives, which are estimated with the highest uncertainty and strongly differ from model to model. In spite of the minute chances for success, it seems reasonable to perform the investigations in the region $Z \leqslant 110$, but with considerably increased experimental sensitivity.

Considering different nuclei as an object for such studies, it turns out that for element 108—Hs, the chemical homologue of Os, an extremely high sensitivity can be reached when searched for in natural samples and cosmic rays [218]. Given the same chemical behaviour of Hs and Os, which was demonstrated experimentally [154], the search for rare decays may be undertaken with a natural sample of Os, where atoms of Hs can be present. Leaving aside the open question about the half-life of the long-lived β^--stable isotope of Hs, we may assume that it will directly undergo SF or SF will be observed for the product of its α-decay. In any case, as a first step, it seems reasonable to register rare events of spontaneous fission.

Spontaneous fission in the initial Os sample (up to 1 kg) can be registered by the outburst of prompt fission neutrons. For the nuclei with $Z = 106$–108, the estimated average neutron number per fission is $\overline{\nu} \approx 4.5$–$6.0$ [5] (see also the measurement of $\overline{\nu} \approx 4.2$ in the spontaneous fission of ^{268}Db/^{268}Rf [126]). The construction of the neutron detector for such measurements

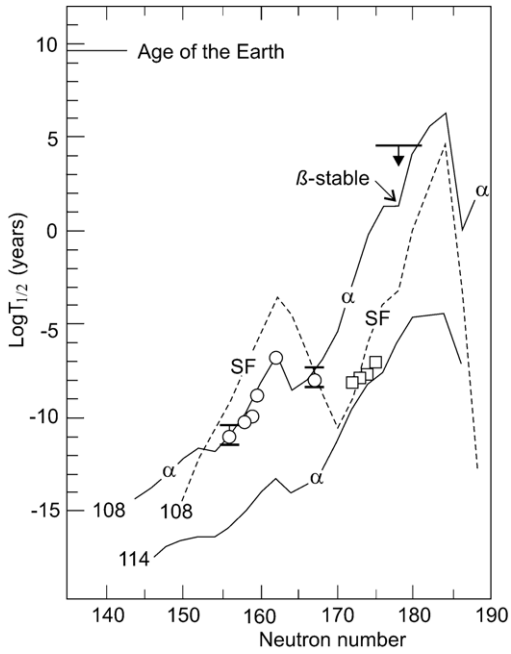

Figure 35. Calculated values of partial half-lives T_α(th) of the isotopes of elements 108 and 114 together with T_{SF} ($Z = 108$), obtained in the MM-model in [7, 39]. Circles and squares denote experimental values T_α(exp), obtained in cold fusion reactions and in the Act. + ^{48}Ca reactions for the isotopes of elements 108 and 114, respectively. The limiting value of the half-life is shown for the β-stable nucleus ^{286}Hs according to the data from measurements of rare events of spontaneous fission from the metallic Os (500 g) sample during a period of about 1 year (see the text).

is similar to the setup used for registering the spontaneous fission of ^{268}Db/^{268}Rf in the chemical experiment (see above). In order to exclude the background of neutrons arising from the interaction of cosmic fast muons, the detector has been placed in the underground laboratory in Modane (France), protected by a 4000 m water-equivalent layer. In such conditions, with the efficiency being $\approx 60\%$ (for three or higher fold coincidences), it is possible to detect rare SF-decays with counting rate up to 1 SF/year. Assuming that the half-life of Hs is $T_{1/2} = 10^9$ years, the observation of 1 SF/year corresponds to the content of Hs in Os of about 5×10^{-15} g g^{-1} or 5×10^{23} g g^{-1} in the Earth's crust. Such a concentration is approximately a factor of 10^{16} lower than the abundance of ^{238}U. On the other hand, given the intensity of the flux of cosmic Os and ^{238}U [219], it can be shown that the observation of 1 SF/year from a 500 g–Os sample corresponds to a ratio of the intensities Hs/^{238}U $\sim 10^{-5}$.

Such an experiment has been now running for more than 340 days (it will be continued for about 2 years). If we assume that the *r*-process leads to the formation of heavy nuclei with mass up to $A \sim 290$ [220] in the ratio Hs/U $\geqslant 0.1$, then given the remoteness of the cosmic ray sources $\sim 10^{23}$cm and the velocity of the heavy nucleus $v \approx 0.2c$, the preliminary results of this experiment let us determine the upper limit of the half-life of the long-lived isotope of element 108 as $T_{1/2} \leqslant 5 \times 10^4$ years (as shown in figure 35).

In spite of the high sensitivity of this particular experiment, exceeding all earlier attempts to observe superheavy nuclei in natural samples or in cosmic rays, the search for the most long-lived nuclei again makes us turn to the artificial production of superheavy elements.

Acknowledgments

Discussing the issue of the properties of the heaviest nuclei we confined ourselves to the results obtained during the recent few years in Act. + ^{48}Ca reactions. For these investigations we used intense ^{48}Ca beams, produced at the heavy-ion cyclotron U-400 of the Flerov Laboratory of Nuclear Reactions (FLNR, JINR, Dubna). The experiments at DGFRS were carried out in collaboration with the Analytical and Radiochemical Division of the Lawrence Livermore National Laboratory (LLNL, Livermore); the experiments on the chemical identification of the isotopes ^{268}Db and ^{283}112 within the collaboration: Paul Scherrer Institute (PSI, Villigen), Department for Chemistry and Biochemistry of the University of Bern, FLNR (Dubna), LLNL (Livermore), Institute of Electronic Technology (IET, Warsaw) with the participation of Dr M Hussonois from the Institute of Nuclear Physics (IPN, Orsay). It is my pleasure to convey my gratitude to my colleagues and co-authors of the majority of original publications for their hard work and active participation in the experimental programme on the synthesis and study of the properties of superheavy elements. It is my duty to thank Professors W Greiner, S Hoffman, M G Itkis, G Muenzenberg, A Sobiczewski, W J Świątecki, V V Pashkevich, K Siwek-Wilczyńska, J Wilczyński and H W Gäeggeler, as well as Dr V K Utyonkov, Professors V I Zagrebaev and S N Dmitriev, who have taken the trouble to read this manuscript and have made useful remarks. I would like to thank Dr R Kalpakchieva for preparing the English version of the manuscript and for the many valuable suggestions. Thanks are due to E V Prokhorova for her assistance in preparing the manuscript for publication. I am grateful to the JINR Directorate, in particular to Professors V G Kadyshevsky, A N Sissakian and Ts Vylov for the help and support we received during all stages of the experiments. The investigations reported in this review have been performed with the support of the Russian Ministry of Atomic Energy, grants of RFBR Nos. 04-02-17186 and 04-03-32047 and the Swiss National Scientific Foundation. Much of the support for the LLNL authors was provided through the US DOE under Contract No. W-7405-Eng-48.

Note added in proof. Early in 2007 (after the present review had already been submitted), in GSI at the recoil separator SHIP, a new attempt to synthesize the isotope ^{283}112 in the reaction ^{238}U + ^{48}Ca was undertaken. The decay sequences R-α-SF, observed in this experiment, the corresponding energies and decay times of nuclei—members of the decay chains—were found to be in good agreement with the results presented in figure 20(c) and confirm the decay properties of ^{283}112, listed in table 3 (row 17). I am grateful to Professor S Hofmann for this private communication.

References

[1] Bohr N and Wheeler J A 1939 *Phys. Rev.* **56** 426
[2] Frenkel J 1937 *Phys. Rev.* **55** 987
[3] Myers W D and Swiatecki W J 1966 *Nucl. Phys.* **81** 1
[4] Nilsson S G, Thompson S G and Tsang C F 1969 *Phys. Lett.* **28 B** 458
[5] Oganessian Yu Ts and Lazarev Yu A 1985 *Treatise on Heavy-Ion Science* vol 4 ed D A Bromley (New York: Plenum) p 3
[6] Myers W D and Swiatecki W J 1967 *Ark Fys.* **36** 343
[7] Smolańczuk R 1997 *Phys. Rev.* C **56** 812
[8] Polikanov S M, Druin V A, Karnaukhov V A, Mikheyev V L, Pleve A A, Skobelyev N K, Subbotin V G, Ter-Akopian G M and Fomichev V A 1962 *Sov. Phys.—JETP* **15** 1016
[9] Bjørnholm S and Linn J 1980 *Rev. Mod. Phys.* **52** 725
[10] Holden N E and Hoffman D C 2000 *Pure Appl. Chem.* **72** 1525 (and references therein)
[11] Haxel O, Jensen J H D and Suess H E 1949 *Phys. Rev.* **75** 1766
[12] Mayer M G 1949 *Phys. Rev.* **75** 1969
[13] Strutinsky V M 1967 *Nucl. Phys.* A **95** 420
[14] Strutinsky V M 1968 *Nucl. Phys.* A **122** 1
[15] Brack M, Damgaard J, Jensen A S, Pauli H C, Strutinsky V M and Wong C Y 1972 *Rev. Mod. Phys.* **44** 320

[16] Nilsson S G, Tsang C F, Sobiczewski A, Szymański Z, Wycech S, Gustafson C, Lamm I-L, Möller P and Nilsson B 1969 *Nucl. Phys.* A **131** 1
[17] Mottelson B R and Nilsson S G 1955 *Phys. Rev.* **99** 1615
[18] Möller P and Nix J R 1994 *J. Phys. G: Nucl. Part. Phys.* **20** 1681
[19] Greiner W 1995 *Int. J. Mod. Phys.* E **5**
[20] Sobiczewski A 1994 *Phys. Part. Nucl.* **25** 119
[21] Sobiczewski A, Gareev F A and Kalinkin B N 1966 *Phys. Lett.* **22** 500
[22] Meldner H 1967 *Ark. Fys.* **36** 593
[23] Mosel U and Greiner W 1969 *Z. Phys.* **222** 261
[24] Patyk Z and Sobiczewski A 1991 *Nucl. Phys.* A **533** 132
[25] Smolańczuk R, Skalski J and Sobiczewski A 1995 *Phys. Rev.* C **52** 1871
[26] Patyk Z and Sobiczewski A 1991 *Phys. Lett.* B **256** 307
[27] Ćwiok S, Nazarevicz W and Heenen P H 1999 *Phys. Rev. Lett.* **83** 1108
[28] Skyrme T H R 1958 *Phil. Mag. Nucl. Phys.* **9** 615
[29] Vautherin D and Brink D M 1972 *Phys. Rev.* C **5** 626
[30] Flocard H, Quentin P, Kerman A K and Vautherin D 1973 *Nucl. Phys.* **203** 3
[31] Patra S K, Greiner W and Gupta R K 2000 *J. Phys. G: Nucl. Part. Phys.* **26** L65
[32] Gogny D 1975 *Nuclear Self-Consistent Fields* ed G Ripka and M Pomeuf (Amsterdam: North-Holland) p 333
[33] Dechargé J and Gogny D 1980 *Phys. Rev.* C **21** 1568
[34] Berger J F, Girod M and Gogny D 1984 *Nucl. Phys.* A **428** 23c
[35] Serot B D and Walecka J D 1986 *The Relativistic Nuclear Many-Body Problem (Advances in Nuclear Physics* vol 16*)* ed J W Negele and E Vogt (New York: Plenum)
[36] Ring P 1996 *Prog. Part. Nucl. Phys.* **37** 193
[37] Sobiczewski A and Pomorski K 2007 *Prog. Part. Nucl. Phys.* **58** 292
[38] Berger J F, Bitaud L, Dechargé J, Girod M and Dietrich K 2001 *Nucl. Phys.* A **685** 1c
[39] Muntian I, Patyk Z and Sobiczewski A 2003 *Acta Phys. Pol.* B **34** 2073
[40] Bender M, Rutz K, Reinhard P-G, Maruhn J A and Greiner W 1998 *Phys. Rev.* C **58** 2126
[41] Bender M, Rutz K, Reinhard P-G, Maruhn J A and Greiner W 1999 *Phys. Rev.* C **60** 034304
[42] Bürvenich T, Bender M, Maruhn J A and Reinhard P-G 2004 *Phys. Rev.* C **69** 014307
[43] Lunney D, Pearson J M and Thibault C 2003 *Rev. Mod. Phys.* **75** 1021
[44] Rikovska Stone J 2005 *J. Phys. G: Nucl. Part. Phys.* **31** R211
[45] Smolańczuk R and Sobiczewski A 1995 *Proc. XV Nuclear Physics Divisional Conference on Low Energy Nuclear Dynamics (St. Petersburg, Russia, 18–22 April 1995)* ed Yu Ts Oganessian, R Kalpakcheva and W von Oertzen (Singapore: World Scientific) p 313
[46] Moller P, Nix J R, Myers W D and Swiatecki W J 1995 *At. Data Nucl. Data Tables* **59** 185
[47] Hofmann S and Munzenberg G 2000 *Rev. Mod. Phys.* **72** 733
[48] Hulet E K *et al* 1977 *Phys. Rev. Lett.* **39** 385
[49] Illige J D, Hulet E K, Nitschke J M, Dougan R J, Lougheed R W, Ghiorso A and Landrum J H 1978 *Phys. Lett.* B **78** 209
[50] Otto R J, Morrissey D J, Lee D, Ghiorso A, Nitschke J M, Seaborg G T, Fowler M M and Silva R J 1978 *J. Inorg. Nucl. Chem.* **40** 589
Otto R J, Morrissey D J, Lee D, Ghiorso A, Nitschke J M, Seaborg G T, Fowler M M and Silva R J 1977 *LBL Report No.* LBL-6509 pp 1–29
[51] Oganessian Yu Ts *et al* 1978 *Nucl. Phys* A **294** 213
[52] Ter-Akopian G M, Bruchertseifer H, Buklanov G V, Orlova O A, Pleve A A, Chepigin V I and Sek C V 1979 *Sov. J. Nucl. Phys.* **29** 608
[53] Lougheed R W, Landrum J H, Hulet E K, Wild J F, Dougan R J, Dougan A D, Gäggeler H, Schädel M, Moody K J, Gregorich K E and Seaborg G T 1985 *Phys. Rev.* C **32** 1760
[54] Armbruster P *et al* 1985 *Phys. Rev. Lett.* **54** 406
[55] Flerov G N and Ter-Akopian G M 1985 *Treatise on Heavy-Ion Physics* vol 4 ed D A Bromley (New York: Plenum) p 333
[56] Seaborg G T 1963 *Man-Made Transuranium Elements* (New York: Prentice-Hall)
[57] Hulet E K, Lougheed R W, Wild J F, Dougan R J, Moody K J, Hahn R L, Henderson C M, Dupzyk R J and Bethune G R 1986 *Phys. Rev.* C **34** 1394
[58] Seaborg G T and Loveland W D 1990 *The Elements Beyond Uranium* (New York: Wiley)
[59] Oganessian Yu Ts 1975 *Lecture Notes in Physics* vol 33 ed J Echlers (Berlin: Springer) p 222
[60] Oganessian Yu Ts, Hussonoise M, Demin A G, Kharitonov Yu P, Bruchertseifer H, Constantinescu O, Korotkin Yu S, Tretiakova S P, Shirokovsky I V and Estevez I *et al* 1984 *Radiochim. Acta* **37** 113

[61] Flerov G N, Oganessian Yu Ts, Pleve A A, Pronin N V and Tretyakov Yu P 1976 *Nucl. Phys.* A **267** 359
[62] Oganessian Yu Ts *et al* 2001 *Phys. Rev.* C **64** 054606
[63] Belozerov A V *et al* 2003 *Eur. Phys. J.* A **16** 447
[64] Gaeggeler H W 1989 *Nucl. Phys.* A **502** 561c
[65] Hofmann S 1998 *Rep. Prog. Phys.* **61** 639
[66] Bock R *et al* 1982 *Nucl. Phys.* A **388** 334
[67] Pacheco A J, Fernandez Niello J O, DiGrigorio D E, di Tada M, Testoni J E, Chan Y, Chavez E, Gazes S, Plagnol E and Stokstad R G 1992 *Phys. Rev.* C **45** 2861
[68] Itkis M G *et al* 1998 *Nuovo Cimento* A **111** 783
[69] Zagrebaev V I 2001 *Phys. Rev.* C **64** 034606
[70] Siwek-Wilczyńska K, Skwira-Chalot I and Wilczyński J 2005 *Proc. 12th Workshop on Nuclear Physics 'Marie and Pierre Curie' (Kazimierz Dolny, Poland, 21–25 September 2005)* ed A Baran, J Bartel and K Pomorski
Siwek-Wilczyńska K, Skwira-Chalot I and Wilczyński J 2006 *Int. J. Mod. Phys.* E **15** 405
[71] Armbruster P 1985 *Annu. Rev. Nucl. Part. Sci.* **35** 135
[72] Munzenberg G 1988 *Rep. Prog. Phys.* **51** 57
[73] Morita K *et al* 2004 *J. Phys. Soc. Japan* **73** 2593
[74] Zagrebaev V I, Itkis M G and Oganessian Yu Ts 2003 *Phys. At. Nucl.* **66** 1033
[75] Świątecki W J, Siwek-Wilczyńska K and Wilczyński J 2004 *Int. J. Mod. Phys.* E **13** 261
[76] Aritomo Y, Wada T, Ohta M and Abe Y 1999 *Phys. Rev.* C **59** 796
[77] Zagrebaev V I and Greiner W 2005 *J. Phys. G: Nucl. Part. Phys.* **31** 825
[78] Oganessian Yu Ts, Itkis M G, Popeko A G, Utyonkov V K and Yeremin A V 2001 *Nucl. Phys.* A **682** 108c
[79] Gupta R K *et al* 1977 *Z. Naturf.* **a 32** 704
[80] Kondratiev N A, Kozulin E M, Pokrovski I V and Prokhorova E V 1999 *Proc. 4th Int. Conf. on Dynamical Aspects of Nuclear Fission (DANF 1998) (Casta-Papiernichka, Slovac Republic, October 1998)* (Singapore: World Scientific) p 431
[81] Prokhorova E V *et al Nucl. Phys.* A (submitted)
[82] Itkis M G *et al* 2001 *Proc. Int. Conf. on Fusion Dynamics at the Extremes (Dubna, 2000)* (Singapore: World Scientific) p 93
[83] Itkis M G *et al* 2000 *Proc. 2nd Int. Conf. on Fission and Properties of Neutron- Rich Nuclei (St. Andrews, Scotland, 28 June–3 July 1999)* ed J H Hamilton (Singapore: World Scientific) p 268
[84] Itkis I M *et al* 2005 *Proc. Int. Simp. on Exotic Nuclei (EXON2004) (Peterhof, Russia, 5–12 July 2004)* ed Yu E Penionzhkevich and E A Cherepanov (Singapore: World Scientific) p 317
[85] Heßberger F P *et al* 1997 *Z. Phys.* A **359** 415
[86] Itkis M G *et al* 2003 *Proc. 5th Int. Conf. on Dynamical Aspects of Nuclear Fission (DANF 2001) (23–27 October 2001, Casta-Papiernichka, Slovac Republic)* ed J Kliman (Singapore: World Scientific) p 1
[87] Itkis M G *et al* 2004 *Nucl. Phys.* A **734** 136
[88] Itkis M G *et al* 2003 *Phys. At. Nucl.* **66** 1118
[89] Pokrovsky I V *et al* 2000 *Phys. Rev.* C **62** 014615
[90] Hulet E K *et al* 1989 *Phys. Rev.* C **40** 770
[91] Oganessian Yu Ts 2001 *Nature* **413** 122
[92] Möller P, Nix J R, Myers W D and Świătecki W J 1995 *At. Data Nucl. Data Tables* **59** 185
[93] Bürvenich T, Bender M, Maruhn J A and Reinhard P-G 2004 *Phys. Rev.* C **69** 014307
[94] Donetz E D, Schegolev V A and Ermakov V A 1965 *Sov. J. Nucl. Phys.* **2** 1015
[95] Lazarev Yu A *et al* 2000 *Phys. Rev.* C **62** 064307
[96] Flerov G N, Oganesian Yu Ts, Lobanov Yu V, Lasarev Yu A, Tretiakova S P, Kolesov I V and Plotko V M 1971 *Nucl. Phys.* A **160** 181
[97] Lazarev Yu A *et al* 1994 *Phys. Rev. Lett.* **73** 624
[98] Wilk P A *et al* 2000 *Phys. Rev. Lett.* **85** 2697
[99] Türler A *et al* 2005 *The Third Sandanski Coordination Meeting on Nuclear Science (Albena, Bulgaria, 26–30 September)* (unpublished)
[100] Lazarev Yu A *et al* 1996 *Phys. Rev.* C **54** 620
[101] Oganessian Yu Ts and Penionzhkevich Yu E 1976 *Nucleonica* **21** 237
[102] Schädel M *et al* 1978 *Phys. Rev. Lett.* **41** 469
[103] Schädel M *et al* 1982 *Phys. Rev. Lett.* **48** 852
[104] Schädel M *et al* 1986 *Phys. Rev.* C **33** 1547
[105] Münzenberg G, Faust W, Hofmann S, Armbruster P, Güttner K and Ewald H 1979 *Nucl. Instrum. Methods* **161** 65
Hofmann S *et al* 1995 *Z. Phys.* A **350** 277

[106] Yeremin A V, Bogdanov D D, Chepigin V I, Gorshkov V A, Kabachenko A P, Malyshev O N, Popeko A G, Sagaidak R N, Ter-Akopian G M and Lavrentjev A Yu 1997 *Nucl. Instrum. Methods* **B126** 329
[107] Cohen B L and Fulmer C B 1958 *Nucl. Phys* **6** 547
[108] Armbruster P 1961 *Nukleonika* **3** 188
[109] Karnaukhov V A, Rubinskaya L A, Ter-Akopyan G M, Titov V N and Chugreev V A 1969 *JINR Preprint* P13-4454 (Dubna)
Bacho I, Bogdanov D D, Daroczy Sh, Karnaukhov V A, Petrov L A and Ter-Akopyan G M 1970 *Prib. Tekh. Eksp*. **2** 43
[110] Ghiorso A, Yashita S, Leino M E, Frank L, Kalnins J, Armbruster P, Dufour J-P and Lemmertz P K 1988 *Nucl. Instrum. Methods* A **269** 192
[111] Ninov V and Gregorich K E 1999 *ENAM98* ed B M Sherrill, D J Morrissey and C N Davids (Woodbury: AIP) p 704
[112] Oganessian Yu Ts *et al* 2000 *Proc. 4th Int. Conf. on Dynamical Aspects of Nuclear Fission (Casta-Papiernicka, Slovak Republic, 19–23 October 1998)* (Singapore: World Scientific) p 334
[113] Subotic K, Oganessian Yu Ts, Utyonkov V K, Lobanov Yu V, Abdullin F Sh, Polyakov A N, Tsyganov Yu S and Ivanov O V 2002 *Nucl. Instrum. Methods* A **481** 71
[114] Leino M, Uusitalo J, Enqvist T, Eskola K, Jokinen A, Loberg K, Trzaska W H and Aysto J 1994 *Z. Phys.* A **348** 151
[115] Miyatake H, Nomura T, Kawakami H, Tanaka J, Oyaizu M, Morita K, Shinozuka T, Kudo H, Sueki K and Iwata Y 1987 *Nucl. Instrum. Methods* B **26** 309
[116] Ninov V, Armbruster P, Hebberger F P, Hofmann S and Münzenberg G 1995 *Nucl. Instrum. Methods* A **357** 486
[117] Bohr N 1940 *Phys. Rev.* **58** 654
Bohr N 1941 *Phys. Rev.* **59** 270
[118] Oganessian Yu Ts *et al* 2001 *Phys. Rev.* C **64** 064309
[119] Oganessian Yu Ts, Lobanov Yu V, Popeko A G, Abdullin F Sh, Gulbekian G G, Mezentsev A N, Kharitonov Yu P, Ledovskoy A A, Polikanov A N and Tsyganov Yu S 1991 Heavy Ion Physics *JINR LNR Scientific Report* 1989–1990 p 158 (Dubna)
[120] Skobelev N K *et al* 2005 *Nucl. Instrum. Methods* B **227** 471
[121] Oganessian Yu Ts *et al* 2004 *Phys. Rev.* C **70** 064609
Oganessian Yu Ts *et al* 2004 *JINR Preprint* E7-2004-160 (http://www.jinr.ru/publish/Preprints/2004/160(E7-2004-160).pdf)
[122] Oganessian Yu Ts *et al* 2000 *Phys. Rev.* C **62** 041604
Oganessian Yu Ts 2000 *Phys. At. Nucl*. **63** 1679
[123] Oganessian Yu Ts *et al* 2004 *Phys. Rev.* C **69** 054607
[124] Oganessian Yu Ts *et al* 2004 *Phys. Rev.* C **69** 021601
[125] Oganessian Yu Ts *et al* 2005 *Phys. Rev.* C **72** 034611
[126] Dmitriev S N *et al* 2005 *Mendeleev Commun*. **15** 1
[127] Schumann D *et al* 2005 *Radiochim. Acta* **93** 727
[128] Stoyer N J *et al* 2006 *Proc. 9th Int. Conf. Nucleus–Nucleus Collisions (Rio de Janeiro, Brazil, 28 August–1 September 1 2006)*
[129] Oganessian Yu Ts *et al* 2001 Observation of the Decay of $^{292}116$ *Phys. Rev.* C **63** 011301
Oganessian Yu Ts, Utyonkov V K and Moody K J 2001 *Phys. At. Nucl*. **64** 1349
[130] Oganessian Yu Ts *et al* 2002 *JINR Communication* D7-2002-287
Oganessian Yu Ts *et al* 2003 *Lawrence Livermore National Laboratory Report* UCRL-ID-151619
Oganessian Yu Ts *et al* http://www.jinr.ru/publish/Preprints/2002/287(D7-2002-287)e.pdf
[131] Oganessian Yu Ts 2006 *Phys. Scr.* **125** 57
[132] Oganessian Yu Ts *et al* 2004 *Nucl. Phys*. A **734** 109
[133] Subbotin V G, Iliev S N, Sukhov A M, Tsyganov Yu S, Polyakov A N, Tomin V I and Voinov A A 2003 *Acta Phys. Pol*. B **34** 2159
Tsyganov Yu S, Subbotin V G, Polyakov A N, Iliev S N, Sukhov A M, Voinov A A and Tomin V I 2004 *Nucl. Instrum. Methods* A **525** 213
[134] Oganessian Yu Ts *et al* 2004 *Phys. Rev.* C **69** 021601
[135] Firestone R B and Shirley V S 1996 *Table of Isotopes* 8th edn (New York: Wiley)
[136] Wild J F, Hulet E K, Lougheed R W, Moody K J, Bandong B B, Dougan R J and Veeck A 1994 *J. Alloys Compounds* **213/214** 86–92
[137] Zagrebaev V I 2004 *Nucl. Phys*. A **734** 164c
[138] Bass R 1980 Fusion reactions: successes and limitations of a one-dimensional description *Proc. Symposium on Deep Inelastic and Fusion Reactions with Heavy Ions (West Berlin, 1979) (Lecture Notes in Physics* vol 117*)* ed W von Oertzen (Berlin: Springer) p 281

[139] Hofmann S *et al* 1996 *Z. Phys.* A **354** 229–30
Hofmann S *et al* 2002 *Eur. Phys. J.* A **14** 147
[140] Morita K 2005 *Proc. Int. Symp. on Exotic Nuclei 'EXON 2004' (Peterhof, Russia, 5–12 July 2004)* ed Yu E Penionzhkevich and E A Cherepanov (Singapore: World Scientific) p 188
[141] Loveland W, Gregorich K E, Patin J B, Peterson D, Rouki C, Zielinski P M and Aleklett K 2002 *Phys. Rev.* C **66** 044617
Gregorich K E *et al* 2005 *Phys. Rev.* C **72** 014605
[142] Hofmann S *et al* 2005 *Contribution to the 'Carpathian Summer School of Physics' (Mamaia, Romania, 13–24 June 2005)* (http://mare.tamu.edu/cssp05)
[143] Oganessian Yu Ts *et al* 1999 *Eur. Phys. J.* A **5** 63
Oganessian Yu Ts *et al* 1999 *Nature* **400** 242
Oganessian Yu Ts *et al* 2004 *Eur. Phys. J.* A **19** 3
[144] Muntian I, Patyk Z and Sobiczewski A 2003 *Phys. At. Nucl.* **66** 1015
[145] Ćwiok S, Heenen P-H and Nazarewicz W 2005 *Nature* **433** 705
[146] Bender M 2000 *Phys. Rev.* C **61** 031302
[147] Smolańczuk R 1999 *Phys. Rev.* C **59** 2634
Smolańczuk R 2001 *Phys. Rev.* C **63** 044607
[148] Hofmann S and Münzenberg G 2000 *Rev. Mod. Phys.* **72** 733
[149] Moritomo K *et al* 2001 *Proc. Tours Symp. on Nuclear Physics IV (Tours, France, 2000)* (New York: AIP) p 354
[150] Stodel C *et al* 2001 *Proc. Tours Symp. on Nuclear Physics IV (Tours, France, 2000)* (New York: AIP) p 344
[151] Gregorich K E *et al* 2003 *Eur. Phys. J.* A **18** 633
[152] Oganessian Yu Ts *et al* 2006 *Phys. Rev.* C **74** 044602
[153] Lazarev Yu A *et al* 1994 *Phys. Rev. Lett.* **73** 624–627
Türler A, Dressler R, Eichler B, Gäggeler H W, Jost D T, Schädel M, Brüchle W, Gregorich K E, Trautmann N and Taut S 1998 *Phys. Rev.* C **57** 1648
[154] Düllmann Ch E *et al* 2002 *Nature* **418** 859
Türler A *et al* 2003 *Eur. Phys. J.* A **17** 505
[155] Hofmann S *et al* 1995 *Z. Phys.* A **350** 281
[156] Morita K *et al* 2004 *J. Phys. Soc. Japan* **73** 1738
[157] Audi G, Wapstra A H and Thibault C 2003 *Nucl. Phys.* A **729** 337
[158] Kolesnikov N N, Krylova A P and Kandybarov V K 1963 *Izv. AN SSSR, Ser. Fiz.* **27** 132
Kolesnikov N N and Demin A G 1975 *JINR Communication* P6-9421 (in Russian)
[159] Hyde E K, Perlman I and Seaborg G T 1964 *The Nuclear Properties of the Heavy Elements, Detailed Radioactive Properties* (Englewood Cliffs, NJ: Prentice-Hall)
[160] Paulus W *et al* 1999 *Radiochim. Acta* **84** 69
[161] Gäggeler H W and Türler A 2003 *The Chemistry of Superheavy Elements* ed M Schädel (Dordrecht: Kluwer) p 237
Kratz J V 2003 *The Chemistry of Superheavy Elements* ed M Schädel (Dordrecht: Kluwer) p 159
[162] Schädel M 2002 *J. Nucl. Radiochem. Sci.* **3** 113
[163] Yakushev A B *et al* 2001 *Radiochim. Acta* **89** 743
[164] Pitzer K S 1975 *J. Chem. Phys.* **63** 1032
[165] Eliav E, Kaldor U and Ishikawa Ya 1995 *Phys. Rev.* A **52** 2765–9
Seth M, Schwerdtfeger P and Dolg M 1997 *J. Chem. Phys.* **106** 3623
[166] Pershina V, Bastug T, Jacob T, Fricke B and Varga S 2002 *Chem. Phys. Lett.* **365** 176
[167] Yakushev A B *et al* 2003 *Radiochim. Acta* **91** 433
Eichler R *et al* 2006 *Radiochim. Acta* **94** 181
[168] Düllmann Ch E, Eichler B, Eichler R, Gäggeler H W, Jost D T, Piguet D and Türler A 2002 *Nucl. Instrum. Methods* A **479** 631
Soverna S *et al* 2005 *Radiochimica Acta* **93** 1
[169] Eichler R and Schädel M 2002 *J. Phys. Chem.* B **106** 5413
[170] Eichler B, Zimmermann P and Gäggeler H W 2000 *J. Phys. Chem.* A **104** 3126
[171] Zvara I 1985 *Radiochim. Acta* **38** 95
[172] Eichler R *et al* 2007 *Nature* (at press)
[173] Geiger H and Nuttal J M 1911 *Phil. Mag.* **22** 613
[174] Viola V E Jr and Seaborg G T 1966 *J. Inorg. Nucl. Chem.* **28** 741
[175] Dong T and Ren Zh 2005 *Eur. Phys. J.* A **26** 69
[176] Chowdhury P R, Samanta C and Basu D N 2006 *Phys. Rev.* C **73** 014612

[177] Parkhomenko A and Sobiczewski A 2005 *Acta Phys. Pol.* B **36** 3095
[178] Poenaru D N, Plonski I-H and Greiner W 2006 *Phys. Rev.* C **74** 014312 (and references therein)
[179] Zhang H, Zuo W, Li J and Royer G 2006 *Phys. Rev.* C **74** 017304
[180] Oganessian Yu Ts *et al* 1999 *Phys. Rev. Lett.* **83** 3154
[181] Berger J F, Hirata D and Girod M 2003 *Acta Phys. Pol.* B **34** 1909
[182] Typel S and Brown B A 2003 *Phys. Rev.* C **67** 034313
[183] Gupta M and Burrows T W 2005 *Nucl. Data Sheets* **106** 251
[184] Goriely S, Samyn M, Heenen P-H, Pearson J M and Tondeur F 2002 *Phys. Rev.* C **66** 024326
[185] Warda M, Egido J L and Robledo L M *Proc. 12th Workshop on Nuclear Physics 'Marie and Pierre Curie' (Kazimierz Dolny, Poland, 21–25 September 2005)* ed A Baran, J Bartel and K Pomorski
Warda M, Egido J L and Robledo L M 2006 *Int. J. Mod. Phys.* E **15** 504
[186] Gambhir Y K, Bhagwat A and Gupta M 2005 *Ann. Phys.* **320** 429
Gambhir Y K, Bhagwat A and Gupta M 2005 *Phys. Rev.* C **71** 037301
[187] Baran A, Łojewski Z, Sieja K and Kowal M 2005 *Phys. Rev.* C **72** 044310
Baran A, Łojewski Z, Sieja K and Kowal M 2005 *Acta Phys. Pol.* B **36** 1369
[188] Baran A, Łojewski Z and Sieja K 2006 *Int. J. Mod. Phys.* E **15** 452
[189] Hoffman D S 1989 *Nucl. Phys.* A **502** 21c
[190] Iwamoto A, Möller P, Nix J R and Sagawa H 1996 *Nucl. Phys.* A **596** 329
[191] Nishio K, Ikezoe H, Mitsuoka S and Lu J 2000 *Phys. Rev.* C **62** 014602
[192] Gupta R K, Manhas M and Greiner W 2006 *Phys. Rev.* C **73** 054307
[193] Oganessian Yu Ts *et al* 2003 *Nucl. Instrum. Methods* B **204** 606
[194] Oganessian Yu Ts 2002 *JINR Preprint* E7-2002-64
(http://www.jinr.ru/publish/Preprints/2002/064(E7-2002-64).pdf)
[195] Oganessian Yu Ts 2006 *Phys. At. Nucl* **69** 932
[196] Strutinski V M and Muzychka Yu A 1996 *Proc. Int. Conf. on Heavy Ion Physics (JINR, Dubna, 1966)* Part 2 p 51
[197] Muzychka Yu A, Pashkevich V V and Strutinski V M 1968 *Yad. Fiz.* **8** 716
[198] Muzychka Yu A 1969 *Phys. Lett.* B **28** 539
[199] Randrup J *et al* 1974 *Phys. Scr.* A **10** 60
[200] Fiset E O and Nix J R 1972 *Nucl. Phys.* A **193** 647
[201] Nix J R 1972 *Ann. Rev. Nucl. Sci.* **22** 65
[202] Sobiczewski A 1974 *Phys. Scr.* A **10** 47
[203] Sobiczewski A 1978 *Proc. Int. Sump. on Superheavy Elements (Lubbock, Texas)* ed M A K Lodhi (Oxford: Pergamon) p 274
[204] Nilsson S G 1978 *Proc. Int. Sump. on Superheavy Elements (Lubbock, Texas)* ed M A K Lodhi (Oxford: Pergamon) p 237
[205] Flerov G N and Ter-Akopian G M 1983 *Rep. Prog. Phys.* **46** 817
[206] Bisnovatyi-Kogan G S and Chechetkin V M 1973 *Astrophys. Space Sci. Rev.* **26** 25
[207] Lattimer J M, Mackie F, Ravenhall D G and Schramm D N 1977 *Astrophys. J.* **213** 225
[208] Klapdor H V, Oda T, Metzinger J, Hillebrandt W and Thielemann F K 1981 *Z. Phys.* A **299** 213
[209] Kratz K-L 2006 *Proc. 12th Int. Symposium Capture Gamma Ray Spectroscopy and Related Topics (Notre Dame, Indiana, 4–9 September 2006)* ed A Woehr and A Aprahamian AIP Conf. Proc. 819 409
[210] Pearson J M, Nayak R C and Goriely S 1996 *Phys. Lett.* B **387** 455
[211] Goriely S, Tondeur F and Pearson J M 2001 *At. Data Nucl. Data Tables* **77** 311
[212] Samyn M, Goriely S, Bender M and Pearson J M 2004 *Phys. Rev.* C **70** 044309
[213] Goriely S, Samyn M, Pearson J M and Onsi M 2005 *Nucl. Phys.* A **750** 425
[214] Hoffman D C, Lawrence F O and Rourke F M 1971 *Nature* **234** 132
[215] Ćwiok S, Dobaczewski J, Heenen P-H, Magierski P and Nazarewicz W 1996 *Nucl. Phys.* A **611** 211
[216] Patyk Z and Sobiczewski A 1998 *Proc. VI Int. School-Seminar on Heavy Ion Physics (Dubna, Russia, 1997)* ed Yu Ts Oganessian and R Kalpakchieva (Singapore: World Scientific) p 417
[217] Reihardt P-G and Maruhn J A 1999 *Heavy Elements and Related New Phenomena* vol I ed W Greiner and R K Gupta (Singapore: World Scientific) p 332
[218] Oganessian Yu Ts 2004 *Pure Appl. Chem.* **76** 1715
[219] Israel M H 1981 *Proc. 17th Int. Cosmic Ray Conf. (Paris, France)* vol 12 p 53
[220] Pearson J M, Nayak R C and Goriely S 1996 *Phys. Lett.* B **387** 455